

Politehnica University
Timișoara
Department of Mechanics
and Strength of Materials



Habilitation thesis

Constitutive models for the viscoplasticity and damage of thermoplastic polymers

PhD Domain: Mechanical engineering

Dr. Eng. Dan-Andrei ȘERBAN

Timișoara

2020

Table of Contents

Abstract	5
Rezumat.....	7
1. Introduction	9
1.1. Scientific background.....	9
1.2. Academic background.....	11
1.3. Outline of the dissertation	12
2. Viscoplasticity of thermoplastic polymers	13
2.1. Introduction	13
2.2. Experimental investigations	13
2.2.1. Monotone tests.....	14
2.2.2. Cyclic tests.....	17
2.3. Numerical models.....	21
2.3.1. Viscoelastic rheological models	21
2.3.2. Rate- and temperature-dependent elastic-plastic formulations.....	29
2.3.3. Viscoplastic formulations	43
2.4. Conclusions	47
3. Damage and failure of polymers	49
3.1. Introduction	49
3.2. Spatial state of stress	50
3.2.1. Tensor invariants	50
3.2.2. Haigh-Westergaard stress space	51
3.3. Basis for damage onset in ductile materials	54
3.3.1. The ductile damage model.....	55
3.3.2. The shear damage model	57
3.4. Calibration and validation of damage models	58
3.4.1. Tensile tests on notched flat specimens.....	58
3.4.2. Compression tests on notched cylindrical specimens.....	62
3.4.3. Arcan tests	66

3.4.4.	Model validation for rapid prototyped polymers.....	70
3.5.	Conclusions	73
4.	Scientific achievements	75
4.1.	Overview	75
4.2.	Complete list of publications.....	76
4.2.1.	Publications in ISI Journals	76
4.2.2.	Articles in ISI Proceedings	79
4.2.3.	Articles in International Databases Journals	80
4.3.	Research Grants.....	81
4.3.1.	National Grants.....	81
4.3.2.	International Grants	82
4.4.	Research stages.....	83
4.5.	Other research topics	85
4.5.1.	Research into polymeric foams	85
4.5.2.	Research into metamaterial structures	95
4.5.3.	Research into geopolymer composites	100
5.	Scientific and academic development plan	107
5.1.	Viscosity, plasticity, fatigue and failure of polymers	107
5.1.1.	Mechanical testing.....	107
5.1.2.	Numerical models.....	108
5.2.	Metamaterial structures	109
5.2.1.	Manufacturing	109
5.2.2.	Structure design and optimization	109
5.2.3.	Composite metamaterial structures	109
5.3.	Woven fibre reinforced polymers.....	110
5.3.1.	Mechanical testing.....	110
5.3.2.	Multi-scale modelling.....	110
5.4.	Academic development plan	112
6.	Bibliography	115

Abstract

This thesis presents a summary of the author's main scientific contributions between 2012 (the date of the author's PhD thesis defence) and 2020, in the field of experimental analysis and simulation of the mechanical behaviour of advanced materials. The focus of the Habilitation is represented by the numerical modelling approaches used for thermoplastic polymers. Results from other research topics that the author was concerned with will also be briefly presented.

The Habilitation thesis is divided into three sections. The first section consists of a short introduction, where the author's scientific and academic backgrounds are briefly presented, along with an outline of the thesis.

The second section of the thesis, which encompasses the main topic of the Dissertation, is composed of two chapters: *Viscoplasticity of thermoplastic polymers* and *Damage and failure of polymers*.

The first of the two chapters begins with a brief presentation of the experimental results on various polymeric compounds. The main focus was the showcasing of the viscoplastic behaviour of this class of materials through both monotone and cyclic tests. Two parameters were identified as major factors for the non-linear behaviour: temperature and time (through the effects of the strain rate and long-term loading). Apart from the significant effect on stiffness and strength (which increase proportionally with the strain rate and decrease with temperature), a peculiarity of thermoplastic polymers is that, at different temperatures, the same compound can exhibit either brittle or ductile characteristics.

In the second part of this chapter, three formulations were evaluated for their accuracy in modelling the stress-strain response of thermoplastic polymers at different strain rates and temperatures: the viscoelastic formulation, the elastic-plastic formulation and the viscoplastic formulation. For the viscoelastic formulation, the Wiechert model showed the best results, when compared to the other investigated rheological models. For the elastic-plastic formulations, three models were presented: the Zerilli-Armstrong model, the Johnson-Cook model and the Multi-linear hardening model, with the latter exhibiting the optimal response. Two viscoplastic models were investigated: the Bingham-Maxwell model and the Two-layer viscoplastic model. Even though the TLV model can yield the best results in modelling the viscoplastic effects, its calibration is rather cumbersome. In consequence, for simpler applications, the MLH model is recommended in the case of monotone loadings and the Wiechert model for the case of cyclic loadings at low strains.

The chapter entitled *Damage and failure of polymers* is concerned with the experimental determination and numerical approximation of the failure of thermoplastic polymers when subjected to various loading conditions. The considered failure model

was initially developed for metals and it assumes that the failure in ductile materials is caused by the nucleation and subsequent growth of voids in the material during straining (phenomenon also observed in polymers). From a mathematical standpoint, this formulation considers that the critical plastic strain (responsible for the void nucleation) is a function of three tensor invariants: the first invariant of the total stress tensor (the hydrostatic pressure) and the second (through the von Mises equivalent stress) and third (through the Lode angle) invariants of the stress deviator tensor.

For the calibration of the model, several experimental procedures were considered: tensile tests on flat notched specimens, compression tests on round notch specimens and Arcan tests. Numerical analyses were performed with identical test conditions in order to determine the critical plastic strain, stress triaxiality and Lode angle parameter. The results were combined into a damage model that accounts for a wide range of stress triaxiality variation and it was evaluated using simulations that replicate the compression of a metamaterial structure with open Kelvin cells, yielding accurate results.

The third section of the thesis presents the scientific achievements (complete list of publications and research Grants), the scientific development plan and results from other research topics, which are divided in three categories: polymeric foams, metamaterial structures and geopolymer composites.

The research into polymeric foams was mainly centred on un-reinforced and long fibre reinforced polyurethane rigid foams and was concern with the static and dynamic characterization, morphology and microstructural analyses and damage/fracture. For the topic of metamaterial structures, various types of periodic geometries were analysed, manufactured and tested, with the goal of determining optimal configurations. Concerning the geopolymer composites topic, wood fibre reinforced fly ash composites were investigated experimentally and concrete damage plasticity models were calibrated with good results.

The scientific development plan contains a brief presentation of the future research topics. The first topic represents a continuation of the current research into the viscosity, plasticity and fatigue of polymers. The focus will be on the development of yield surfaces and yield potentials specific for polymers and the investigation of the ductile failure hypothesis for a wider range of materials. Another topic of interest is related to metamaterial structures and the continued search for structure optimization in terms of mechanical properties as well as manufacturing. The multi-scale modelling of woven fibre reinforced polymers will also be a priority, with the aim of developing macro-scale constitutive models for elasticity, plasticity and damage based on limited data provided by pre-impregnate manufacturers.

Rezumat

Această teză prezintă pe scurt principalele contribuții științifice ale autorului între anii 2012 (data susținerii tezei de doctorat) și 2020, în domeniul analizei experimentale și numerice a comportamentului mecanic pentru materiale avansate. Tema principală a acestei teze este prezentarea diverselor abordări în modelarea comportamentului polimerilor termoplastici. Rezultatele din alte domenii de cercetare abordate de autor vor fi de asemenea prezentate.

Această lucrare este împărțită în trei secțiuni, prima fiind reprezentată de o scurtă introducere, unde autorul prezintă succint evoluția carierei științifice și academice, alături de o prezentare generală a conținutului tezei.

A doua secțiune a tezei, care cuprinde tema principală a Disertației, cuprinde două capitole: *Viscoplasticitatea polimerilor termoplastici* și *Degradarea și cedarea polimerilor*.

Primul din aceste capitole începe cu o scurtă prezentare a rezultatelor experimentale obținute pentru diferiți compuși polimerici. Scopul principal este evidențierea comportamentului viscoplastic al acestei clase de materiale prin intermediul testelor monotone și ciclice. Doi parametri au fost identificați ca având o influență semnificativă asupra comportamentului neliniar: temperatura și timpul (prin efectele vitezei de deformare și încărcări de lungă durată). Pe lângă efectele considerabile asupra rigidității și rezistenței (care cresc proporțional cu viteza de deformare și scad cu creșterea temperaturii), o particularitate a acestor polimeri este că, la diferite temperaturi, același compus poate avea comportament fragil sau ductil.

În a doua parte a acestui capitol a fost evaluată acuratețea în modelarea caracteristicilor tensiune-deformație la diferite viteze de deformare și temperaturi pentru trei formulări diferite: formularea viscoelastică, formularea elastic-plastică și formularea viscoplastică. În cazul formulării viscoelastice, dintre modelele reologice evaluate, cele mai bune rezultate au fost determinate de modelul Wiechert. Pentru formularea elastic-plastică au fost prezentate trei modele: Zerilli-Armstrong, Johnson-Cook și modelul ecruisării multi-liniare (MLH), cel din urmă determinând cele mai bune rezultate. Două modele viscoplastice au fost investigate: Bingham-Maxwell și modelul viscoplastic în două niveluri (TLV). Deși modelul TLV a determinat cele mai exacte rezultate, calibrarea acestuia este destul de dificilă. În consecință, pentru aplicații mai simple, se recomandă utilizarea modelului MLH pentru solicitări monotone și modelul Wiechert pentru solicitări ciclice la deformații mici.

În capitolul intitulat *Degradarea și cedarea polimerilor* sunt prezentate rezultatele încercărilor experimentale și ale analizelor numerice efectuate în scopul aproximării cedării polimerilor termoplastici pentru diferite stări de solicitare. Modelul de degradare studiat a fost dezvoltat pentru metale și are ca principiu nucleația și creșterea progresivă a vidurilor în timpul deformației (fenomen observat și în cazul

polimerilor). Din punct de vedere matematic, această formulare presupune existența unor deformații critice (responsabile de nucleația vidurilor), care variază cu trei parametri: primul invariant al tensorului tensiunilor totale (presiunea hidrostatică), al doilea invariant al componentei distorsionare a tensorului tensiunilor (prin tensiunea echivalentă von Mises) și al treilea invariant al componentei distorsionare a tensorului tensiunilor (prin așa-numitul parametru al unghiului Lode).

Pentru calibrarea acestui model au fost efectuate trei tipuri de teste: teste de tracțiune pe epruvete plate cu concentrator, teste de compresiune pe epruvete cilindrice cu concentrator și teste Arcan. O serie de analize numerice au fost efectuate în condiții identice cu cele experimentale în scopul determinării deformației plastice critice și valorile corespunzătoare pentru starea de triaxialitate a tensiunii și parametrul unghiului Lode. Rezultatele au fost compuse într-un model care exprimă variația deformației plastice critice pentru un interval larg al stării de triaxialitate a tensiunii. Acest model a fost evaluat pe analize numerice care au replicat încercări de compresiune pe structuri de metamateriale cu celule deschise de tip Kelvin.

A treia secțiune a tezei prezintă realizările științifice (lista completă a publicațiilor și a Grant-urile de cercetare), planul de dezvoltare al activității științifice și rezultatele obținute în alte domenii de cercetare: spume polimerice, structuri de metamateriale și compozite geopolimerice.

Cercetările privind spumele polimerice au fost axate în principal pe caracterizarea statică și dinamică, analiza morfologică și microstructurală și cedarea/ruperea spumelor poliuretanică rigide neranforsate și ranforsate cu fibre de sticlă. În domeniul structurilor de metamateriale au fost proiectate, simulate, fabricate și testate diferite tipuri de structuri periodice în scopul determinării configurațiilor optime. În studiul compozitelor geopolimerice, cercetările au fost concentrate asupra materialelor alcătuite din matrice din cenușă zburătoare armate cu fibre lemnoase, ale căror proprietăți au fost determinate experimental și modelate utilizând formularea plasticității și degradării betoanelor.

Planul de dezvoltare al activității științifice prezintă viitoarele direcții de cercetare ale autorului. Prima temă este reprezentată de o continuare a studiilor referitoare la vâscozitatea, plasticitatea și oboseala polimerilor. Accentul va fi pus pe dezvoltarea unor suprafețe și potențiale de curgere specifice polimerilor precum și investigații referitoare la aplicarea modelului cedării ductile pentru alte clase de polimeri. A doua temă este reprezentată de studiul structurilor de metamateriale în scopul optimizării geometriilor și facilitării fabricației. A treia temă de interes este modelarea *multi-scale* a polimerilor armați cu țesături de fibre, având ca scop dezvoltarea de ecuații constitutive la scară macro pentru elasticitate, plasticitate și cedare, bazate doar pe informații provenite de la fabricanții pre-impregnatelor.

1. Introduction

1.1. Scientific background

The research theme of the candidate's doctoral studies was the determination of the mechanical properties of a semi-crystalline thermoplastic polymer and based on the obtained experimental data, the development of a number of constitutive material models that could accurately replicate the mechanical characteristics of the studied material in finite element analysis simulations. The main use of the studied material is Sports industry as components of running footwear soles. The numerical material models have been used in the footwear design process in order to obtain a sensible component dimensioning (assurance of the required properties at the lowest possible mass). Thus an experimental programme was developed that included tests which would account for the viscoelastic nature of the polymer, namely the time and temperature dependency of the material properties. With the help of gathered data several software implemented constitutive models were calibrated, each presenting both advantages and drawbacks from an accuracy and time expenditure point of view. This research was the result of a joint collaboration between four institutions:

„Politehnica” University of Timișoara, Romania, the host institution, provided financial support (by means of a doctoral scholarship funded by the program POSDRU/88/1.5/S/50783) as well as material resources;

Adidas Innovation Team (AIT), Adidas AG (Herzogenaurach, Germany) proposed the research topic, provided the materials and offered know-how regarding material testing and simulation, the opportunity to perform a research stage at AIT and material resources during the stay;

Sports Technology Institute (STI), Loughborough University, United Kingdom, offered know-how in setting up the experimental plan and concerning material testing as well as the opportunity to perform a research stage at STI and material resources during the stay;

Institut für Leichtbau und Kunststofftechnik, Technical University of Dresden, Germany offered material resources and the opportunity to perform a research stage.

An important aspect regarding the practicality of this research is the direct applicability of the results, the developed material models being used by *Adidas Innovation Team* in the process of designing sports footwear as early as the doctoral studies and are continuing to use them to this day.

After the conclusion of the doctoral studies the candidate maintained collaborations with the partners. Through the collaboration protocol signed between “Politehnica” University of Timișoara and the Technical University of Dresden the candidate attended three research stages at *Institut für Leichtbau und Kunststofftechnik*, being integrated in a research project that aims at the development of glass fibre reinforced cellular materials and the optimization of the manufacturing process by increasing productivity. In the first stages, the candidate’s tasks were the elaboration of an experimental plan for the mechanical characterization of the studied composites in order to determine the optimal parameters. The collaboration with Adidas continued in the area of virtual material models used in finite-element analysis by expanding the developed material models, so that damage and failure models were included and by developing material models for other hyperelastic materials (synthetic leather).

During the doctoral research the candidate was co-opted into a research team that studied the determination and modelling of the mechanical behaviour of cellular materials, this research being supported by the Grant UEFISCDI PN-II-ID-PCE-2011-3-0456, contract number 172/2011. In this Grant the candidate is responsible for developing 2D micromechanical models of the studied cellular materials, the development of finite-element analysis simulations in order to determine the influence of the geometrical parameters on the mechanical properties as well as the development of constitutive models at a macro scale for simulating parts and components manufactured from the studied foams. Up until this point the research concluded by the submission for reviewing of three articles at ISI journals.

Starting with the month of May 2014 the candidate won a postdoctoral scholarship offered by POSDRU (POSDRU/159/1.5/S/137070) that spans over 18 months, following a competition held by “Politehnica” University of Timișoara. The project’s theme belongs to research field of *Products, Processes and Innovative Materials*, with a principal research direction of *Materials and Technologies for Energy Conversion*. The project objective is the development of constitutive models used in simulation composite sandwich structures.

In 2016, the candidate was awarded an 18-month Grant for the project entitled “Transfer of knowledge for dashboard and Head-Up Display optimization through testing and modelling of advanced materials”, performed in collaboration with Continental Automotive Timișoara (value of ~75.000 €). The objectives of the project were the determination of the static, dynamic and fatigue properties of 7 types of polymer compounds and composites used by Continental Automotive in manufacturing dashboards and head-up display units. With the experimental results, material models were developed for each compound, which are currently used by Continental in the design process of the aforementioned components.

In 2017, a consortium of 8 partners led by the Technical University of Krakow was awarded a 36-month Era-Net LAC Grant for the project entitled “Development of ecofriendly composite materials based on geopolymer matrix and reinforced with waste fibers”, the candidate being the coordinator of the Politehnica University Timișoara (UPT) team (partner budget of around 87.000 €). The role of UPT in the project was the investigation of the mechanical properties of fibre-reinforced geopolymers and the development of constitutive models.

In 2018, the candidate was awarded a 24-month Grant for the project entitled “Development of polymer-based metamaterial structures for safety equipment applications”, where several structures were developed and simulated, the results being validated by experimental procedures on prototyped models (budget of ~55.000 €).

1.2. Academic background

The candidate began his academic activity in 2010 as a volunteer, during his PhD studies, holding applications in the topics of Strength of materials (Faculty of Mechanical Engineering, Politehnica University Timișoara) and Fundamentals of Mechanical Engineering (Faculty of Electrotechnical and Electroenergetic Engineering, Politehnica University Timișoara).

While working as a scientific researcher, the candidate was employed as an associate lecturer to the Department of Mechanics and Strength of Materials, Politehnica University Timișoara, holding lectures and applications in the topics of The Finite Element Method (Faculty of Mechanical Engineering, Politehnica University Timișoara) and Fundamentals of Mechanical Engineering and Robotics (Faculty of Automation and Computer Science, Politehnica University Timișoara)

In 2017, the candidate was appointed Lecturer at the Department of Mechanics and Strength of Materials, Politehnica University Timișoara, holding lectures and applications in the topics of:

- Introduction to Numerical Methods (Faculty of Mechanical Engineering, Politehnica University Timișoara)
- Numerical Analyses of Biomechanical Structures (Faculty of Mechanical Engineering, Politehnica University Timișoara)
- The Finite Element Method (Faculty of Mechanical Engineering, Politehnica University Timișoara)
- Numerical Methods in the Analyses of Thermomechanical Stresses (Faculty of Mechanical Engineering, Politehnica University Timișoara)

- Numerical Methods in the Analyses of Stresses (Faculty of Mechanical Engineering, Politehnica University Timișoara)
- Mechanical Engineering and Robotics (Faculty of Automation and Computer Science, Politehnica University Timișoara)

From 2019, the candidate was appointed as Associate Professor at the Department of Mechanics and Strength of Materials, Politehnica University Timișoara, teaching similar topics to his Lecturer position.

1.3. Outline of the dissertation

The main topic of this dissertation is the presentation of the main results from the continuation of the candidate's studies into the mechanical behaviour of polymeric materials. The results are structured in two chapters: *Viscoplasticity of thermoplastic polymers* and *Damage and failure of polymers*.

The first chapter is divided into two sections. The first one deals with the most relevant experimental results that showcase the viscoelastic behaviour of thermoplastic polymers, namely the significant influence of temperature and time on their response. The second section will present several approaches in modelling this behaviour, namely viscoelasticity, elastoplasticity and viscoplasticity.

In the second chapter, the modelling of progressive damage and failure of polymers will be evaluated using the ductile damage model (which presumes that damage occurs due to the nucleations of voids during straining). Several experimental procedures on various specimens will be presented, that determine the failure strain for different stress triaxiality values. The results will then be replicated using finite element analyses, in order to obtain a valid damage model.

Other research topics not related to the study of polymers, that the candidate studied after the completion of his doctoral studies will also be briefly covered.

2. Viscoplasticity of thermoplastic polymers

2.1. Introduction

The first step in the development of constitutive models is the determination of their mechanical properties and their variation with different parameters such as time, temperature, humidity etc. There is a very wide range of standardized mechanical test protocols designed for polymers, from standard tensile, compressive or flexural loadings, to biaxial or multiaxial tests and fatigue to more specific procedures such as crazing or scratch resistance [1]. This work presents uniaxial and cyclic test data performed on various polymers with the aim of determining their basic mechanical properties (Young's modulus, strength, plastic and viscous flow behaviours).

The gathered experimental data is used in calibrating constitutive models. Due to the complex nature of the mechanical behaviour of polymers, there is an issue with calibrating existing material models in order to account for strain rate or temperature effects. This chapter presents various types of constitutive formulations (elastic-plastic, viscoelastic and viscoplastic), their calibration and the comparison between the experimental data and the numerical results.

2.2. Experimental investigations

During his scientific career, the author performed a large number of experimental tests on a wide variety of polymer compounds, such as polyamides, ABS, polycarbonates, PMMA, PBT, PPS etc.

The experimental investigation into the mechanical properties of thermoplastic polymers presented in this work were carried out with the intent of determining the influence of temperature and strain rate on the mechanical properties on both monotone and cyclic loadings. This paragraph will briefly present experimental results gathered from a variety of polymeric compounds, with the aim of highlighting the particularities of this class of materials.

2.2.1. Monotone tests

Monotone tests were performed in order to determine the influence of the strain-rate and temperature on the stiffness, strength and yielding of polymers.

Strain rate dependency

The influence of strain rate was investigated for a wide variety of tests speeds, from quasi-static to dynamic loadings. The typical stress-strain response for various strain rates is presented in Figure 2.1 for a polyamide compound [2].

As with other types of materials, the stiffness and strength of the polymers increases with strain rate (as seen in Figure 2.2), though the influence is more pronounced as the mechanisms associated with this behaviour differ due to their microstructure (consisting on long, covalent bonded entangled macromolecules).

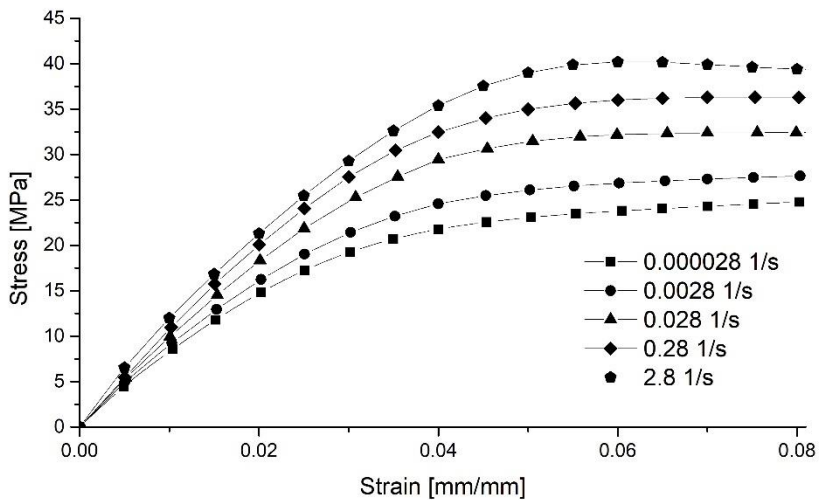


Figure 2.1 Strain rate dependency for a PA compound

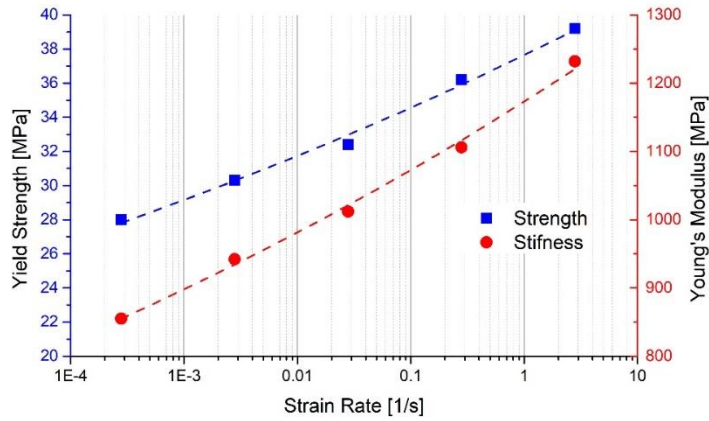


Figure 2.2 Variation of yield strength and Young’s modulus with strain rate for a PA compound [3]

There is a rather wide array of mechanisms associated with the deformation of polymers [4]. A linear elastic region is usually observed at very small deformations ($< 0.01 \text{ mm/mm}$), usually caused by the stretching of the macromolecules, which regain their initial shape after the loading is ceased. The non-linear response (Figure 2.3) can have different causes, which can cause long-time reversible deformations (viscous strains, caused by chain slippage, bond interchange or Thirion relaxation) or irreversible deformations (plastic strains, caused by chain detanglement or fracture). For this reason, it is often difficult to distinguish the reversible and irreversible strains, which represents a serious challenge in modelling the mechanical response.

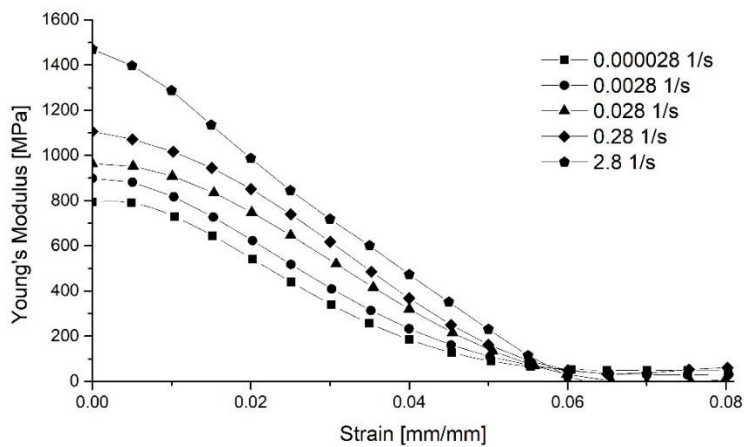


Figure 2.3 Variation of Young’s modulus with strain for different strain rates [3]

Temperature dependency

The influence of temperature on the mechanical properties of polymers was studied for temperature intervals that the given compounds can be subjected during service (from $-25\text{ }^{\circ}\text{C}$ up to $90\text{ }^{\circ}\text{C}$). A typical variation of the stress-strain response with temperature is presented in Figure 2.4 for a PMMA compound.

Apart from the rather significant influence of temperature on the stiffness and strength of the polymers (which is caused by their microstructure, as with the strain rate influence), a phenomenon specific to thermoplastics is often observed. A ductile polymer may become brittle at low temperatures and a brittle polymer may become ductile at high temperature, as seen in Figure 2.4.

In theory, every thermoplastic polymers can have brittle as well as ductile behaviour depending on the temperature. The transition between the two states is called the glass transition temperature, and it can be determined with the help of specific tests (DMA tests, which will be discussed in the next paragraph). The temperature influence is higher in the vicinity of the glass transition temperature and thus, in order to obtain a more predictable response, polymer compositions should be considered so that the GTT is not near the in-service temperature.

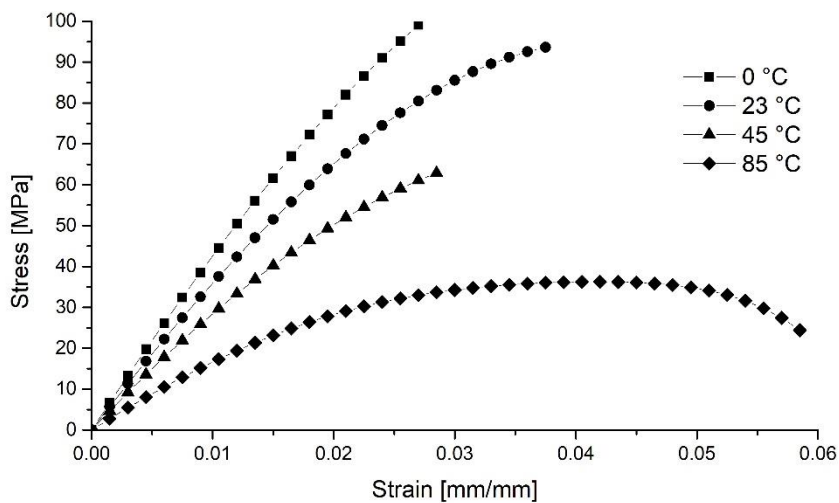


Figure 2.4 Temperature dependency for a PMMA compound

2.2.2. Cyclic tests

The cyclic tests were performed in order to gain insight on the flow behaviour of polymers and to try to differentiate the viscous strains from the plastic ones. Three types of tests are presented: dynamic mechanical analyses (DMA), tensile cyclic tests at variable strains and low-cycle fatigue tests.

DMA Tests

Dynamic mechanical analyses represent a type of tests specifically designed for polymers with the aim of the determination of the influence of temperature (and of the glass transition temperature) and of the influence of frequency [5]. The tests consist of the application of a strain with a sinusoidal amplitude for a variety of loadings (tensile, single or double cantilever, shear etc.) and the recording of the stress and of the phase angle shift determined by the viscous nature of the polymers.

A typical temperature sweep DMA test result is presented in Figure 2.5 and it highlights the variation of the dynamic stiffness (storage modulus) with temperature and the glass transition temperature (corresponding to the peak region of the loss modulus).

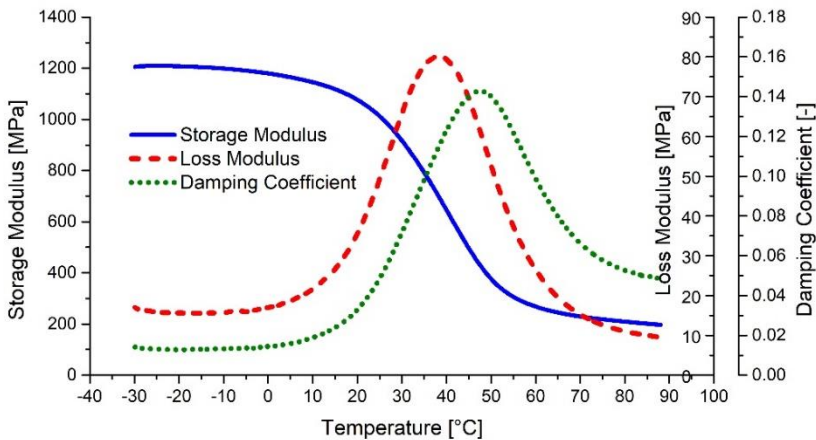


Figure 2.5 Temperature sweep DMA test results for a ABS compound [5]

Frequency sweep DMA tests are performed in order to determine the viscoelastic properties of the polymers at high strain rates. A typical variation of the storage modulus with frequency is presented in Figure 2.6 for a PC-ABS compound, for different temperatures.

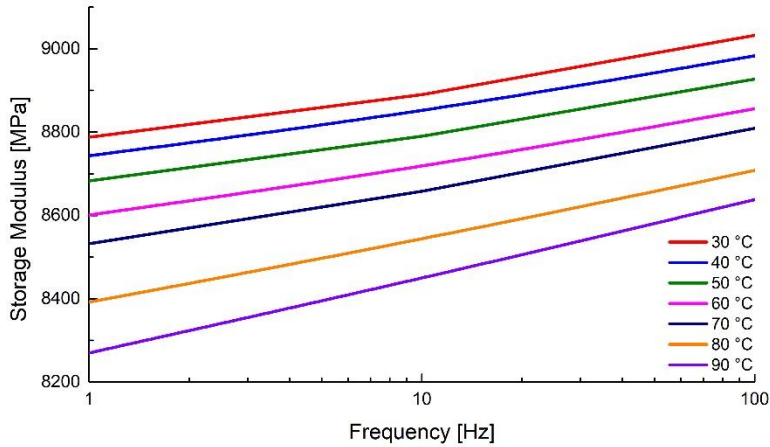


Figure 2.6 Frequency sweep DMA test results for a PC-ABS compound

Cyclic tests at variable strains

The cyclic viscoplasticity of thermoplastic polymers was investigated using repeated tensile loadings at variable strains. Several test protocols were considered, including constant stress increments (stress control, Figure 2.7), constant strain increments (strain control) and several blocks of repeated cycles at equal strain (strain control Figure 2.8) [6].

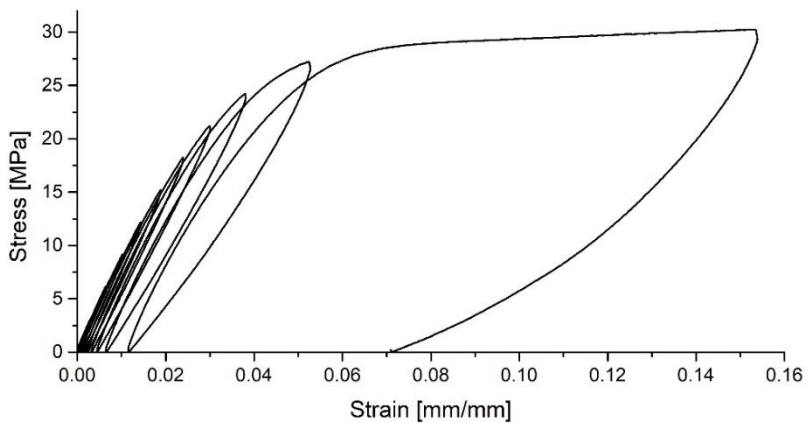


Figure 2.7 Behaviour of a PA compound subjected to cyclic loading at variable strains [7]

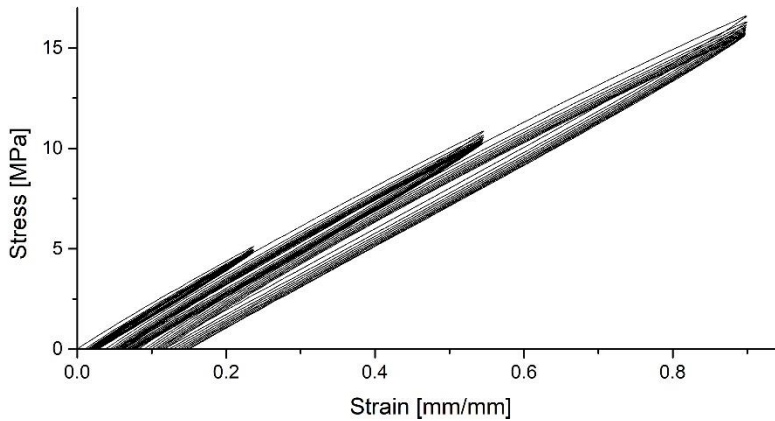


Figure 2.8 Behaviour of a PA compound subjected to several blocks of repeated cycles at equal strain [8]

Results show that remnant deformations occur when unloading from a certain strain, however, unlike metal plasticity, the unloading curve is not linear as some strain recovers instantaneously due to viscous effects.

For the cyclic tests with blocks of repeated cycles at the same strain, a gradual softening is observed, which tends to stabilise after a given number of cycles.

Low-cycle fatigue tests

Low cycle fatigue tests were performed in strain control for $R = 0$ at different frequencies and mean strains (situated in the inelastic region, below the strain corresponding to the tensile strength) [9].

The aim of the tests was to determine the induced softening and to investigate whether the damage was recoverable or permanent. Thus, specimens were tested in tensile loading immediately after the low-cycle fatigue tests were completed and after a recovery time of 24 hours.

During the tests, several loading-unloading cycles were recorded after fixed number of cycles. From the obtained curves, several characteristics were determined, such as stress values, stiffness and dissipated energy.

A variation of the normalized stiffness (stiffness recorded at a given number of cycles divided by the initial stiffness) with the number of cycles is presented in Figure 2.9.

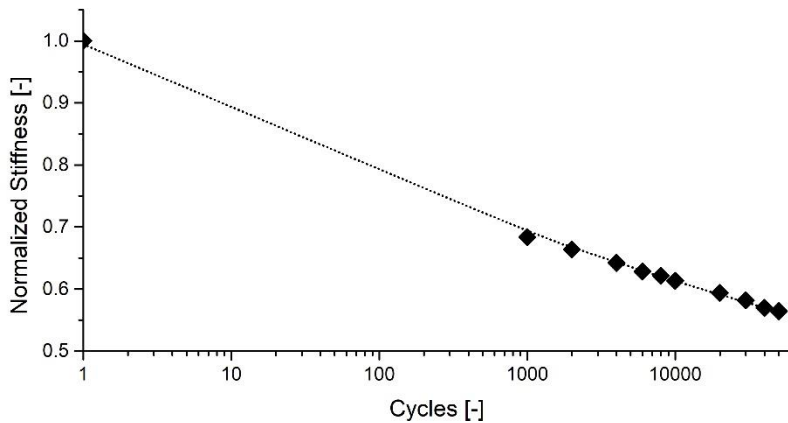


Figure 2.9 Low-cycle fatigue induced softening [9]

The apparent stiffness reduced substantially during the low-cycle fatigue tests due to the drop in the recorded stress. In order to see if the drop in stress is caused by damage to the microstructure or it was caused by stress relaxation, tensile tests were performed immediately after the LCF tests were completed. Results show that the stress-strain response was very similar to that of a previously untested specimen (Figure 2.10), concluding that most of the softening observed was due to the viscous flow of the macromolecules. Furthermore, tests performed after 24 hours of the LCF completion show an even greater degree of similarity to the initial material response, concluding that a part of the observed softening was recovered due to viscous effects.

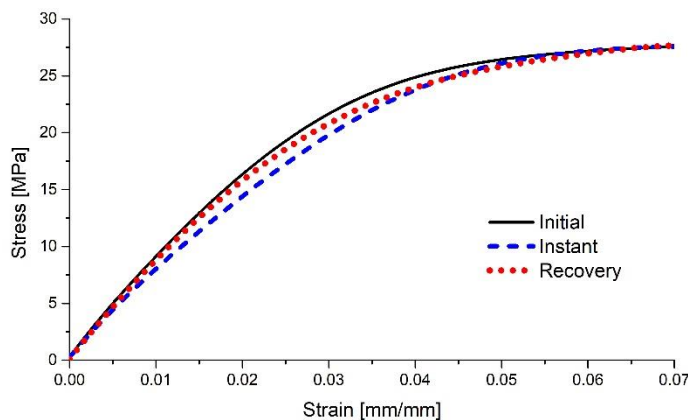


Figure 2.10 Low-cycle fatigue induced softening

2.3. Numerical models

Due to the very large number of applications in which thermoplastic polymers are used, there is a proportionally large number of types of loadings that they can be subjected to. The complex behaviour presented in the previous section is very hard if nearly impossible to model using a universal material model. Thus, several formulations are considered, each having its advantages and disadvantages, and, in consequence, are suitable for specific types of loadings.

This chapter presents three types of constitutive models that the author used in modelling the behaviour of thermoplastic polymers: viscoelastic rheological models, temperature- and rate-dependent plasticity models and viscoplastic models.

2.3.1. Viscoelastic rheological models

Experimental observations which conclude that some materials have both an elastic component and a viscous component of deformation was observed as early as the 19th century, through the work of Ludwig Boltzmann, who coined the term "viscoelasticity" [10]. Based on those observations, James Clerk Maxwell and Sir William Thomson, Lord Kelvin developed the first mathematical models, based on a rheological approach: the elasticity was modeled through a spring while the viscosity was model through a dashpot [10, 11].

The Maxwell fluid

The Maxwell model consists of a spring and a dashpot connected in series (Figure 2.11). The total strain of the model equals the sum of the strains in the elements

$$\varepsilon(t) = \varepsilon_s + \varepsilon_d = \frac{E}{\sigma(t)} + \frac{\sigma(t)}{\mu} t \quad (2.1)$$

and the stress is equal in both elements.

$$\sigma_s = \sigma_d = \sigma \quad (2.2)$$

Thus, the equation of motion of the Maxwell model is

$$\frac{d}{dt} \varepsilon = \frac{1}{E} \cdot \frac{d}{dt} \sigma(t) + \frac{\sigma(t)}{\mu} \quad (2.3)$$



Figure 2.11 The Maxwell rheological model

When subjected to creep, the model determines a linear increase in strain, behaviour similar to that of a fluid, hence the name.

In order to determine the stress variation with strain, Equation (2.3) can be solved for a constant strain rate

$$\varepsilon(t) = tk \quad (2.4)$$

$$\frac{d}{dt} \varepsilon = k \quad (2.5)$$

resulting in the variation of stress with strain after an exponential law.

$$\sigma(\varepsilon) = k\mu \left(1 - e^{-\frac{\varepsilon E}{k\mu}} \right) \quad (2.6)$$

The Kelvin solid

The Kelvin model consists of a spring and a dashpot connected in parallel (Figure 2.12). In this case, the strain is equal in both elements

$$\varepsilon = \varepsilon_s = \varepsilon_d \quad (2.7)$$

while the total stress is the sum of the stresses in an element

$$\sigma(t) = \sigma_s + \sigma_d = \varepsilon(t) \cdot E + \mu \frac{d}{dt} \varepsilon(t) \quad (2.8)$$

When subjected to creep, the model determines a negative exponential increase in strain, reaching an asymptote, behaviour similar to that of a solid.

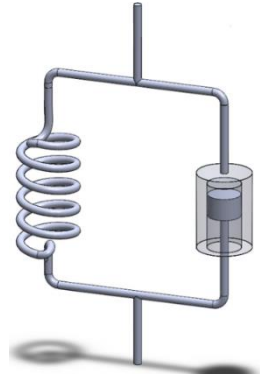


Figure 2.12 The Kelvin rheological model

For a constant strain rate, the stress-strain relation becomes:

$$\sigma(t) = \varepsilon(t) \cdot E + \mu k \quad (2.9)$$

The Zenner model

The Maxwell and Kelvin elements have simple formulations and are not capable of accurately modelling complex material behaviour. To overcome this aspect, several models were developed, linking more elements. Such an example is the Zenner model (sometimes referred to as the Standard Linear Solid), which consists of a Kelvin element linked in series with a spring (Figure 2.13).

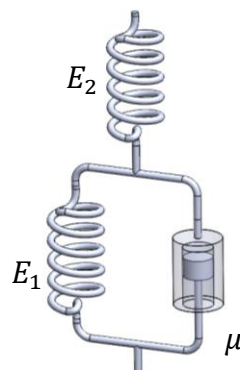


Figure 2.13 The Zenner rheological model

Similar to the Maxwell model, the stress in the elements is equal while the strains add up

$$\sigma(t) = \sigma_1(t) = \sigma_2(t) \quad (2.10)$$

$$\varepsilon(t) = \varepsilon_1(t) + \varepsilon_2(t) \quad (2.11)$$

The stress in the Kelvin element was expressed before and the stress in the spring follows Hooke's law

$$\sigma_1(t) = \varepsilon_1(t) \cdot E_1 + \mu \frac{d}{dt} \varepsilon_1(t) \quad (2.12)$$

$$\sigma_2(t) = \varepsilon_2(t) \cdot E_2 \quad (2.13)$$

From these equations, the strain in each element is derived

$$\varepsilon_1(t) = \frac{\sigma_1(t)}{E_1 + \mu \frac{d}{dt}} \quad (2.14)$$

$$\varepsilon_2(t) = \frac{\sigma(t)}{E_2} \quad (2.15)$$

The dashpot viscosity can be constant (Newtonian viscosity), or non-linear, expressed as a function of strain rate

$$\mu = C \left[\frac{d}{dt} \varepsilon(t) \right]^{n-1} \quad (2.16)$$

After some algebraic manipulations, the constitutive equation of the Zenner model can be shown to have the form

$$\sigma(t) + \frac{\mu \left[\frac{d}{dt} \varepsilon(t) \right]}{E_1 + E_2} \frac{d\sigma(t)}{dt} = \frac{E_1 E_2}{E_1 + E_2} \varepsilon(t) + \frac{\mu \left[\frac{d}{dt} \varepsilon(t) \right] E_2}{E_1 + E_2} \frac{d\varepsilon(t)}{dt} \quad (2.17)$$

For a constant strain rate, Equation (2.17) becomes

$$\sigma(t) + \frac{C k^{n-1}}{E_1 + E_2} \frac{d\sigma(t)}{dt} = \frac{E_1 E_2}{E_1 + E_2} \varepsilon(t) + \frac{C k^{n-1} E_2}{E_1 + E_2} k \quad (2.18)$$

This differential equation can be solved, resulting in the stress variation with strain for the Zenner model at a constant strain rate

$$\sigma(t) = \left[\frac{E_1 E_2}{E_1 + E_2} \varepsilon(t) + \frac{C k^n E_2}{E_1 + E_2} \right] \left[1 - e^{-\frac{\varepsilon(t)(E_1 + E_2)}{C k^n}} \right] \quad (2.19)$$

In Equation (2.19), E_1, E_2, C and n are material constants. An example of the constant fitting for a PA compound for various strain rate values is presented in Figure 2.14.

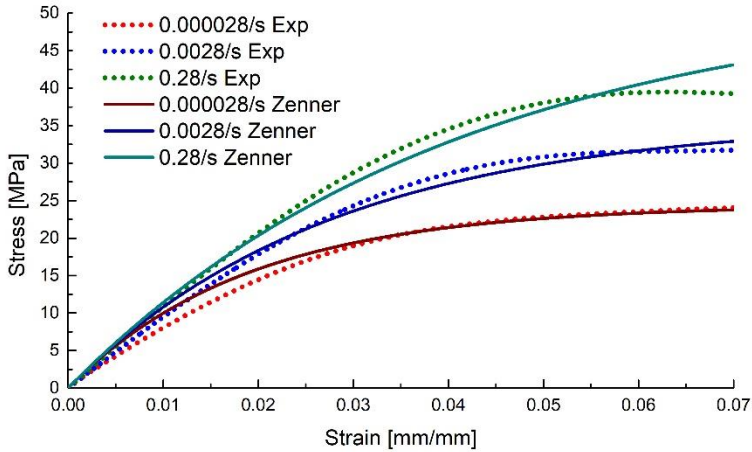


Figure 2.14 Strain rate dependency of the Zener model compared with experimental values

The Wiechert model

The Wiechert model, also referred to as the generalized Maxwell model consists of a series of n Maxwell elements connected in parallel with a free spring (Figure 2.15).

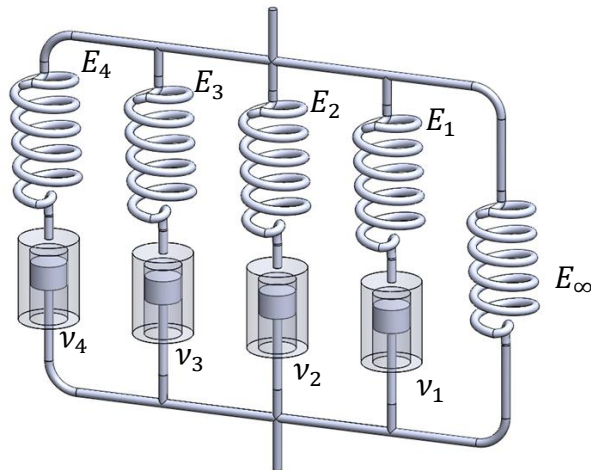


Figure 2.15 The Wiechert rheological model

For this model, the strain is equal for all elements while the total stress is the sum of the stresses in all elements

$$\sigma(t) = \sigma_S(t) + \sigma_{M1}(t) + \sigma_{M2}(t) + \dots + \sigma_{Mn}(t) \quad (2.20)$$

$$\varepsilon(t) = \varepsilon_S(t) = \varepsilon_{M1}(t) = \varepsilon_{M2}(t) = \dots = \varepsilon_{Mn}(t) \quad (2.21)$$

The stress-strain relationship can be written as

$$\sigma(t) = E(t)\varepsilon_0 + \int_0^{t_f} \left[E(t_f - t) \frac{\partial}{\partial t} \varepsilon(t) \right] dt \quad (2.22)$$

where the variation of the stiffness with time is expressed through Prony series [5]

$$E(t) = E_\infty + \sum_{i=1}^n (E_i e^{-t/\tau_i}) \quad (2.23)$$

the relaxation times being defined as

$$\tau_i = \frac{\mu_i}{E_i} \quad (2.24)$$

Considering the strain rate $\frac{\partial}{\partial t} \varepsilon$ can be expressed as

$$\frac{\partial}{\partial t} \varepsilon = \frac{\Delta \varepsilon}{\Delta t} \quad (2.25)$$

an incremental numerical formulation for the constitutive equation can be written [12]:

$$\sigma_{j+1} = \tilde{E} \varepsilon_{j+1} + \sigma_{res} \quad (2.26)$$

where the instantaneous modulus \tilde{E} is

$$\tilde{E} = E_\infty + \sum_{i=1}^n \left[\frac{E_i \tau_i}{\Delta t_{j+1}} \left(1 - e^{-\frac{\Delta t_{j+1}}{\tau_i}} \right) \right] \quad (2.27)$$

and the residual stress σ_{res} is

$$\sigma_{res} = [E(t_{j+1}) - E(t_j)]\varepsilon_0 + \sum_{i=1}^n \left[\left(e^{-\frac{\Delta t_{j+1}}{\tau_i}} - 1 \right) \alpha_i^j \right] \quad (2.28)$$

$$\alpha_i^j = e^{-\frac{\Delta t_{j+1}}{\tau_i}} \alpha_i^j + \frac{E_i \tau_i}{\Delta t_j} \left(1 - e^{-\frac{\Delta t_j}{\tau_i}} \right) \Delta \varepsilon_j \quad (2.29)$$

$$\alpha_i^0 = 0 \quad (2.30)$$

The presented model assumes linear viscosity and thus, the only parameters required for calibration are the long term stiffness (free spring) E_∞ and the stiffness E_i and relaxation times τ_i of the elements. This model was calibrated for the same experimental data as the Zenner model, yielding more accurate results (Figure 2.16).

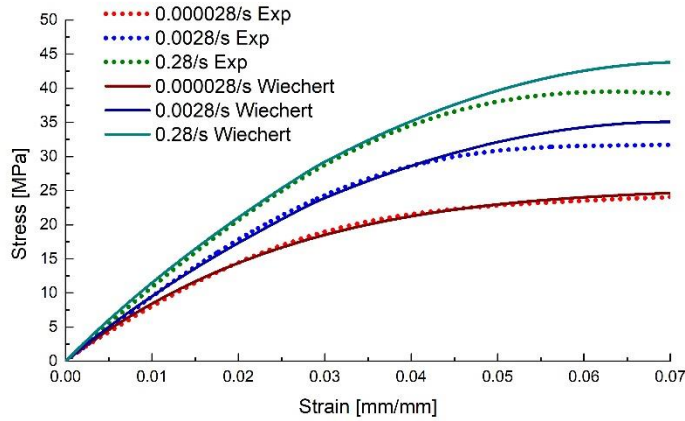


Figure 2.16 Strain rate dependency of the Wiechert model compared with experimental values [13]

Cyclic loadings were also applied to this model, resulting in rather accurate results, presented in Figure 2.17.

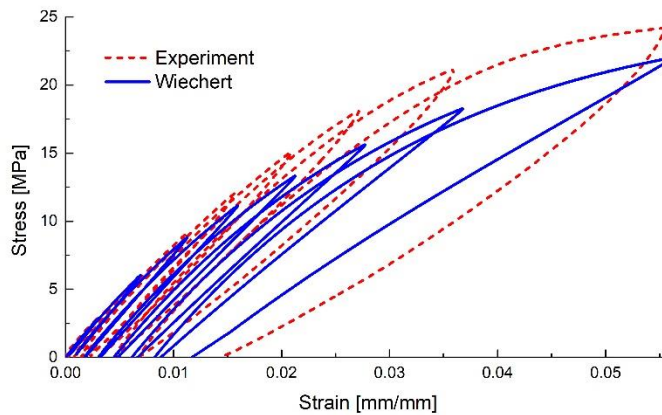


Figure 2.17 Cyclic loading response of the Wiechert model compared with experimental values

Spatial formulation

The implementation of the model in finite element analysis software requires a spatial formulation, accounting for all the components of the stress, strain and stiffness/compliance tensors.

Written in Voigt notation, Equation (2.26) can be expanded for the spatial formulation as

$$\begin{Bmatrix} \sigma_x \\ \sigma_y \\ \sigma_z \\ \tau_{xy} \\ \tau_{yz} \\ \tau_{zx} \end{Bmatrix}_{j+1} = \frac{\tilde{E}}{1-\nu^2} \begin{bmatrix} 1 & \nu & \nu & 0 & 0 & 0 \\ \nu & 1 & \nu & 0 & 0 & 0 \\ \nu & \nu & 1 & 0 & 0 & 0 \\ 0 & 0 & 0 & \frac{1-\nu}{2} & 0 & 0 \\ 0 & 0 & 0 & 0 & \frac{1-\nu}{2} & 0 \\ 0 & 0 & 0 & 0 & 0 & \frac{1-\nu}{2} \end{bmatrix} \begin{Bmatrix} \varepsilon_x \\ \varepsilon_y \\ \varepsilon_z \\ \gamma_{xy} \\ \gamma_{yz} \\ \gamma_{zx} \end{Bmatrix}_{j+1} + \begin{Bmatrix} \sigma_x \\ \sigma_y \\ \sigma_z \\ \tau_{xy} \\ \tau_{yz} \\ \tau_{zx} \end{Bmatrix}_{res} \quad (2.31)$$

where the normalised stiffness matrix is

$$[A] = \frac{1}{1-\nu^2} \begin{bmatrix} 1 & \nu & \nu & 0 & 0 & 0 \\ \nu & 1 & \nu & 0 & 0 & 0 \\ \nu & \nu & 1 & 0 & 0 & 0 \\ 0 & 0 & 0 & \frac{1-\nu}{2} & 0 & 0 \\ 0 & 0 & 0 & 0 & \frac{1-\nu}{2} & 0 \\ 0 & 0 & 0 & 0 & 0 & \frac{1-\nu}{2} \end{bmatrix} \quad (2.32)$$

The equation for the residual stress tensor becomes

$$\begin{Bmatrix} \sigma_x \\ \sigma_y \\ \sigma_z \\ \tau_{xy} \\ \tau_{yz} \\ \tau_{zx} \end{Bmatrix}_{res} = [E(t_{j+1}) - E(t_j)][A] \begin{Bmatrix} \varepsilon_x \\ \varepsilon_y \\ \varepsilon_z \\ \gamma_{xy} \\ \gamma_{yz} \\ \gamma_{zx} \end{Bmatrix}_0 + \sum_{i=1}^n \left[e^{-\frac{\Delta t_{j+1}}{\tau_i}} - 1 \right] \begin{Bmatrix} \alpha_x \\ \alpha_y \\ \alpha_z \\ \alpha_{xy} \\ \alpha_{yz} \\ \alpha_{zx} \end{Bmatrix}_i \quad (2.33)$$

$$\begin{Bmatrix} \alpha_x \\ \alpha_y \\ \alpha_z \\ \alpha_{xy} \\ \alpha_{yz} \\ \alpha_{zx} \end{Bmatrix}_i^j = e^{-\frac{\Delta t_{j+1}}{\tau_i}} \begin{Bmatrix} \alpha_x \\ \alpha_y \\ \alpha_z \\ \alpha_{xy} \\ \alpha_{yz} \\ \alpha_{zx} \end{Bmatrix}_i^{j-1} + \frac{E_i \tau_i}{\Delta t_j} \left(1 - e^{-\frac{\Delta t_j}{\tau_i}} \right) [A] \Delta \begin{Bmatrix} \varepsilon_x \\ \varepsilon_y \\ \varepsilon_z \\ \gamma_{xy} \\ \gamma_{yz} \\ \gamma_{zx} \end{Bmatrix}_j \quad (2.34)$$

$$\begin{Bmatrix} \alpha_x \\ \alpha_y \\ \alpha_z \\ \alpha_{xy} \\ \alpha_{yz} \\ \alpha_{zx} \end{Bmatrix}_i^0 = \begin{Bmatrix} 0 \\ 0 \\ 0 \\ 0 \\ 0 \\ 0 \end{Bmatrix} \quad (2.35)$$

2.3.2. Rate- and temperature-dependent elastic-plastic formulations

Another approach in modelling the non-linearity of thermoplastic polymers is through the use of rate- and temperature-dependent elastic-plastic formulations. Viscoelastic formulations do not explicitly account for temperature dependency and the material parameters must be input individually for each set of temperature data. The parameter values for temperatures different from the input values must therefore be calculated through interpolations, increasing computational time. In contrast, several plasticity models account for temperature dependency (as well as for strain rate dependency) through hardening function parameters integrated in the equation.

In this section, four plasticity models are presented, calibrated and evaluated for tensile tests at different strain rates and temperatures

The Zerilli–Armstrong model

In order to model plasticity, Frank Zerilli and Ronald Armstrong developed a mechanistic model based on dislocation mechanics [14]

$$\sigma = \begin{cases} E\varepsilon, & \sigma \leq \sigma_0^y \\ \sigma_a + B \cdot e^{-\beta T} + B_0 \sqrt{\dot{\varepsilon}^p} \cdot e^{-\alpha T}, & \sigma > \sigma_0^y \end{cases} \quad (2.36)$$

where σ_a is an additional stress dependent on the strain rate and micromechanical characteristics

$$\sigma_a = A + K(\dot{\varepsilon}^p)^n \quad (2.37)$$

while α and β are defined as

$$\alpha = \alpha_0 - \alpha_1 \ln \left(\frac{d}{dt} \varepsilon^p \right) \quad (2.38)$$

$$\beta = \beta_0 - \beta_1 \ln \left(\frac{d}{dt} \varepsilon^p \right) \quad (2.39)$$

This model has 11 constants, namely the Young's modulus E , the yield stress σ_0^y and $A, K, n, B, B_0, \alpha_0, \alpha_1, \beta_0$ and β_1 are material parameters that need to be determined.

For the same experimental data, the calibrated Zerilli-Armstrong model yields the results presented in Figure 2.18 for the strain rate influence and in Figure 2.19 for the temperature influence.

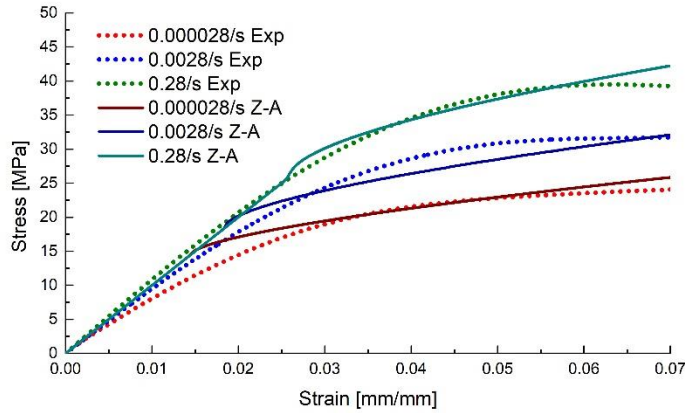


Figure 2.18 Strain rate dependency of the Zerilli-Armstrong model compared with experimental values

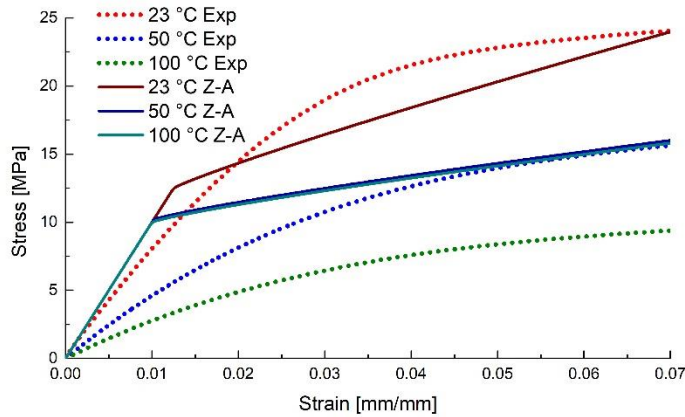


Figure 2.19 Temperature dependency of the Zerilli-Armstrong model compared with experimental values

Due to the interdependence between the strain rate influence and the temperature influence expressed in the model's equation, the Zerilli-Armstrong model is unable to yield accurate results for both cases.

The Johnson-Cook model

The plasticity model developed by Gordon Johnson and William Cook is based on the power law plasticity function, while accounting for the influence of strain rate and temperature [15].

$$\sigma = \begin{cases} E\varepsilon, & \sigma \leq \sigma_0^y \\ [A + B(\varepsilon^p)^n] \left[1 + C \ln\left(\frac{d}{dt} \varepsilon^p\right) \right] [1 - (\tilde{T})^m], & \sigma > \sigma_0^y \end{cases} \quad (2.40)$$

The model assumes normalized values for the strain rate and temperature, referred to a baseline value as

$$\frac{d}{dt} \varepsilon^p = \frac{\frac{d}{dt} \varepsilon^p}{\frac{d}{dt} \varepsilon_0^p} \quad (2.41)$$

where $\frac{d}{dt} \varepsilon^p$ is the current strain rate, $\frac{d}{dt} \varepsilon_0^p$ is the reference strain rate and

$$\tilde{T} = \frac{T - T_0}{T_{melt} - T_0} \quad (2.42)$$

where T is the current temperature, T_0 is the reference temperature and T_{melt} is the melting temperature of the material.

The Johnson-Cook model has 7 parameters: the Young's modulus E , the yield stress σ_0^y and the material constants A, B, n, C and m .

This formulation can model the strain rate effects independent of the temperature effects, which makes it easier to calibrate for both scenarios. The results from the calibrated model are presented in Figure 2.20 for the strain rate influence and in Figure 2.21 for the temperature influence.

Though yielding more accurate results than the Zerilli-Armstrong model, the Johnson-Cook model is still unable to model the high degree of non-linearity of polymers, as well as the strain rate dependent stiffness. For this reason, a new model is proposed.

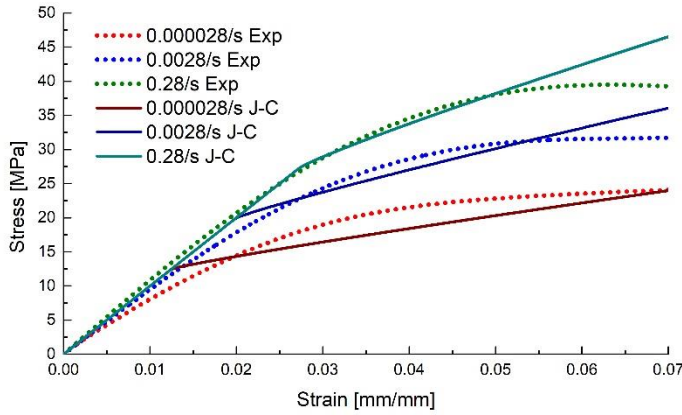


Figure 2.20 Strain rate dependency of the Johnson-Cook model compared with experimental values

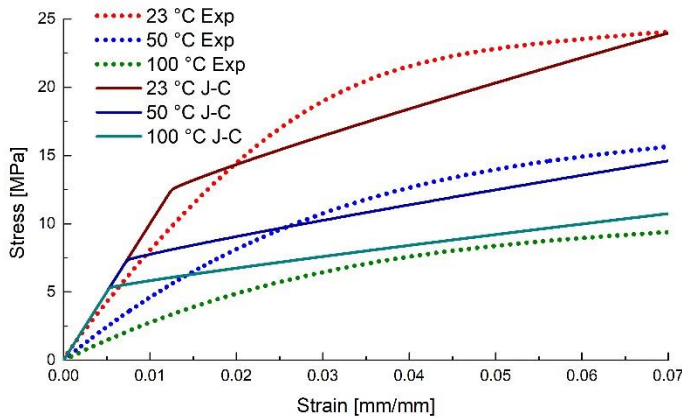


Figure 2.21 Temperature dependency of the Johnson-Cook model compared with experimental values

Modified Johnson-Cook model

The modified Johnson-Cook model is based on the exponential hardening formulation (which results in an asymptotic curve represented by the mechanical strength), as opposed to the power law. Experimental observations yielded that the influence of strain rate and temperature on the stiffness, yield stress and mechanical strength is similar, in the form of a power law. Thus both the linear elastic response and the flow stress will be multiplied by the same factors to account for both dependencies:

$$\sigma = \begin{cases} (E\varepsilon) \left(\frac{d}{dt} \tilde{\varepsilon}^p\right)^n [1 - (\tilde{T})^m], & \sigma < \sigma^y \\ [\sigma_0^y + K \cdot (1 - e^{-\alpha \cdot \varepsilon^p})] \left(\frac{d}{dt} \tilde{\varepsilon}^p\right)^n [1 - (\tilde{T})^m], & \sigma \geq \sigma^y \end{cases} \quad (2.43)$$

$$K = (\sigma_0^{max} - \sigma_0^y) \quad (2.44)$$

This model has 6 parameters: the reference Young’s modulus E , the reference yield stress σ_0^y , the reference mechanical strength σ_0^{max} and the material constants n, m and α .

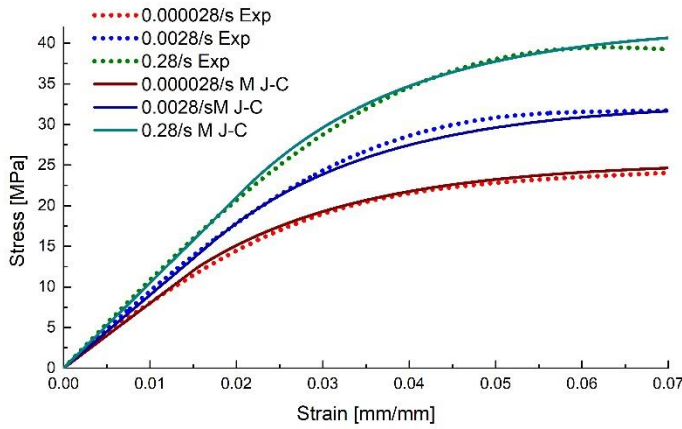


Figure 2.22 Strain rate dependency of the Modified Johnson-Cook model compared with experimental values

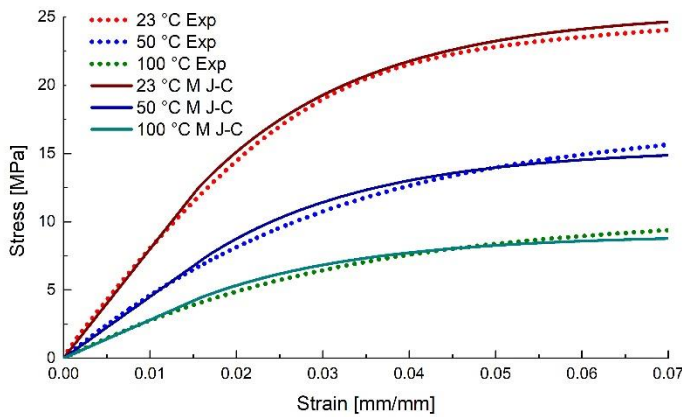


Figure 2.23 Strain rate dependency of the Modified Johnson-Cook model compared with experimental values

The results for the calibrated model are presented in Figure 2.22 for the strain rate influence and in Figure 2.23 for the temperature influence.

It can be observed that this model yields accurate results when accounting for both strain rate and temperature effects. When subjected to cyclic loadings, the model overestimates the remnant plastic deformation, as it cannot account for the material recovery (Figure 2.24).

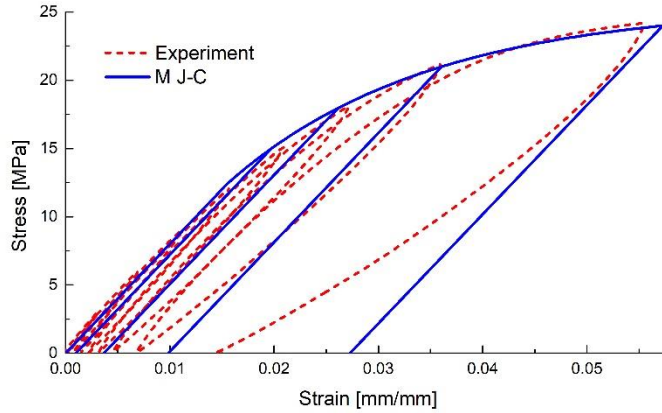


Figure 2.24 Cyclic loading response of the Johnson-Cook model compared with experimental values

Multi-linear hardening model

The multi-linear hardening model consists of a series of n elastic-plastic networks (Saint-Venant elements) connected in parallel with a spring (Figure 2.25). Usually, the limit strain ε_i^p of the friction elements are arranged in ascending order ($\varepsilon_1^p < \varepsilon_2^p < \dots < \varepsilon_n^p$). Consequently, a stress value of σ_j situated between σ_j^y and σ_{j+1}^y can be evaluated with the relation

$$\sigma_j = \begin{cases} \sum_{i=1}^n E_i \varepsilon, & \sigma < \sigma_1^y \\ \sum_{i=1}^j \sigma_i^y + \sum_{i=j+1}^n E_i \varepsilon, & \sigma \geq \sigma_1^y \end{cases} \quad (2.45)$$

The resulting hardening curve will consist of straight lines of varying slopes that connect the yield stress values corresponding the Saint-Venant elements.

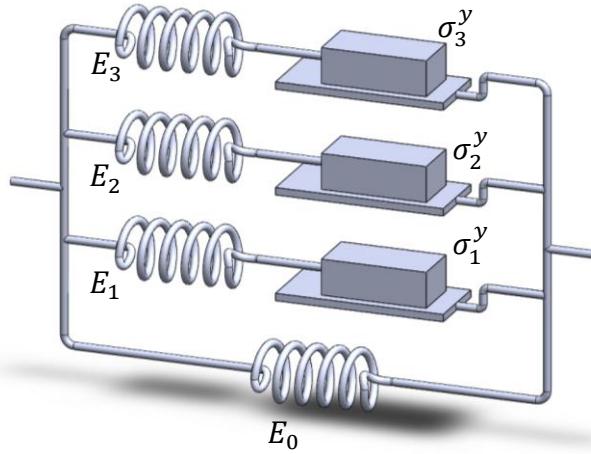


Figure 2.25 Rheological model of the multi-linear hardening model

This model can include a large number of elements in order to determine accurate results. In order to overcome this issue, the material hardening can be expressed through a curve that describes the yield stress variation with plastic strain, plastic strain rate and temperature

$$\sigma_j = \begin{cases} E\varepsilon & \sigma < \sigma_0^y \\ \sigma_0^y + f\left(\varepsilon^p, \frac{d}{dt}\varepsilon^p, T\right) & \sigma \geq \sigma_0^y \end{cases} \quad (2.46)$$

For a given total strain, the plastic strain and the yield stress are evaluated and if the values fall between the input data, linear interpolations are performed.

The most facile way to calibrate this model is to choose reference plastic strain values and generate lines with the slope equal to Young's modulus that pass through the chosen points. The corresponding yield stresses are obtained through the intersection of the lines with the stress-strain curve [2].

As with other plasticity models, the linear elastic region is not strain rate dependent. To overcome this issue, one can set the Young's modulus equal to the value determined by the tests performed at the highest strain rate and set the initial yield stress very low. Thus, only a very small region will have linear elastic deformations as the material softening occurs very early (similar to the experimental observations)

An example for such hardening curves is presented in Figure 2.26 for the same experimental data showcased throughout this section.

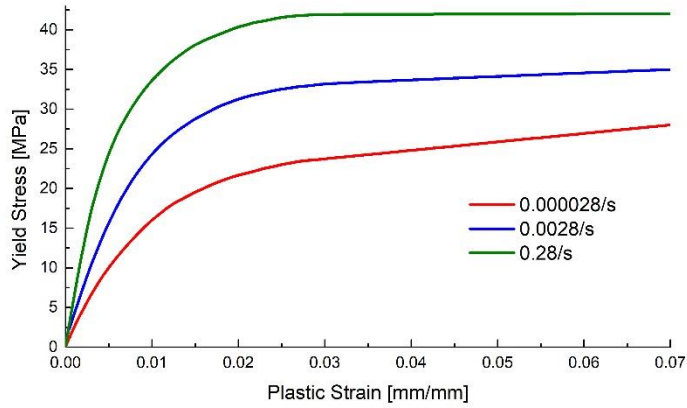


Figure 2.26 Yield stress-plastic strain hardening curves for various strain rates

Numerical analyses performed with this material model showed excellent correlation with the experimental data for both strain rate (Figure 2.27) and temperature influence (Figure 2.28).

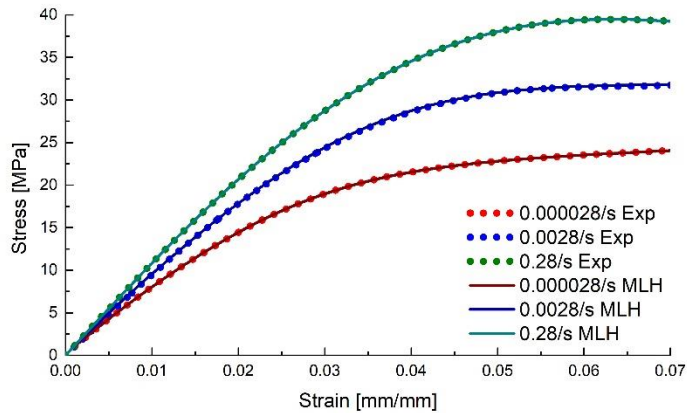


Figure 2.27 Strain rate dependency of the multi-linear hardening model compared with experimental values

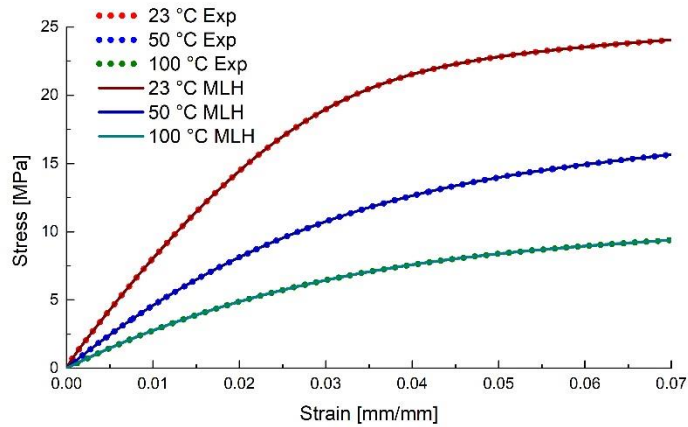


Figure 2.28 Strain rate dependency of the of the multi-linear hardening model compared with experimental values

The behaviour of the multi-linear hardening model subjected to cyclic loadings is presented in Figure 2.29, yielding similar results to the modified Johnson-Cook model.

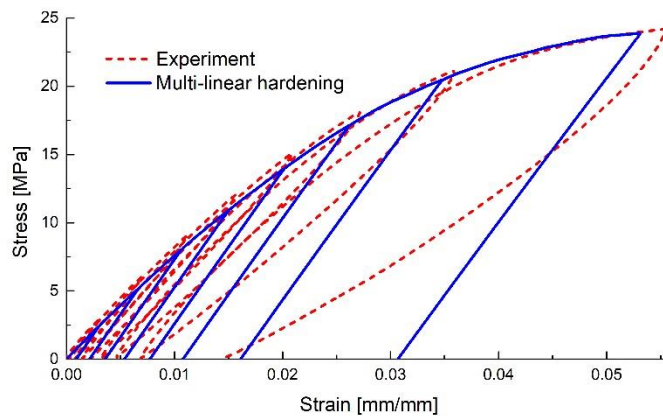


Figure 2.29 Cyclic loading response of the multi-linear hardening model compared with experimental values

Spatial formulations

During service, polymers are rarely subjected only to uniaxial loadings. In the case of multiaxial loadings, the yielding of materials is usually evaluated with various relations of equivalent stresses, based on several yielding hypotheses.

Classical metal plasticity assumes that the yield surface of a material is dependent on the second invariant of the deviatoric stress tensor [16]

$$J_2 = \frac{1}{2} \sum_{i,j=1}^3 (\sigma'_{ii}\sigma'_{jj} - \sigma'_{ij}\sigma'_{ji}) \quad (2.47)$$

The most commonly used yield criterion was formulated by Richard von Mises, who defined the yield surface as

$$\sqrt{3J_2} - \sigma^y = 0 \quad (2.48)$$

where σ^y represents the yield stress of the material in uniaxial tension.

Thus hypothesis assumes that the material is isotropic and the yield strength in tension is equal to the yield stress in compression. For plane stress loadings, the von Mises yield surface becomes an ellipse in the principal stress plane (Figure 2.30). The hardening of the material is evaluated in terms of equivalent stresses (Equation (2.48)) and strains

$$\tilde{\epsilon} = \sqrt{\frac{2}{3} \boldsymbol{\epsilon}^{dev} : \boldsymbol{\epsilon}^{dev}} \quad (2.49)$$

where $\boldsymbol{\epsilon}^{dev}$ is the deviatoric component of the strain tensor $\boldsymbol{\epsilon}$

$$\boldsymbol{\epsilon}^{dev} = \boldsymbol{\epsilon} - tr(\boldsymbol{\epsilon})\mathbf{I} \quad (2.50)$$

A particularity of some polymeric materials is that they exhibit different properties in tension and compression [17]. In order to model this behaviour, the influence of the first invariant of the stress tensor

$$I_1 = tr(\boldsymbol{\sigma}) = \sum_{i=1}^3 \sigma_{ii} \quad (2.51)$$

is accounted for in models such as the Drucker-Prager criterion,

$$\sqrt{J_2} = A + BI_1 \quad (2.52)$$

where A and B are material constants dependent on the yield stress in tension and compression [18]. The sign of the first invariant of the stress tensor I_1 denotes whether the body is subjected mainly to tensile loadings (positive sign) or compressive loadings (negative sign).

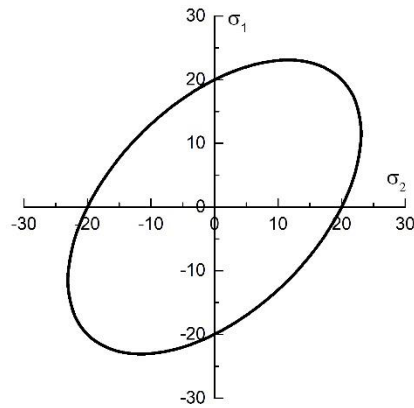


Figure 2.30 Von Mises yield surface in plane stress

The shape of the Drucker-Prager yield function in the principal stress plane is presented in Figure 2.31 for plane stress.

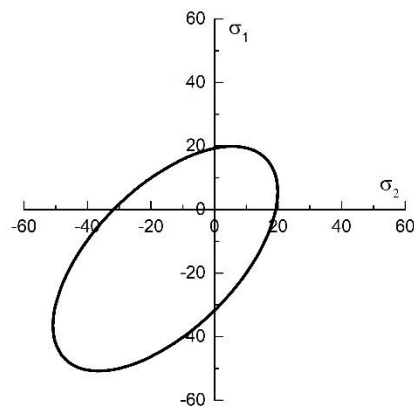


Figure 2.31 Drucker-Prager yield surface in plane stress

An example of the variation in tensile and compressive behaviour modelled using the Drucker-Prager model is presented in Figure 2.32.

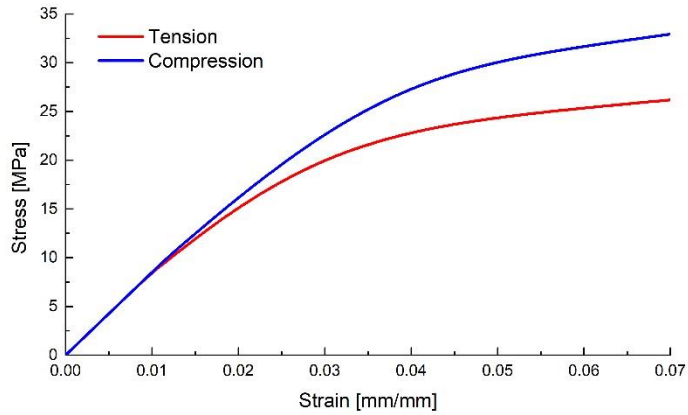


Figure 2.32 Tensile and compressive response modelled using the Drucker-Prager model

Due to the manufacturing process, polymeric parts may exhibit anisotropy due to residual stresses, as seen in Figure 2.33 [19].

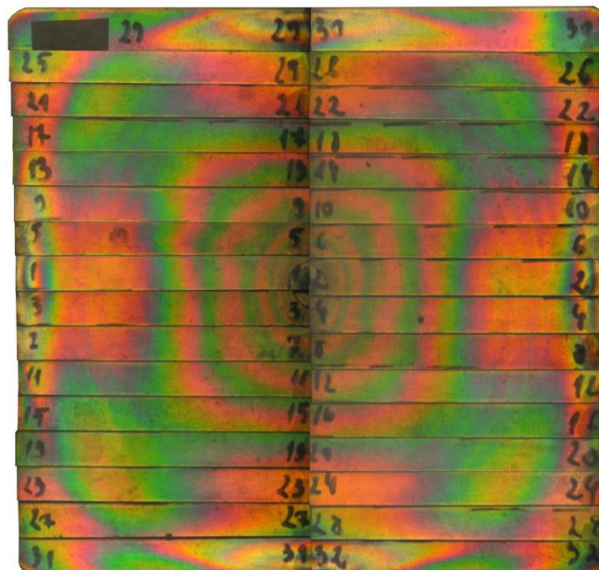


Figure 2.33 Residual stress in injected PA plate [19]

A commonly used criterion for modelling anisotropic plasticity was described by Rodney Hill and is expressed as [20]

$$F(\sigma_{yy} - \sigma_{zz})^2 + G(\sigma_{zz} - \sigma_{xx})^2 + H(\sigma_{xx} - \sigma_{yy})^2 + 2L\tau_{yz}^2 + 2M\tau_{zx}^2 + 2N\tau_{xy}^2 = 1 \quad (2.53)$$

where the material parameters are defined as

$$\begin{aligned} F &= \frac{1}{2} \left[\frac{1}{(\sigma_2^y)^2} + \frac{1}{(\sigma_3^y)^2} - \frac{1}{(\sigma_1^y)^2} \right]; & L &= \frac{1}{2(\tau_{23}^y)^2}; \\ G &= \frac{1}{2} \left[\frac{1}{(\sigma_3^y)^2} + \frac{1}{(\sigma_1^y)^2} - \frac{1}{(\sigma_2^y)^2} \right]; & M &= \frac{1}{2(\tau_{31}^y)^2}; \\ H &= \frac{1}{2} \left[\frac{1}{(\sigma_1^y)^2} + \frac{1}{(\sigma_2^y)^2} - \frac{1}{(\sigma_3^y)^2} \right]; & N &= \frac{1}{2(\tau_{12}^y)^2}; \end{aligned} \quad (2.54)$$

A generalized form of the Hill criterion borrows elements from the Hosford model [21] and is expressed as a function of principal stresses as

$$F(\sigma_2 - \sigma_1)^m + G(\sigma_3 - \sigma_1)^m + H(\sigma_1 - \sigma_2)^m + L(2\sigma_1 - \sigma_2 - \sigma_3)^m + M(2\sigma_2 - \sigma_3 - \sigma_1)^m + N(2\sigma_3 - \sigma_1 - \sigma_2)^m = \sigma_y^m \quad (2.55)$$

The Hill yield surface in 2D principal stress space is exemplified in Figure 2.34.

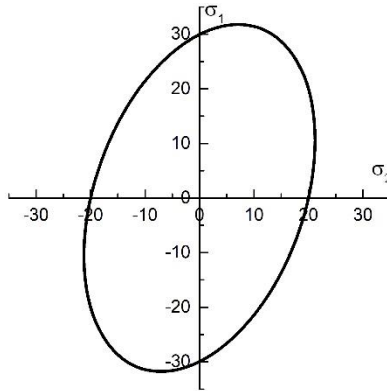


Figure 2.34 Hill yield surface in plane stress

Specimens cut from the PA plate presented in Figure 2.33 were subjected to three-point bending tests and a difference in stiffness and strength was observed for specimens situated parallel and perpendicular to the injection direction. Numerical analyses were performed with the calibrated Hill model resulting in accurate responses (Figure 2.35).

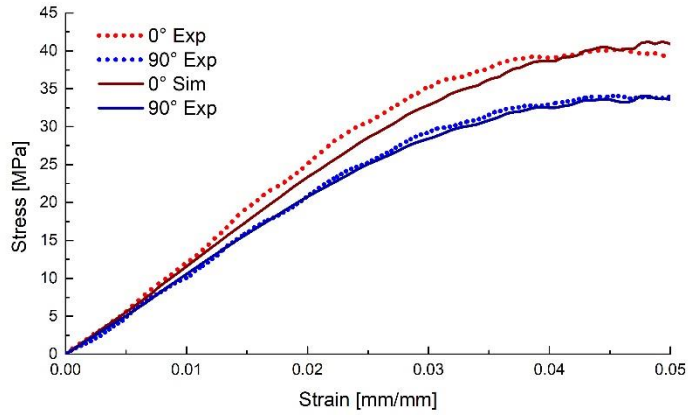


Figure 2.35 Flexural results for experiments and simulations for a PA compound at different orientations

2.3.3. Viscoplastic formulations

As their name implies, viscoplastic models include both viscous and plastic elements. Throughout the years, a number of models were developed, starting from simple rheological models to more complex formulations that cannot determine explicit stress-strain relationships and can only be numerically evaluated through incremental procedures (i.e. the backward Euler integration method) [22].

The Bingham-Maxwell model

One of the first viscoplastic models was based on the Maxwell fluid but incorporated a viscoplastic element, as described by Eugene C. Bingham [23].

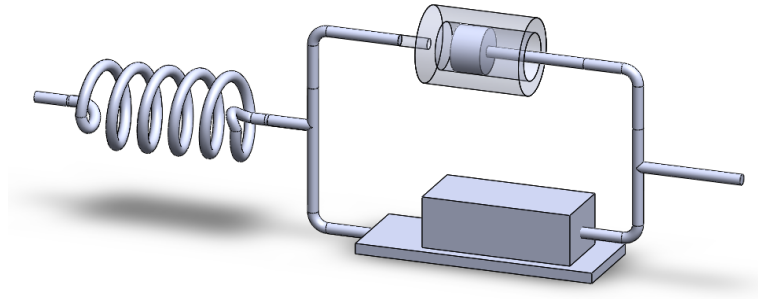


Figure 2.36 Bingham-Norton rheological model

As with the Maxwell model, the stress is equal in both elements while the total strain is the summation of the strains in each element. The constitutive equation of the spring is that of a linear elastic material

$$\sigma(t) = E\varepsilon(t) \quad (2.56)$$

The friction block of the rheological model assumes plasticity with a hardening function $f(\varepsilon^{vp})$, so that the viscoplastic strain ε^{vp} is 0 for stress values below the yield point. For stress values above the yield point, the viscoplastic strain is evaluated with the relation

$$\varepsilon^{vp}(t) = \begin{cases} 0, & \sigma < \sigma^y \\ \frac{\sigma(t)}{\mu} t - [\sigma^y + f(\varepsilon^{vp})]t, & \sigma \geq \sigma^y \end{cases} \quad (2.57)$$

Thus, the total strain is

$$\varepsilon(t) = \varepsilon^{el}(t) + \varepsilon^{vp}(t) = \frac{\sigma(t)}{E} + \frac{\sigma(t)}{\mu(\sigma)} \left[1 - \frac{\sigma^y + f(\varepsilon^{vp})}{\sigma(t)} \right] t \quad (2.58)$$

The time variation is eliminated through derivation, yielding

$$\frac{d}{dt} \varepsilon(t) = \frac{1}{E} \frac{d}{dt} \sigma(t) + \frac{\sigma(t)}{\mu(\sigma)} \left[1 - \frac{\sigma^y + f(\varepsilon^{vp})}{\sigma(t)} \right] \quad (2.59)$$

After some algebraic manipulation, the constitutive relation becomes

$$\sigma(t) = [k\mu(\sigma) + \sigma^y + f(\varepsilon^{vp})] \left(1 - e^{-\frac{\varepsilon E}{k\mu}} \right) \quad (2.60)$$

The results for the calibrated model, compared to the experimental results is presented in Figure 2.37.

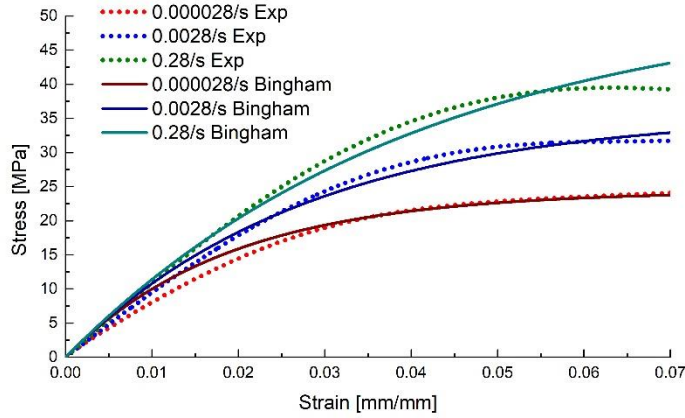


Figure 2.37 Strain rate dependency of the two-layer viscoplastic model compared with experimental values

Two-layer viscoplastic model

A more complex formulation, called the two-layer viscoplastic model, is composed of an elastic-plastic model connected in parallel with a Maxwell model (Figure 2.38).

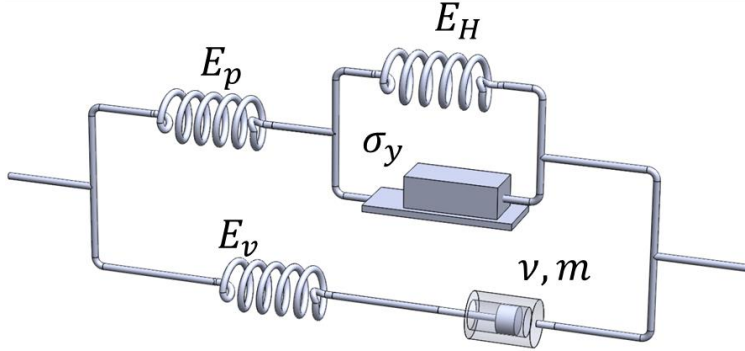


Figure 2.38 Two-layer viscoplastic rheological model

In this case, the stress of the model equals the sum of the stresses from both elements while the strain is equal. For stress values below the yield point, the constitutive relation equals the sum of the stiffness of the two springs multiplied by the strain of the model. After, yielding, the stress can be evaluated with the relation

$$\sigma = \begin{cases} (E_p + E_v) \cdot \varepsilon, & \sigma < \sigma^y \\ \sigma^y \left(1 + \frac{E_p}{\sigma^y} \varepsilon^{pl}\right)^n + \nu^{-\frac{1}{m}} \frac{1}{\dot{\varepsilon}^m}, & \sigma \geq \sigma^y \end{cases} \quad (2.61)$$

where

$$\dot{\varepsilon} = \frac{d}{dt} \varepsilon \quad (2.62)$$

is the strain rate. The elastic strain can be expressed as:

$$\varepsilon^{el} = \frac{E_v}{E_v + E_p} \varepsilon_v^{el} + \left(1 - \frac{E_v}{E_v + E_p}\right) \varepsilon_p^{el} \quad (2.63)$$

and the total strain

$$\varepsilon^{tot} = \frac{E_v}{E_v + E_p} (\varepsilon_v^{el} + \varepsilon_v^v) + \left(1 - \frac{E_v}{E_v + E_p}\right) (\varepsilon_p^{el} + \varepsilon_p^{pl}) \quad (2.64)$$

The numerical results for the calibrated model are presented in Figure 2.39 along with the experimental data.

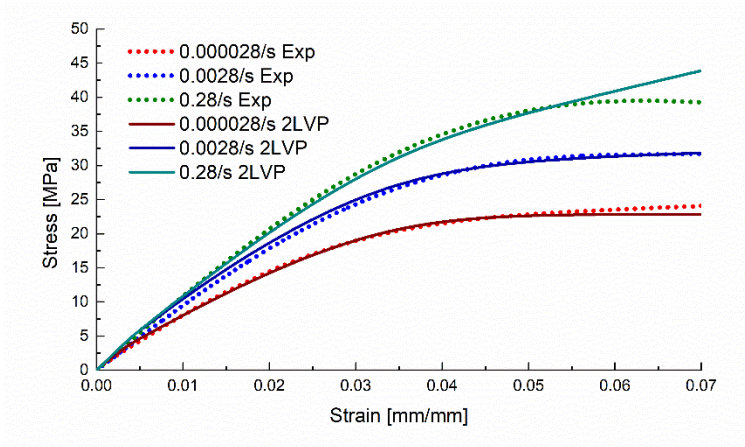


Figure 2.39 Strain rate dependency of the two-layer viscoplastic model compared with experimental values

The simulation results for the cyclic loading is presented in Figure 2.40.

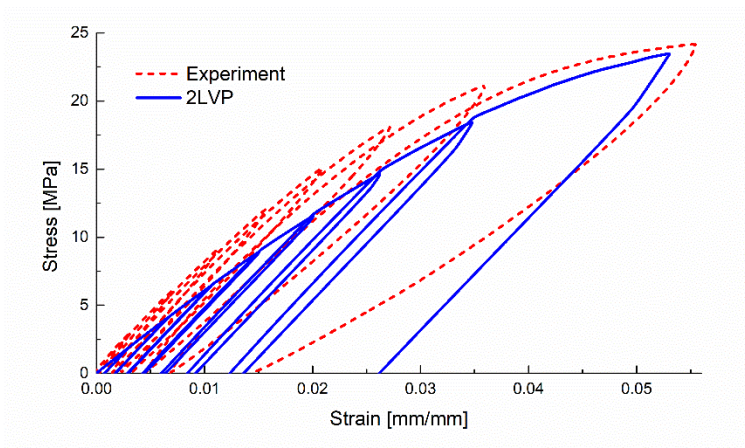


Figure 2.40 Strain rate dependency of the two-layer viscoplastic model compared with experimental values

2.4. Conclusions

The experimental procedures performed showed that thermoplastic polymers have a very wide range of variation in mechanical properties due to their composition. The temperature and strain rate can significantly alter their characteristic, so that the same polymer can have a ductile behaviour at relative high temperatures and low strain rates and a brittle behaviour at relatively low temperatures and high strain rates.

Consequently, a material model that can universally predict the mechanical behaviour of a polymeric compound is very hard to achieve and would require a great number of parameters to calibrate.

Thus, it is recommended to develop material models specific for each type of application. For cyclic loadings at small strains (where the polymer can still be considered to be in the elastic domain, with no plastic deformations), viscoelastic models can yield very good results. Finite element analysis software have several viscoelastic material models implemented in their code (the most common being the generalized Maxwell/Kelvin model), which can be tuned to determine acceptable results [13].

For monotone loadings, the recommended approach is the calibration of elastic-plastic formulations than can incorporate strain rate and temperature dependency. The multi-linear isotropic hardening model is a good contender, as it can predict the stress-strain relationship of polymers in a very accurate manner. This model requires a relatively large number of material parameters, but their determination is facile and it can be automatically generated from experimental data with relative ease [2].

In the case of cyclic loadings at high strains, the only models that can determine accurate responses are the visco-plastic formulations. Their calibration represents a serious challenge and it often requires several calibration iterations [24].

3. Damage and failure of polymers

3.1. Introduction

The previous chapter dealt mostly with uniaxial loadings that are characteristic in defining constitutive laws. The multiaxial response of the investigated material was evaluated using various equivalent stress formulations and yield criteria, briefly discussed in Chapter 2.

In this section, an in-depth look into the multiaxial yielding, damage and failure of materials is presented. In recent years, investigations into the plasticity and damage of ductile metals showed that their behaviour is dependent on three tensor invariants [25, 26, 27]. This aspect is more evident in the case of damage, as varying stress states determine significant differences in failure (i.e. tension versus compression or shear).

Two damage models will be presented (ductile damage model and shear damage model), both expressing critical plastic strain as a function of various parameters based on principal stresses and stress invariants.

The calibration of the damage models requires an extensive experimental plan, with a large number of specimen types [25, 26]. This aspect is relatively easy to achieve for metals, as almost all the required geometries can be obtained through machining. For polymers however, this approach presents a challenge, as the heat generated through machining often times influences the properties of the base materials, and thus the results can get skewed. In addition, the availability of polymeric samples and specimens is directly tied to the manufacturer, as most of the compounds used today are proprietary blends.

A first step in understanding the polymers' behaviour in controlled stress states was to manufacture the desired geometries through rapid prototyping. Though the properties differ substantially from their injected counterparts, this approach is meant to provide an insight and to validate the method.

3.2. Spatial state of stress

3.2.1. Tensor invariants

The modelling of plasticity, damage and failure is based on continuum mechanics approaches and, in consequence, the formulations will be based on the Cauchy (true) stress tensor $\boldsymbol{\sigma}$.

$$\boldsymbol{\sigma} = \begin{pmatrix} \sigma_x & \tau_{xy} & \tau_{xz} \\ \tau_{yx} & \sigma_y & \tau_{yz} \\ \tau_{zx} & \tau_{zy} & \sigma_z \end{pmatrix} \quad (3.1)$$

The spatial state of stress can also be expressed in terms of principal stresses, which represent the extreme values the stresses can reach at a given stress state as a consequence of coordinate transformation. The principal stresses represent the eigenvalues of the stress tensor and are evaluated with the relation

$$(\sigma_i)^3 + I_1^\sigma (\sigma_i)^2 + I_2^\sigma (\sigma_i) + I_3^\sigma = 0 \quad (3.2)$$

where I_1^σ , I_2^σ and I_3^σ are the tensor invariants.

$$I_1^\sigma = \text{tr}(\boldsymbol{\sigma}) = \sum_{i=1}^3 \sigma_{ii} \quad (3.3)$$

$$I_2^\sigma = \frac{1}{2} \sum_{i,j=1}^3 (\sigma_{ii}\sigma_{jj} - \sigma_{ij}\sigma_{ji}) \quad (3.4)$$

$$I_3^\sigma = \det(\boldsymbol{\sigma}) \quad (3.5)$$

The Cauchy stress tensor can be decomposed into a deviatoric component $\boldsymbol{\sigma}'$ (describing the change in shape of the volume element) and a hydrostatic component σ_{Hyd} (a scalar quantity accounting for the change in volume).

$$\boldsymbol{\sigma} = \boldsymbol{\sigma}' + \sigma_{Hyd} \mathbf{I} \quad (3.6)$$

$$\sigma_{Hyd} = \frac{1}{3} I_1^\sigma = \frac{1}{3} \text{tr}(\boldsymbol{\sigma}) = \frac{1}{3} (\sigma_1 + \sigma_2 + \sigma_3) \quad (3.7)$$

As most plasticity formulations are based (at least in part) on the deviatoric stress tensor, it is worthwhile to mention its invariants (expressed in terms of the principal deviatoric stresses). The first invariant, which represents the sum of the principal deviatoric stresses can be shown to be equal to 0.

$$J_1^\sigma = \text{tr}(\boldsymbol{\sigma}') = \sigma'_1 + \sigma'_2 + \sigma'_3 = 0 \quad (3.8)$$

The second invariant is expressed as

$$J_2^\sigma = \frac{1}{2} \sum_{i,j=1}^3 (\sigma'_i \sigma'_j - \sigma'_j \sigma'_i) = \frac{1}{2} [(\sigma'_1)^2 + (\sigma'_2)^2 + (\sigma'_3)^2] \quad (3.9)$$

In terms of the principal stresses, the second invariant of the deviatoric stress is

$$J_2^\sigma = \frac{1}{6} [(\sigma_1 - \sigma_2)^2 + (\sigma_2 - \sigma_3)^2 + (\sigma_3 - \sigma_1)^2] \quad (3.10)$$

The third invariant of the deviatoric stress is the determinant of the tensor

$$J_3^\sigma = \det(\boldsymbol{\sigma}') = \sigma'_1 \sigma'_2 \sigma'_3 \quad (3.11)$$

In terms of the principal stresses, the third invariant of the deviatoric stress is

$$J_3^\sigma = \frac{1}{27} (2\sigma_1 - \sigma_2 - \sigma_3)(2\sigma_2 - \sigma_1 - \sigma_3)(2\sigma_3 - \sigma_1 - \sigma_2) \quad (3.12)$$

3.2.2. Haigh-Westergaard stress space

In order to gain more insight into the multiaxial behaviour of materials, the spatial state of stress can be expressed in different coordinates. Apart from the principal stress space, the most common used frames of reference are the Haigh-Westergaard stress space and the meridional profile [16].

The Haigh-Westergaard stress space is a cylindrical frame of reference defined by the coordinates ζ , ρ and Θ . The axis of the cylinder can be chosen to be the hydrostatic axis ($\sigma_1 = \sigma_2 = \sigma_3$), and the axial coordinate ξ represents the orthogonal projection of the stress onto the axis. The radial coordinate ρ is the magnitude of the stress deviator, and the angular coordinate is called the Lode angle, it represents the angle between the projection of the principal stress and the segment corresponding to the given stress state. Their mathematical expressions are [16]:

$$\begin{cases} \xi = \frac{I_1^\sigma}{\sqrt{3}} = \sqrt{3}\sigma_{Hyd} \\ \rho = \sqrt{2J_2} \\ \theta = \arccos\left(\frac{3}{2}\sqrt{3}\frac{J_3}{J_2^{\frac{3}{2}}}\right) \end{cases} \quad (3.13)$$

By maintaining a constant axial coordinate, the Haigh-Westergaard stress space is reduced to a 2D space with a polar coordinate system, called the deviatoric plane or the octahedral stress plane (Figure 3.1).

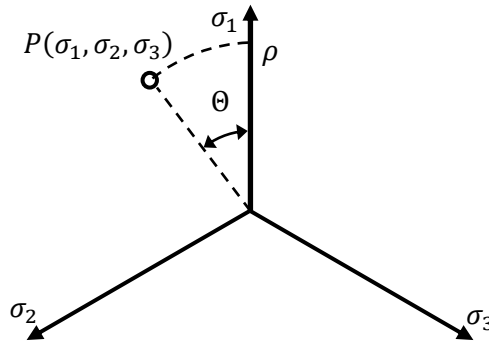


Figure 3.1 Stress state representation in the octahedral stress space

The principal stresses can be expressed in the Haigh-Westergaard coordinate system as

$$\begin{bmatrix} \sigma_1 \\ \sigma_2 \\ \sigma_3 \end{bmatrix} = \frac{1}{\sqrt{3}} \begin{bmatrix} \xi \\ \xi \\ \xi \end{bmatrix} + \sqrt{\frac{2}{3}} \rho \begin{bmatrix} \cos \theta \\ \cos\left(\frac{2\pi}{3} - \theta\right) \\ \cos\left(\frac{2\pi}{3} + \theta\right) \end{bmatrix} \quad (3.14)$$

while the principal deviator stress as

$$\begin{bmatrix} \sigma'_1 \\ \sigma'_2 \\ \sigma'_3 \end{bmatrix} = \frac{2}{\sqrt{3}} \sqrt{J_2} \begin{bmatrix} \cos \theta \\ \cos\left(\frac{2\pi}{3} - \theta\right) \\ \cos\left(\frac{2\pi}{3} + \theta\right) \end{bmatrix} \quad (3.15)$$

Another way to define the Haigh-Westergaard stress space is by using scaled coordinates: the axial coordinate is the measure of the hydrostatic stress, the radial coordinate is the Von Mises equivalent stress and the radial coordinate is transformed into an a-dimensional parameter called the Lode angle parameter.

$$\begin{cases} p = \frac{I_1^\sigma}{3} = \sigma_{Hyd} \\ q = \sqrt{3J_2} = \sigma_{Mises} \\ \xi = \frac{\left[\frac{r}{q}\right]^3}{\frac{3}{2}\sqrt{3}\frac{J_3}{J_2^{\frac{3}{2}}}} \in [-1,1] \end{cases} \quad (3.16)$$

where r is a third invariant dependent equivalent stress (also measured in MPa) defined as

$$r = \left[\frac{27}{2}J_3\right]^{\frac{1}{3}} = \left[\frac{1}{2}(2\sigma_1 - \sigma_2 - \sigma_3)(2\sigma_2 - \sigma_1 - \sigma_3)(2\sigma_3 - \sigma_1 - \sigma_2)\right]^{\frac{1}{3}} \quad (3.17)$$

3.3. Basis for damage onset in ductile materials

This section will briefly present the most common constitutive models used in simulating the damage of ductile materials, namely the ductile damage model and the shear damage model.

The first ductile damage model was proposed by Percy Williams Bridgman in his 1952 book “Studies in large plastic flow and fracture – with special emphasis on the effects of hydrostatic pressure”, where he hypothesised that the damage onset is dependent on the strain rate and the triaxial state of stress [28]. He used analytical methods in approximating the triaxial state of stress for various notches and assigned a failure strain for each stress state. The concept behind this approach is that, at the onset of damage, the local strain increases drastically when compared to the global strain of the body (Figure 3.2).

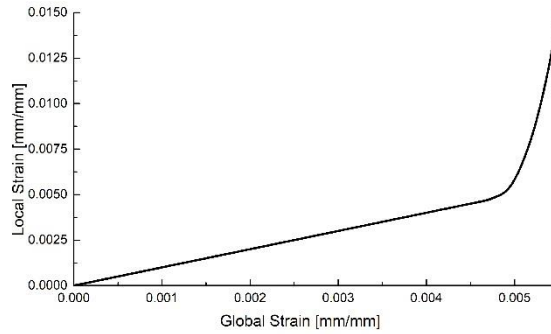


Figure 3.2 Local strain variation with global strain according to the ductile damage hypothesis

These models introduce a damage initiation criterion ω and when the conditions are satisfied ($\omega = 1$), the effective stress $\bar{\sigma}$ will be diminished through a damage evolution parameter D :

$$\sigma = (1 - D)\bar{\sigma} \quad (3.18)$$

The damage evolution parameter D can be defined as a function of the dissipated energy ψ or of the plastic displacement d [29]. The function varies from 0 to 1, at which value the stress tensor becomes null and the material is considered to have failed (Figure 3.3).

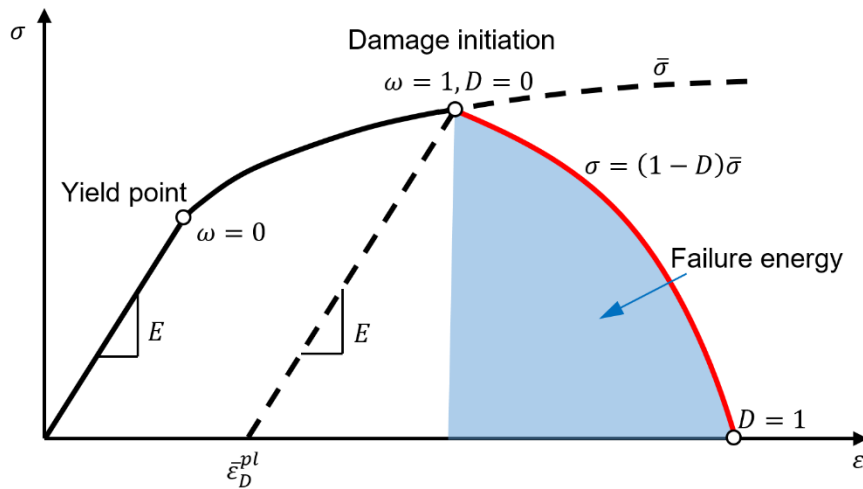


Figure 3.3 Damage evolution model

In the present day, finite element analysis software are able to predict the invariants of the stress tensor with more accuracy, thus becoming an essential tool in determining the damage parameters for the numerical models.

3.3.1. The ductile damage model

The ductile damage model assumes an initiation criterion based on the nucleation of voids during straining (damage onset) and an increase in volume of the voids (damage evolution) that leads to failure. Though initially developed for metals, the failure mechanism of some polymers proves to be similar (Figure 3.4).



Figure 3.4 Void nucleation in a polyamid compound

From a mathematical standpoint, the ductile damage model expresses the equivalent plastic strain at damage onset $\bar{\varepsilon}_D^{pl}$ to be a function of the stress triaxiality η , the Lode angle parameter ξ and the equivalent plastic strain rate $\dot{\bar{\varepsilon}}^{pl}$.

$$\bar{\varepsilon}_D^{pl} = f(\eta, \xi, \dot{\bar{\varepsilon}}^{pl}) \quad (3.19)$$

The equivalent plastic strain $\bar{\varepsilon}^{pl}$ is the correspondent of the equivalent von Mises stress and is defined as

$$\bar{\varepsilon}^{pl} = \int \dot{\bar{\varepsilon}}^{pl} dt = \int \left[\frac{4}{3} \sum_{i,j=1}^3 (\dot{\varepsilon}_{ii}^{pl} \dot{\varepsilon}_{jj}^{pl} - \dot{\varepsilon}_{ij}^{pl} \dot{\varepsilon}_{ji}^{pl})^2 \right]^{\frac{1}{2}} dt \quad (3.20)$$

$$\bar{\varepsilon}^{pl} = \frac{2}{\sqrt{3}} \left[(\varepsilon_1^{pl} - \varepsilon_2^{pl})^2 + (\varepsilon_2^{pl} - \varepsilon_3^{pl})^2 + (\varepsilon_3^{pl} - \varepsilon_1^{pl})^2 \right]^{\frac{1}{2}} \quad (3.21)$$

where ε_i^{pl} are the principal plastic strains.

The stress triaxiality is a scalar value that characterizes the spatial stress state, being expressed as

$$\eta = \frac{\sigma_{Hyd}}{\sigma_{Mises}} = \frac{\sqrt{2}}{3} \frac{\sigma_1 + \sigma_2 + \sigma_3}{[(\sigma_1 - \sigma_2)^2 + (\sigma_2 - \sigma_3)^2 + (\sigma_3 - \sigma_1)^2]^{\frac{1}{2}}} [-] \quad (3.22)$$

The damage initiation parameter for the ductile criterion is expressed as:

$$\omega = \int \frac{d\bar{\varepsilon}^{pl}}{\bar{\varepsilon}_D^{pl}} \quad (3.23)$$

During the analyses, the damage initiation parameter is evaluated at each increment in every integration point, considering the triaxial state of stress, the Lode angle parameter and the strain rate.

3.3.2. The shear damage model

The principle behind the shear damage model is the occurrence of shear bands during loading (Figure 3.5).

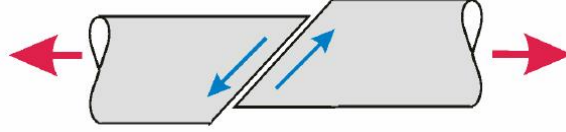


Figure 3.5 Shear band occurrence during tensile loading

In this case, the critical equivalent plastic strain $\bar{\epsilon}_S^{pl}$ is considered a function of the shear stress ratio θ_s and the equivalent strain rate $\dot{\bar{\epsilon}}^{pl}$ [30]

$$\bar{\epsilon}_S^{pl} = f(\theta_s, \dot{\bar{\epsilon}}^{pl}) \quad (3.24)$$

where the shear stress ratio is defined as

$$\theta_s = \frac{\sigma_{Mises} + k_s \cdot \sigma_{Hyd}}{\tau_{max}} \quad (3.25)$$

where k_s is a material parameter and τ_{max} is the maximum shear stress, defined as half the difference between the maximum and minimum principal stresses

$$\tau_{max} = \frac{\sigma_1 - \sigma_3}{2} \quad (3.26)$$

Similar to the ductile model, the damage initiation criterion is evaluated with the relation

$$\omega = \int \frac{d\bar{\epsilon}^{pl}}{\bar{\epsilon}_S^{pl}} \quad (3.27)$$

3.4. Calibration and validation of damage models

The first part of this section will deal with the investigations of the triaxial states of stress on specimens found in literature, and their corresponding failure strain. Due to their rather complex shape, the specimens were manufactured through rapid prototyping.

3.4.1. Tensile tests on notched flat specimens

The investigated notched flat specimens were based on ISO 527 geometries with a double notch radius in the middle region (Figure 3.6) [31]. Four notch radii were chosen along the x axis (1.25 mm, 2.5 mm, 10 mm and 15 mm) and the notches along the z axis were designed so that each specimen would have the same cross section area of 10 mm^2 ($5 \text{ mm} \times 2 \text{ mm}$).

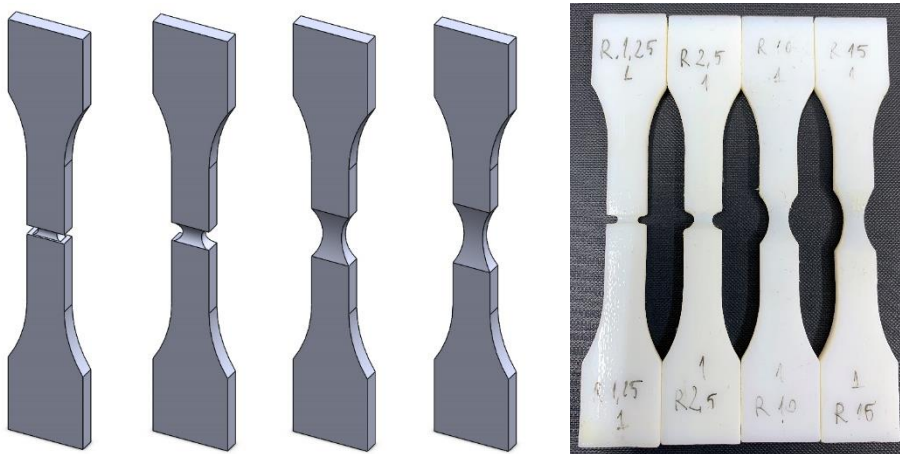


Figure 3.6 Nitched flat specimens models and specimens

The specimens were subjected to tensile loading at a constant strain rate of $2 \text{ mm}/\text{min}$. The deformations of the specimens were evaluated with an extensometer, recording the displacement of a 30 mm calibrated length around the notched region. The load displacement curve for the calibrated region are presented in Figure 3.7.

In order to evaluate the triaxial state of stress, plastic strain and third invariant distribution across the critical region of each specimen, finite element analyses were performed on models representing the volume between the grips of the extensometer. Y-axis symmetry was applied to the bottom region of the specimens and a displacement equal to the failure travel recorded by the extensometer was applied to the top region.

For the material, an elastic-plastic formulation was chosen, determined from tensile tests performed on un-notched specimens.

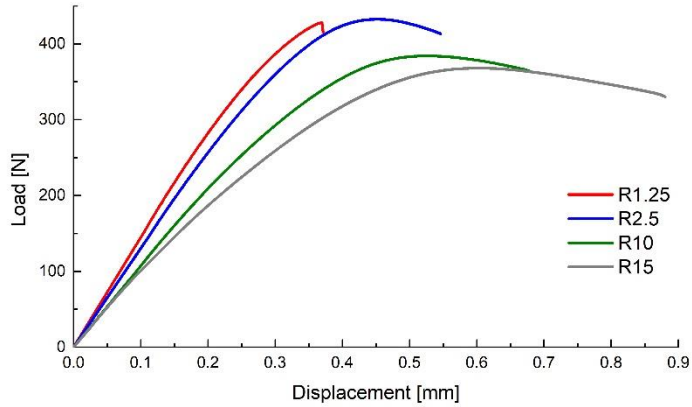


Figure 3.7 Force-deflection curves for the investigated specimens

Following the analyses, the equivalent plastic strain, stress triaxiality, equivalent Von Mises stress and the third invariant of the deviatoric stress tensor (required to evaluate the Lode angle parameter) were recorded (Figure 3.8 and Figure 3.9).

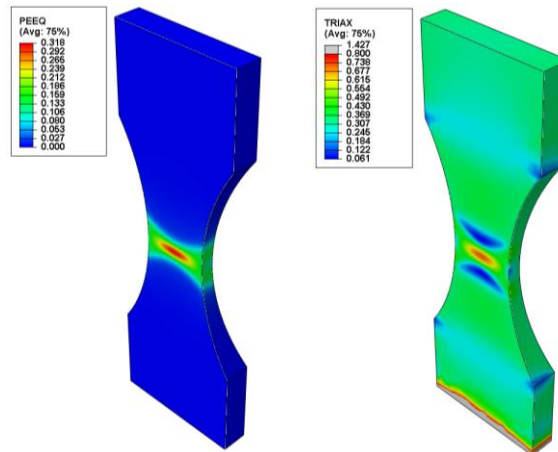


Figure 3.8 Equivalent plastic strain and stress triaxiality variation in the middle of the specimens

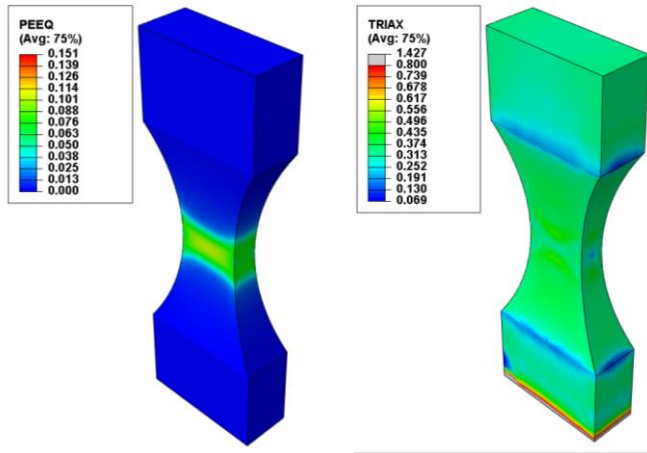


Figure 3.9 Equivalent plastic strain and stress triaxiality variation at the extremities of the specimens

Considering the spatial configuration of the specimens, the variation of the aforementioned parameters was recorded for the middle and for the extremities of the specimens in the fracture region (corresponding with the minimum area for each specimen). The simulation results showed a good agreement with the experimental data, as seen in Figure 3.10.

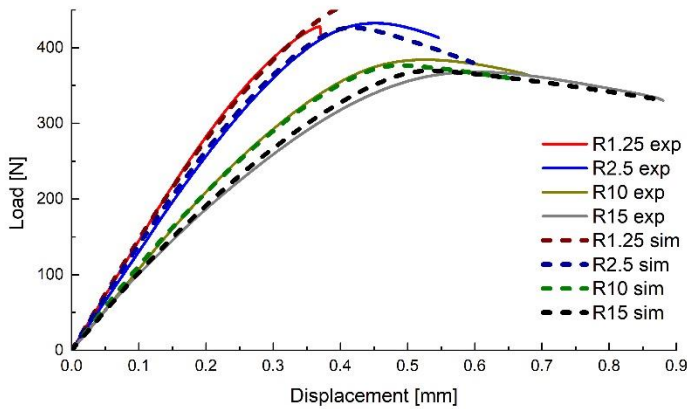


Figure 3.10 Experimental data compared with simulation results

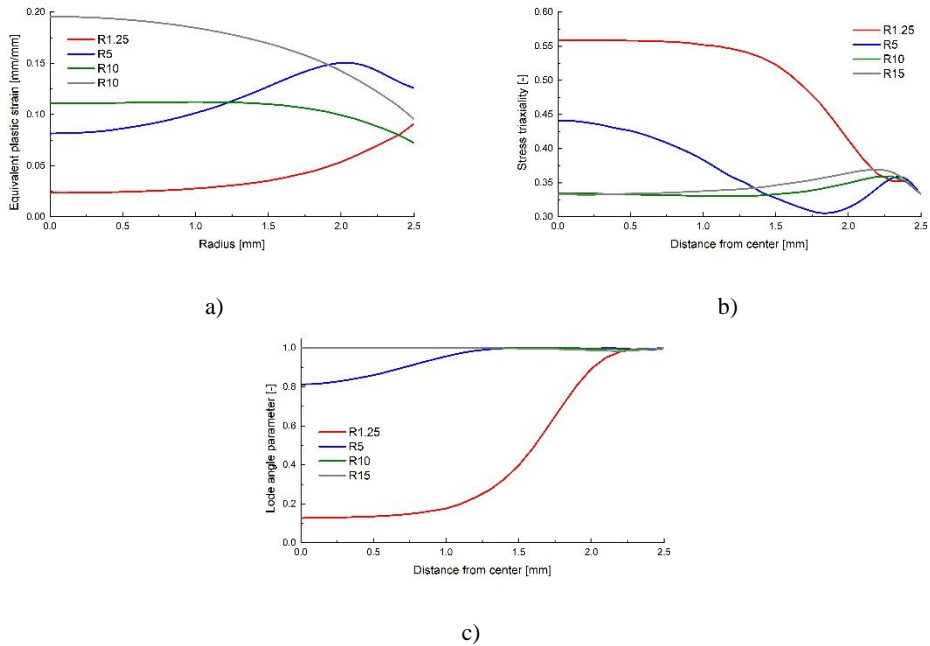


Figure 3.11 Equivalent plastic strain (a), stress triaxiality (b) and Lode angle parameter (c) variation with the distance from the centre of the specimen for the extremities

After the analysis of the equivalent critical plastic strain variation with stress triaxiality for the middle and the extremities of the specimens, it was observed that the values corresponding to the extremities yielded better approximations. The values are presented in Table 1 and the graphical variation of the equivalent plastic strain with stress triaxiality is presented in Figure 3.12.

Table 1. Equivalent critical plastic strain and Lode angle parameter variation with stress triaxiality for the notched flat specimens

Stress triaxiality [-]	Equivalent critical plastic strain [mm/mm]	Lode angle parameter [-]
0.559	0.024	0.128
0.441	0.081	0.814
0.384	0.122	0.999
0.341	0.196	0.999
0.333	0.206	1

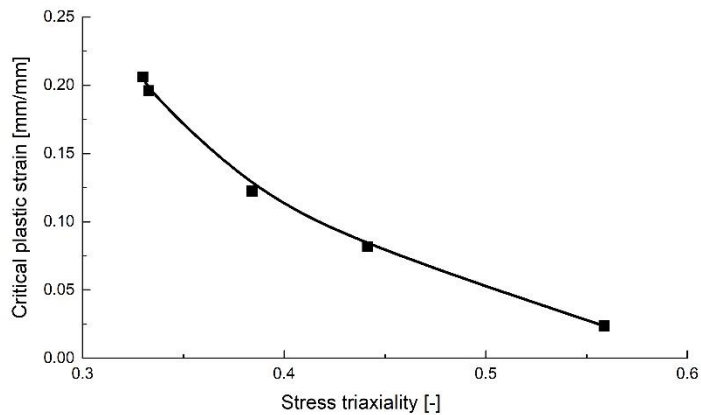


Figure 3.12 Critical plastic strain variation with stress triaxiality for the notched flat tensile specimens

3.4.2. Compression tests on notched cylindrical specimens

Similar to the tensile specimens, several notch radii were chosen (1.67 mm, 3.33 mm, 6.67 mm, 10 mm and infinite radius/un-notched, Figure 3.13) for the round compressive specimens, maintaining the critical surface area (50.26 mm^2) [25, 26]. The specimens were subjected to compression at a constant strain rate of 2 mm/min.



Figure 3.13 Notched cylindrical compressive specimens

The compressive load-displacement curves are presented in Figure 3.14. The tests for the specimens with radii of 1.67 mm , 3.33 mm and 6.67 mm were stopped after the specimens cracked (Figure 3.15), even though they still maintained load bearing capabilities.

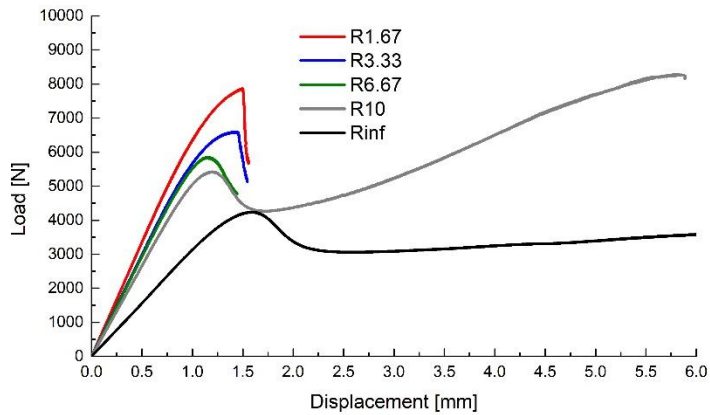


Figure 3.14 Compressive force-displacement curves



Figure 3.15 Specimen condition after the compressive tests

The specimens with the notch radius of 10 mm and the un-notched specimens buckled before showing any signs of damage, and the critical plastic strain could not be evaluated due to the modification of the stress state. This behaviour is highlighted by the hump-like shape of the force-deflection curve. In addition, the apparent softer response

of the un-notched specimen is due to its larger height, as the deflection was considered the variation of the grip separation.

As with the tensile tests, numerical analyses were performed on specimens with identical geometries in order to determine the variation of the equivalent plastic strain, stress triaxiality and Lode angle parameter. For this case, axial symmetrical elements were chosen to simplify the analysis (Figure 3.16).

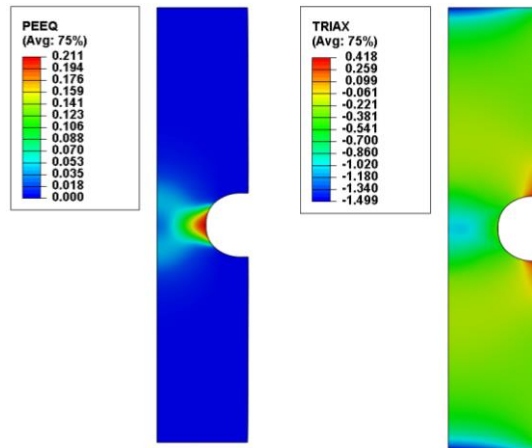


Figure 3.16 Equivalent plastic strain and stress triaxiality distribution

The numerical results, compared with the experimental data, is presented in Figure 3.17, showing good agreement.

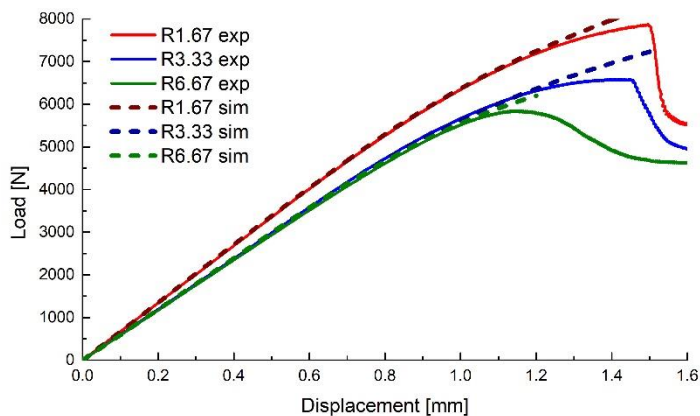


Figure 3.17 Experimental data compared with numerical results for the compression tests

The variation of the critical equivalent plastic strain, stress triaxiality and Lode angle parameter with the radius of the specimens in the critical area is presented in Figure 3.18.

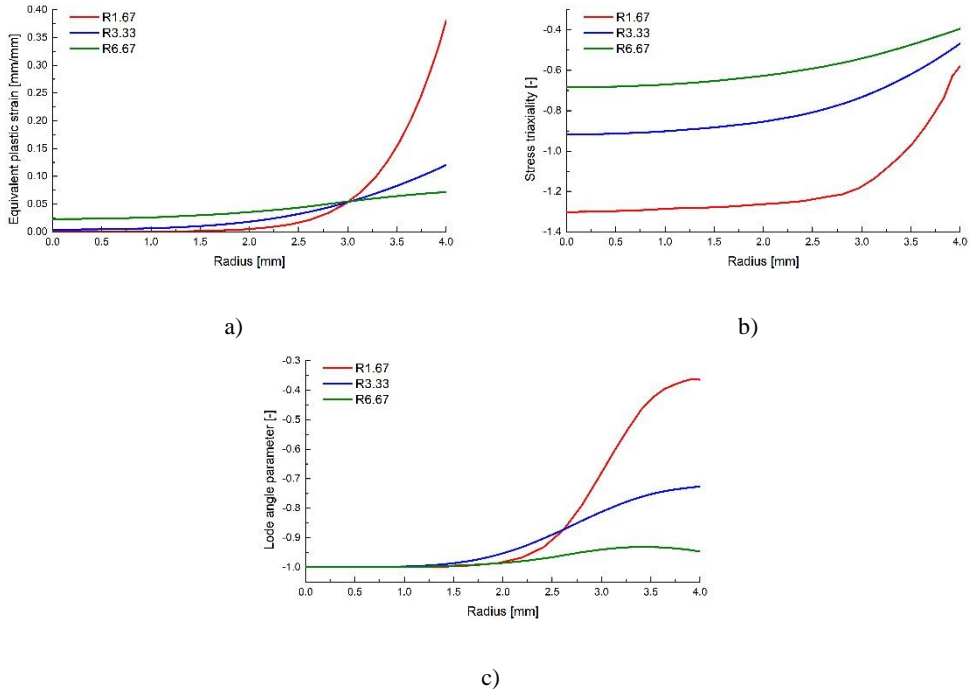


Figure 3.18 Equivalent plastic strain (a), stress triality (b) and Lode angle parameter (c) variation with radius

Considering the numerical data, the critical plastic strain and Lode angle parameter variation with the stress triaxiality is presented in Table 2 and Figure 3.19

Table 2. Equivalent critical plastic strain and Lode angle parameter variation with stress triaxiality for the notched cylindrical specimens

Stress triaxiality [-]	Equivalent critical plastic strain [mm/mm]	Lode angle parameter [-]
-0.578	0.3803	-0.365
-0.466	0.1209	-0.726
-0.394	0.0715	-0.947

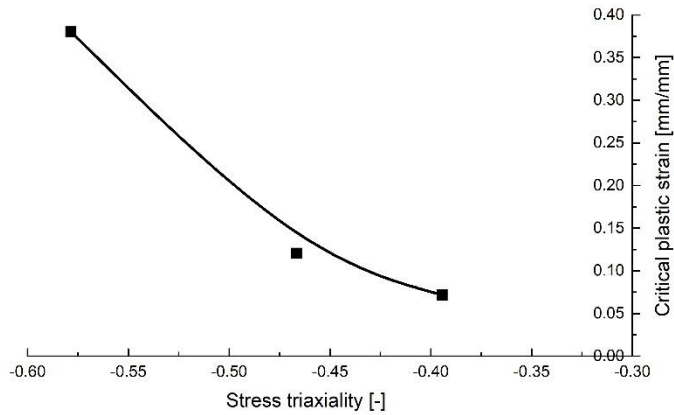


Figure 3.19 Critical plastic strain variation with stress triaxiality for the notched cylindrical specimens

3.4.3. Arcan tests

In order to gather information about the failure of the prototyped material in pure shear loading and other biaxial loading scenarios, Arcan tests were performed on butterfly specimens. These specimens are characterized by a calibrated region with two notch radii (Figure 3.20) so that the failure can be located in the middle of the region. The reduced thickness of the calibrated region assures that the stress along the z axis has very small values compared with the other stresses and thus it can be considered null.

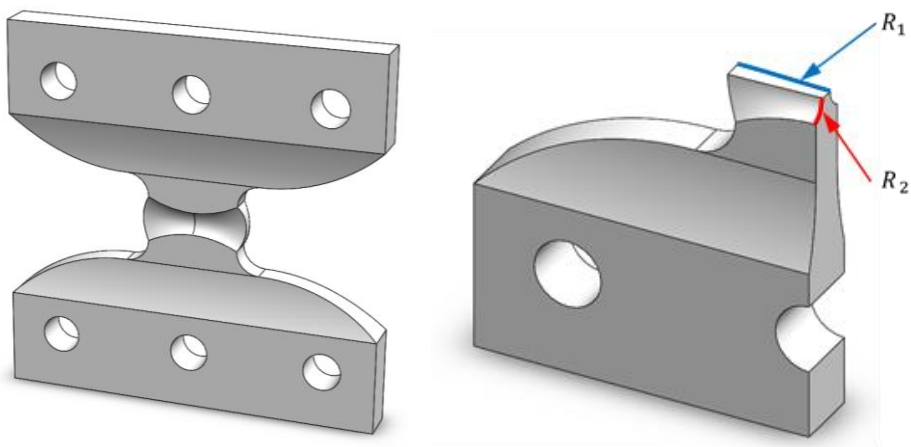


Figure 3.20 The butterfly specimen

Numerical analyses on the butterfly specimen determined various combinations of the principal stresses, as seen in Figure 3.21.

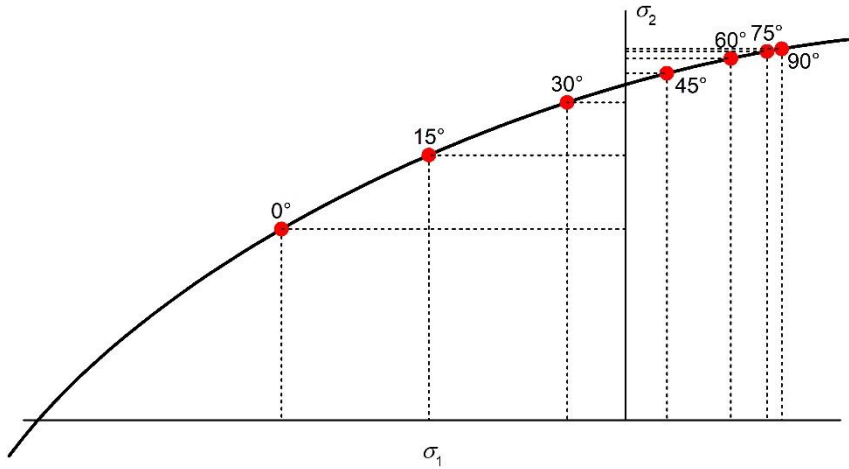


Figure 3.21 Principal stress combinations achievable through the Arcan test

Arcan tests were performed for orientations of 0° , 15° , 30° and 45° , the results being presented in Figure 3.22

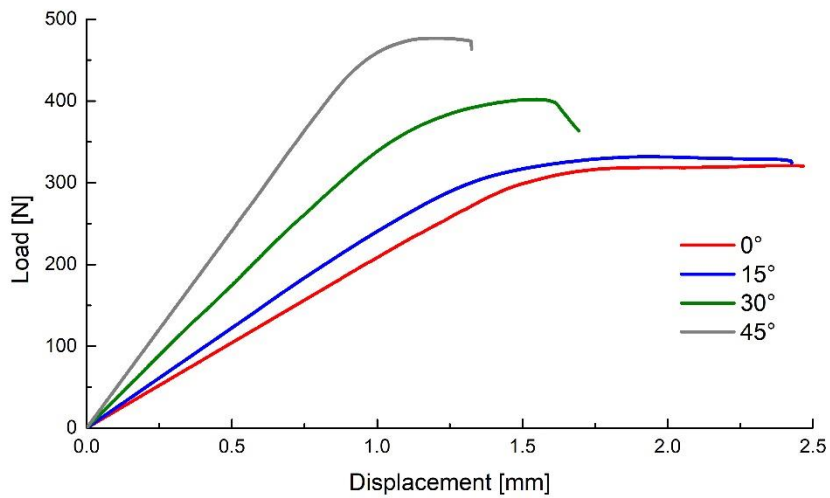


Figure 3.22 Force-deflection curves for the Arcan tests

For all the investigated configurations, the damage initiation mechanism resembled the theoretical assumption, with voids occurring in the critical area (Figure 3.23).

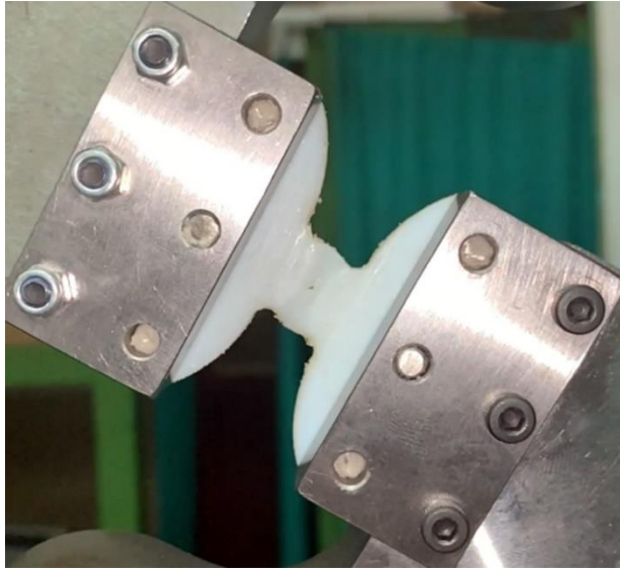


Figure 3.23 Void occurrence during Arcan tests

In order to determine the magnitudes of the failure parameters (critical plastic strain, stress triaxiality and Lode angle parameter) for the Arcan tests, numerical analyses were performed on the butterfly specimen model for the given orientations. The damage initiation strain was considered to be attributed to the deflection of the specimen that corresponded to the deviation of the numerical results from the experimental values (Figure 3.24). The resulted values are presented in Table 3 and the graphical variation in Figure 3.25

Table 3. Equivalent critical plastic strain and Lode angle parameter variation with stress triaxiality for the Arcan tests

Stress triaxiality [-]	Equivalent critical plastic strain [mm/mm]	Lode angle parameter [-]
0.349	0.18	1
0.244	0.513	0.944
0.086	0.78	0.476
-0.012	0.85	0

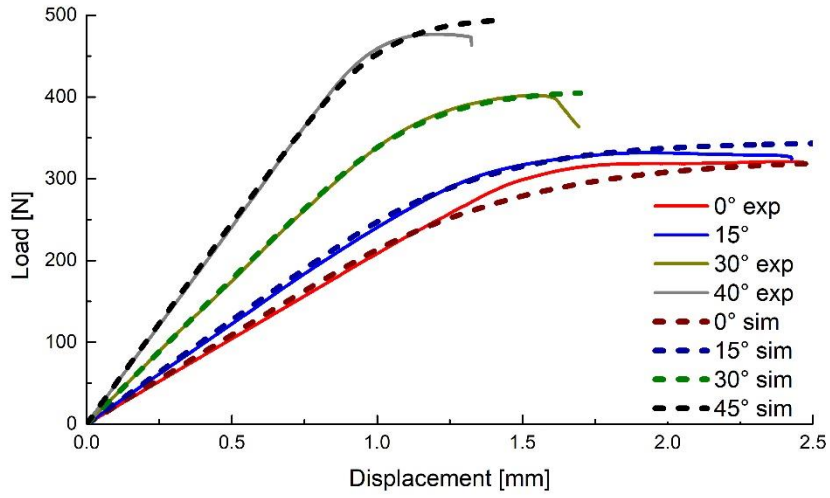


Figure 3.24 Experimental and numerical results for the Arcan tests

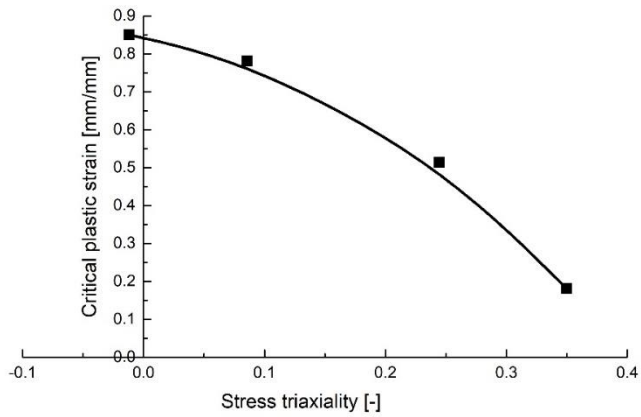


Figure 3.25 Critical plastic strain variation with stress triaxiality for the Arcan tests

3.4.4. Model validation for rapid prototyped polymers

The validation of the damage model was performed through the numerical analyses of metamaterial structures with Kelvin cells subjected to compression.

The chosen Kelvin structure had a relative density of 0.1 and a fillet radius to strut thickness ratio of 0.3, having $9 \times 5 \times 5$ cells and solid faces at the top and bottom. The structure was manufactured using the PolyJet™ technology on a Stratasys ObJet24 3D printer [32].

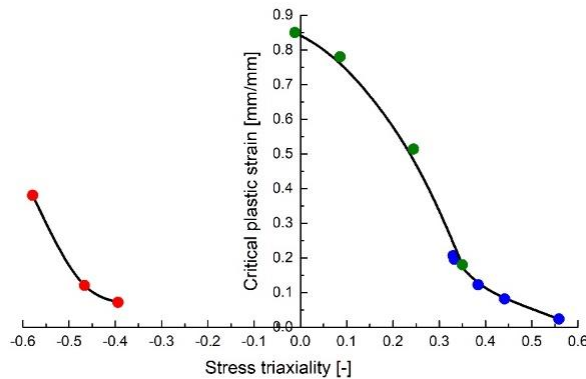


Figure 3.26 Variation of the critical plastic strain with stress triaxialities for all the investigated types of loadings

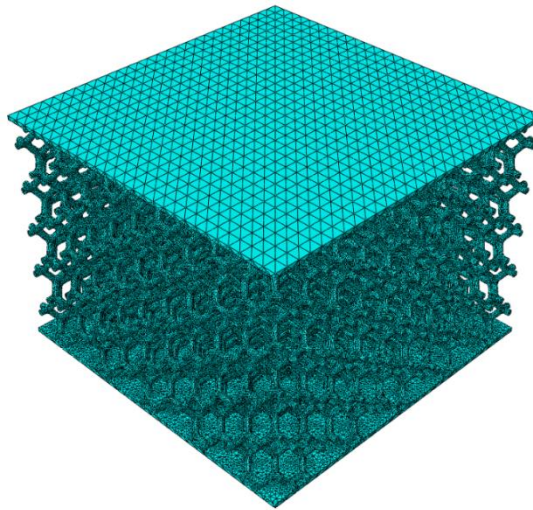


Figure 3.27 Meshed model of the Kelvin structure

The same model used for rapid prototyping was imported into the FEA software Abaqus. For the material model, the elastic-plastic ABS with the damage parameters described above was implemented. The mesh consisted of $2.78 \cdot 10^6$ C3D10M elements (Figure 3.27). Preliminary analyses showed a high degree of variation of the stress triaxiality (Figure 3.28), which prompted this study.

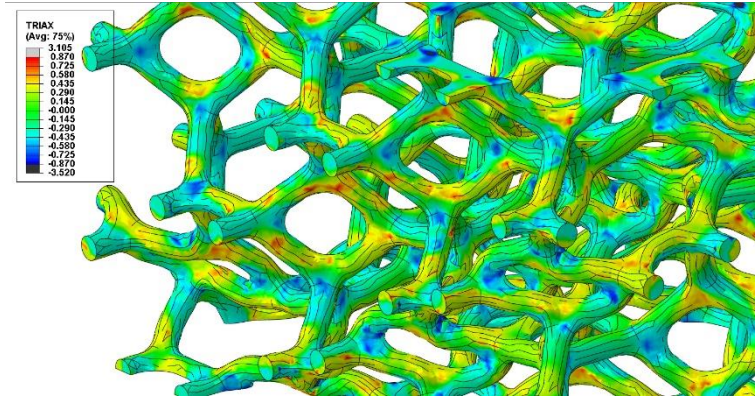


Figure 3.28 Triaxial state of stress of the Kelvin structure during compression

With the updated material model, the analyses results were more accurate in terms of stiffness, yield strength and plateau (Figure 3.29). A comparison between the experimental and numerical behaviour in compression of the structures is presented in Figure 3.30

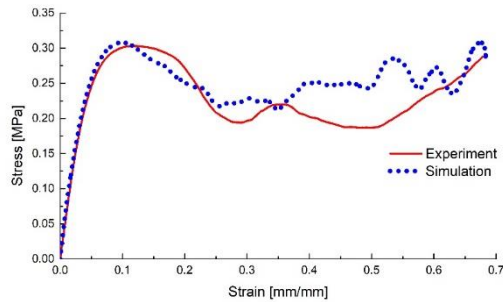


Figure 3.29 Stress-strain curve for the experimental and numerical compression tests on the Kelvin structure

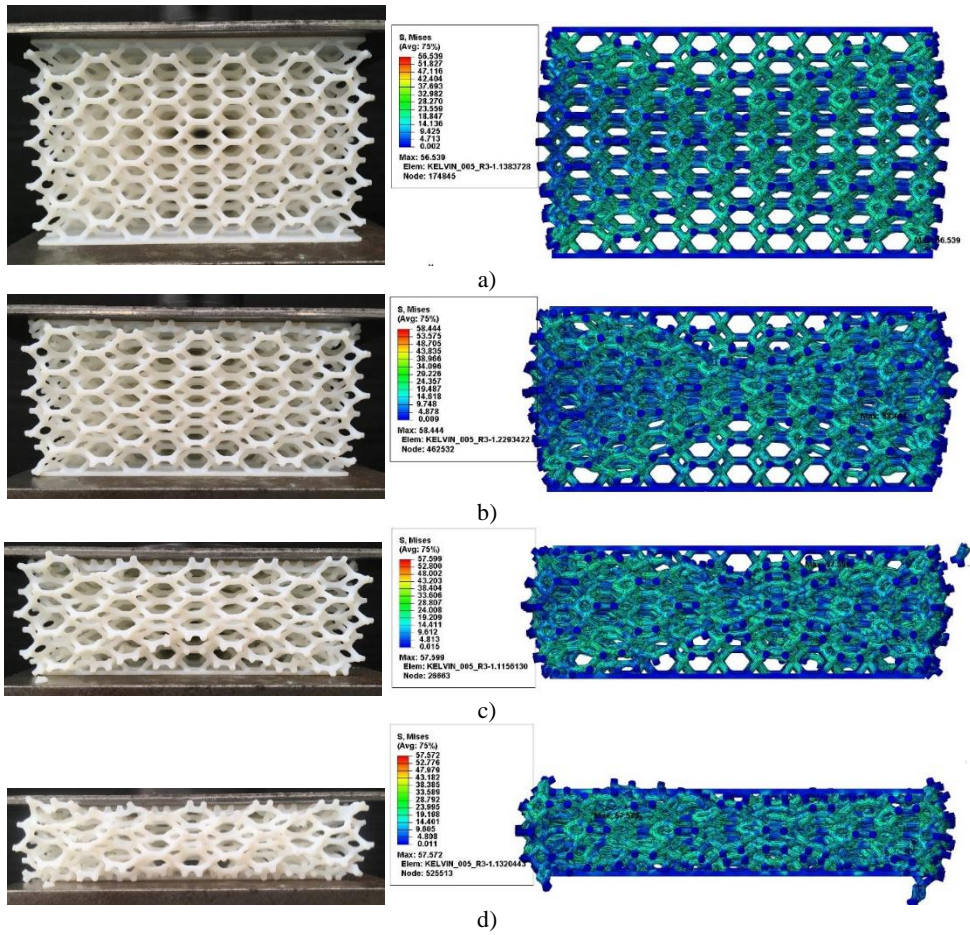


Figure 3.30 Experimental and numerical deformation of the Kelvin structure for a displacement of 10 mm (a), 20 mm (b), 30 mm (c) and 40 mm (d)

3.5. Conclusions

In this chapter, the ductile damage model initially developed for metals was proposed for the damage and failure prediction of polymeric materials, as the theoretical basis for damage onset (the nucleation and growth of voids during straining) is similar.

The determination of the critical plastic strain variation with stress triaxiality can be obtained by performing various tests on notched specimens, where the failure locus can be easily identified.

Considering the rather complex specimen geometries, the first step in investigating if this approach is suitable was to perform tests on rapid prototyped specimens. Tensile, compressive and shear tests were performed, determining the variation of the equivalent plastic strain, stress triaxiality and third invariant with the critical cross section of the specimens.

The validation of the developed damage models was evaluated with numerical analyses on both the test specimens as well as on complex structures, yielding promising results.

The next step in this direction is to manufacture the specific specimens through injection. This aspect requires the manufacturing of specific injection moulds for each geometry.

4. Scientific achievements

4.1. Overview

In this section, the author's statistics will be presented (at the time of the submission of the thesis) for the two leading analytics websites:

On **Web of Science**

- 24 publications from Web of Science Core Collection
- H-index: 10
- Sum of Times Cited: 273
- Citing Articles: 201

On **Scopus**

- Documents by author: 31
- H-index: 11
- Total citations: 350
- Citing documents: 228

4.2. Complete list of publications

At the date of the thesis submission, the author has published a number of 32 articles, of which 20 as main author. Out of the 32 articles, 18 are published in ISI indexed journals (11 as main author) and 10 are published in ISI Proceedings (6 as main author). The complete list of publications is presented below:

4.2.1. Publications in ISI Journals

1. **D.A. Şerban**, L. Marşavina, and V. V. Silberschmidt, "Behaviour of semi-crystalline thermoplastic polymers: Experimental studies and simulations" *Computational Material Science*, vol. 52, pp. 139–146, 2012. (Impact factor: 1.878, Q2), DOI: 10.1016/j.commatsci.2011.02.042;

2. **D.A. Şerban**, L. Marşavina, and V. Silberschmidt, "Response of semi-crystalline thermoplastic polymers to dynamic loading: A finite element study" *Computational Material Science*, vol. 64, pp. 116–121, 2012. (Impact factor: 1.878, Q2); DOI: 10.1016/j.commatsci.2012.05.072

3. **D.A. Şerban**, G. Weber, L. Marşavina, V. V. Silberschmidt, and W. Hufenbach, "Tensile properties of semi-crystalline thermoplastic polymers: Effects of temperature and strain rates," *Polymer Testing*, no. 32, pp. 413–425, 2013. (Impact factor: 1.816, Q1); DOI: 10.1016/j.polymertesting.2012.12.002

4. **D.A. Şerban**, E. Linul, T. Voiconi, L. Marşavina, N. Modler, "Numerical evaluation of two-dimensional micromechanical structures of anisotropic cellular materials: case study for polyurethane rigid foams", *Iranian Polymer Journal*, no. 24, pp. 515–529, 2015 (Impact factor: 1.806, Q3); DOI: 10.1007/s13726-015-0342-3

5. **D.A. Şerban**, L. Marşavina, N. Modler, "Low-cycle fatigue behaviour of polyamides", *Fatigue and Fracture of Engineering Materials*, no. 38, Issue 11, pp. 1383–1394, 2015 (Impact factor: 1.561, Q2); DOI: 10.1111/ffe.12333

6. **D.A. Şerban**, T. Voiconi, E. Linul, L. Marşavina, N. Modler, "Viscoelastic Properties of PUR Foams: Impact excitation and dynamic mechanical analysis", *Materiale Plastice*, no. 52, Issue 4, pp. 537–541, 2015 (Impact factor: 0.903, Q4);

7. **D.A. Şerban**, O. Weissenborn, S. Geller, L. Marşavina, M. Gude, "Evaluation of the mechanical and morphological properties of long fibre reinforced polyurethane rigid foams", *Polymer Testing*, no. 49, pp. 121–127, 2016. (Impact factor: 2.464, Q1). DOI: 10.1016/j.polymertesting.2015.11.007.

8. R. Negru, **D.A. Şerban**, L. Marşavina, A. Magda, "Lifetime prediction in medium-cycle fatigue regime of notched specimens", *Theoretical and Applied Fracture Mechanics*, no. 84, PP. 140-148, 2016, (Impact factor: 2.659, Q1), DOI:10.1016/j.tafmec.2016.03.006.

9. E. Linul, **D.A. Şerban**, L. Marsavina, J. Kovacik, "Low-cycle fatigue behaviour of ductile closed-cell aluminium alloy foams", *Fatigue and Fracture of Engineering Materials and Structures*, no. 40, pp. 597-604, 2017 (Impact factor: 2.335, Q1), DOI: 10.1111/ffe.12535

10. E. Linul, **D.A. Şerban**, L. Marsavina, T. Sadowski, "Assessment of collapse diagrams of rigid polyurethane foams under dynamic loading conditions", *Archives of Civil and Mechanical Engineering* no. 17, pp. 457 – 466, 2017 (Impact factor: 2.216, Q1), DOI: 10.1016/j.acme.2016.12.009

11. L. Marşavina, F. Berto, R. Negru, **D.A. Şerban**, E. Linul, "An engineering approach to predict mixed mode fracture of PUR foams based on ASED and micromechanical modelling", *Theoretical and Applied Fracture Mechanics*, no. 91, pp. 148-154, 2017 (Impact factor: 2.659, Q2), DOI: 10.1016/j.tafmec.2017.06.008

12. R. Negru, **D.A. Şerban**, C. Pop, L. Marşavina, "Notch effect assessment in a PUR material using a ring shaped specimen", *Theoretical and Applied Fracture Mechanics*, no 97, pp 500-506, 2018 (Impact factor: 2.215, Q2), DOI:10.1016/j.tafmec.2018.01.016

13. E. Linul, **D.A. Şerban**, L. Marşavina, "Influence of Cell Topology on Mode I Fracture Toughness of Cellular Structures", *Physical Mesomechanics*, PHYSICAL MESOMECHANICS, no. 21, pp. 178-186, 2018 (Impact factor: 2.38, Q1), DOI: 10.1134/S1029959918020121

14. **D.A. Şerban**, L. Marşavina, L. Rusu, R. Negru, "Numerical study of the behavior of magnesium alloy AM50 in tensile and torsional loadings", *Archive of Applied Mechanics*, no 89, pp 911-917, 2019 (Impact factor: 1.374, Q3), DOI: 10.1007/s00419-018-1492-5

15. **D.A. Şerban**, R. Negru, S. Sărăndan, G. Belgiu, L. Marşavina, "Numerical and experimental investigations on the mechanical properties of cellular structures with open Kelvin cells", *Mechanics of Advanced Materials and Structures* (Impact factor: 2.873, Q1), DOI: 10.1080/15376494.2019.1669093, accepted for publishing on 14.09.2019

16. D. Buncianu, N. Tessier-Doyen, J. Absi, R. Negru, **D.A. Şerban**, Liviu Marşavina, "Multi-Scale Mechanical Behaviour of a Highly Porous Alumina Based Foam", *Metals and Materials International* (Impact factor: 1.99, Q2), DOI: 10.1007/s12540-019-00413-0

17. **D.A. Şerban**, R. Negru, H. Filipescu, L. Marşavina, "Investigations on the influence of the triaxial state of stress on the failure of polyurethane rigid foams", *Continuum Mechanics and Thermodynamics* (Impact factor: 2.139, Q2), DOI: 10.1007/s00161-020-00924-x

18. **D.A. Şerban**, G. Furtos, L. Marşavina, C. Şoşdean, R. Negru, "Numerical modelling of the mechanical behaviour of wood fibre-reinforced geopolymers", *Continuum Mechanics and Thermodynamics* (Impact factor: 2.139, Q2), DOI: 10.1007/s00161-020-00934-9

4.2.2. Articles in ISI Proceedings

1. **D.A. Şerban**, H. Hanson, L. Marşavina, and V. Silberschmidt, "Viscoelastic properties of semi-crystalline thermoplastic polymers: dynamic analysis and creep," *Solid State Phenomena*, Vol. 188, no. *Advanced Materials and Structures IV*, pp. 211-218, 2012;

2. **D.A. Şerban**, T. Voiconi, L. Marşavina, V. Silberschmidt, „Flexural properties of polyamides: influence of strain rate, friction and moulding-induced anisotropy”, *Key Engineering Materials* Vol. 601, *Proceedings of the 14th Symposium on Experimental Stress Analysis and Material Testing*, pp. 29-32, 2014;

3. E. Linul, **D.A. Şerban**, T. Voiconi, L. Marşavina, T. Sadowski, „Energy – absorption and efficiency diagrams of rigid PUR foams”, *Key Engineering Materials* Vol. 601, *Proceedings of the 14th Symposium on Experimental Stress Analysis and Material Testing*, pp. 246-249, 2014;

4. **D.A. Şerban**, L. Marşavina, N. Modler, “Finite Element Modelling of the Progressive Damage and Failure of Thermoplastic Polymers in Puncture Impact”, *Procedia Engineering* Volume 109, *Proceedings of the XXIII Conference of the Italian Group of Fracture Meeting*, pp. 97–104, 2015.

5. **D.A. Şerban**, E. Linul, S. Sărăndan, L. Marşavina, ” Development of parametric Kelvin structures with closed cells”, *Solid State Phenomena* 254, pp 49-54, 6th International Conference on Advanced Materials and Structures, 2016.

6. G. Belgiu, C. Cărăuşu, **D.A. Şerban**, C. G. Turc, ”Product management of making large pieces through Rapid Prototyping PolyJet® technology”, *IOP Conference Series: Materials Science and Engineering* 227, 5th International Conference on Modern Technologies in Industrial Engineering, 2017.

7. L. Marşavina, **D.A. Şerban**, C. Pop, R. Negru, ”Experimental investigation of failure modes for sandwich beams”, *Key Engineering Materials* 754 KEM, 16th International Conference on Fracture and Damage Mechanics pp 115-118, 2017.

8. **D.A. Şerban**, S. Sărăndan, R. Negru, G. Belgiu, L. Marşavina, "A Parametric Study of the Mechanical Properties of Open-Cell Kelvin Structures", IOP Conference Series: Materials Science and Engineering 416, 7th International Conference on Advanced Materials and Structures 2018

9. **D.A. Şerban**, N. Tessier-Doyen, J. Absi, L. Marşavina, R. Negru, "Evaluation of the Elastic Properties of Highly Porous Alumina Foams using Finite Element Analysis", IOP Conference Series: Materials Science and Engineering 416, 7th International Conference on Advanced Materials and Structures 2018

10. E. Linul, K. Korniejenko, **D.A. Şerban**, R. Negru, L. Marşavina, M. Lach, J. Mikula, "Quasi-Static Mechanical Characterization of Lightweight Fly Ash-Based Geopolymer Foams", IOP Conference Series: Materials Science and Engineering 416, 7th International Conference on Advanced Materials and Structures 2018

4.2.3. Articles in International Databases Journals

1. **D.A. Şerban**, L. Marşavina, L. Culea, and V. V. Silberschmidt, "Experimental determination of Mullins effect in semi-crystalline thermoplastic polymers," Acta Technica Napocensis, 53, 2010;

2. V. Putz, D. Ştef, **D.A. Şerban**, "Contributions regarding the optimization of the technological process procedure of draught bars through the development and usage of computational mathematical models that define the manufacturing simulation", Volume XIX (IX), 2010/2.

3. **D.A. Şerban**, E. Linul, C. Neş, L. Marşavina, "Numerical Modelling of Damage and Failure of Ductile Materials in Finite Element Analysis", Buletinul Universităţii Petrol - Gaze Ploieşti. Seria Tehnică, Vol. LXVII, 11-20, 2016/2

4. **D.A. Şerban**, E. Linul, S. Sărăndan, L. Marşavina, "Development of Parametric Kelvin Structures with Closed Cells", Solid State Phenomena 245, Proceedings of the Advanced Materials and Structures IV, pp. 49–54, 2016

4.3. Research Grants

4.3.1. National Grants

As Director

1. Project entitled “Transfer of knowledge for dashboard and Head-Up Display optimization through testing and modelling of advanced materials”, PN-III-P2-2.1-BG-2016-0125, Contract no. 93BG/2016, 2016-2018, founded by the Romanian Ministry of National Education through UEFISCDI, budget: 75000 EUR.

Research team members:

- Prof. Dr. Eng. Liviu Marşavina
- Dr. Eng. Radu Negru
- Dr. Eng. Emanoil Linul
- Dr. Eng. Corina Şoşdean
- PhD Student Eng. Emanuel Praţa
- Eng. Cristian Codrescu
- Eng. Adelin Enescu

2. Project entitled “Development of polymer-based metamaterial structures for safety equipment applications”, PN-III-P1-1.1-PD-2016-0445, Contract no. 13/2018, 2018-2020, founded by the Romanian Ministry of National Education through UEFISCDI, budget: 54350 EUR.

Research team members:

- Prof. Dr. Eng. Nicolae Faur

As research team member

1. Project entitled “Micro-mechanical modelling of cellular materials with refinements on fracture and damage”, Director: Prof. Dr. Eng. Liviu Marşavina, PN-II-ID-PCE-2011-3-0456, Contract no. 172/2011, 2011-2016, founded by the Romanian Ministry of National Education through UEFISCDI, budget: 276080 EUR.

2. Project entitled “High performance lightweight panels with a new optimized design for advanced aircraft structures”, Director: Prof. Dr. Eng. Dan Mihai

Constantinescu, PN-II-PT-PCCA2011-3.2-0068, Contract no. 206/2012, founded by the Romanian Ministry of National Education through UEFISCDI, budget: 31380 EUR.

3. Project entitled “Transfer of knowledge for fatigue strength evaluation of steering wheel armatures”, Director: Prof. Dr. Eng. Liviu Marşavina, PN-III-P2-2.1-BG2016-0060, Contract no. 89BG/2016, 2016-2018, founded by the Romanian Ministry of National Education through UEFISCDI, budget: 100000 EUR.

4. Project entitled “Smart buildings adaptable to the climate change effects”, Director: Prof. Dr. Eng. Viorel Ungureanu, PN-III-P1-1.2-PCCDI-2017-0391, Contract no. 30PCCDI/2018, founded by the Romanian Ministry of National Education through UEFISCDI.

4.3.2. International Grants

As Project coordinator for Politehnica University Timișoara

1. Project entitled “Development of ecofriendly composite materials based on geopolymer matrix and reinforced with waste fibers”, Project leader: Technical University of Krakow, Poland, Horizon 2020 EraNet LAC ELAC2015/T02-0721, Contract no. 18/2017/2017, 2017-2019, budget: 86770 EUR.

Research team members:

- Prof. Dr. Eng. Liviu Marşavina
- Dr. Eng. Radu Negru
- Dr. Eng. Emanoil Linul

As research team member

1. Project entitled “Microstructural-mechanical properties relationship for metallic foams”, Director: Prof. Dr. Eng. Liviu Marşavina, Contract no. 653/2013

4.4. Research stages

1. Date: November 2009 - December 2009

Host institution: Institut für Leichtbau und Kunststofftechnik, Technische Universität Dresden

Main activities and responsibilities: Mechanical testing of polyamides

2. Date: March 2011 - June 2011

Host institution: Sports Technology Institute, Loughborough University

Main activities and responsibilities: Experimental investigations and material modelling for numerical simulations of polyamides

3. Date: July 2011 - August 2011

Host institution: adidas innovation team, adidas AG

Main activities and responsibilities: Material modelling for numerical simulations of polyamides

4. Date: April 2012 - August 2012

Host institution: Institut für Leichtbau und Kunststofftechnik, Technische Universität Dresden

Main activities and responsibilities: Experimental investigations and material modelling for numerical simulations of polymers

5. Date: June 2013 - August 2013

Host institution: Institut für Leichtbau und Kunststofftechnik, Technische Universität Dresden

Main activities and responsibilities: Experimental investigations and material modelling of cellular materials

6. Date: February 2014 - July 2014

Host institution: Institut für Leichtbau und Kunststofftechnik, Technische Universität Dresden

Main activities and responsibilities: Experimental investigations and material modelling of cellular materials

7. Date: February 2015 - April 2015

Host institution: Institut für Leichtbau und Kunststofftechnik, Technische Universität Dresden

Main activities and responsibilities: Experimental investigations and material modelling of cellular materials

8. Date: September 2017 - October 2017

Host institution: University of Limoges

Main activities and responsibilities: Experimental investigations on ceramic foams

4.5. Other research topics

This section briefly presents the research results of the author in fields not related to the viscoplastic behaviour of polymers.

4.5.1. Research into polymeric foams

After the completion of the doctoral studies, the author was co-opted into the research team of Prof. Liviu Marşavina and began studying the mechanical behaviour of polyurethane rigid (PUR) foams. During his research career, the author studied a variety of topics related to the properties, morphology and fracture of PUR foams. Apart from the regular PUR foams, the opportunity of improving the mechanical properties by glass fibre reinforcements was also investigated.

Static and dynamic mechanical characterization of unreinforced and reinforced polymeric foams

The first step in evaluating the mechanical behaviour of the investigated PUR foams was the determination of static tensile and compressive properties. Tensile tests were performed on ISO 527 specimens [33], the strain being recorded with a laser extensometer, showing an elastic-plastic behaviour with low failure strains. The compressive tests were performed on cubes, showing the three stages of deformation characteristic to cellular materials: a linear elastic region, a plateau and a densification region [34, 35], Figure 2.1.

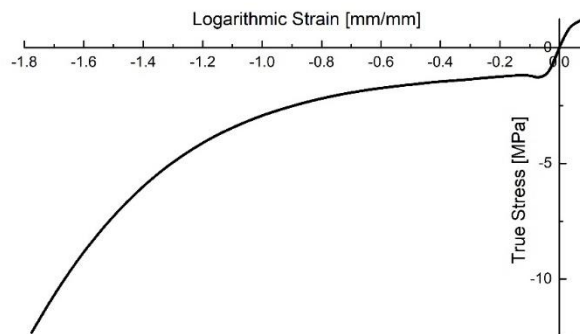


Figure 4.1 Tensile and compressive stress-strain behaviour of an unreinforced PUR foam

In addition, the influence of fibre reinforcements on the stiffness and mechanical strength was also investigated for various fibre lengths and weight contents [36] (Figure 4.2). It was observed that the weight content of fibres increases the stiffness and the plateau stress of the composites, but no clear trends could be set for the increase in fibre length, as the longest investigated fibres (50mm) yielded lower mechanical properties than shorter variants (i.e. 25mm).

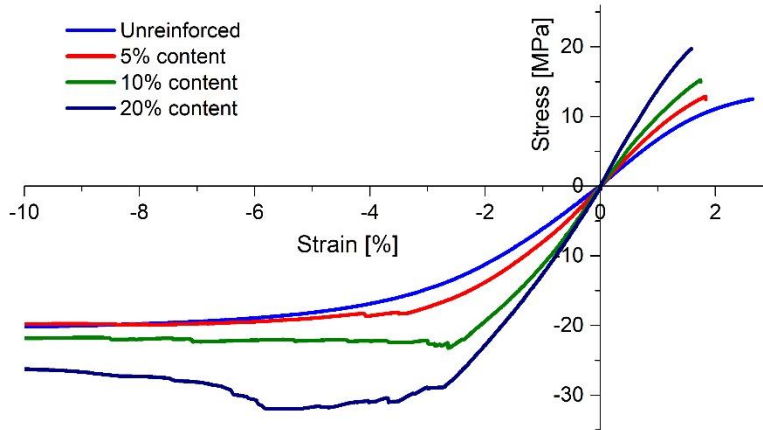


Figure 4.2 Influence of fibreglass reinforcements on the static tensile and compressive behaviour of a PUR foam [36]

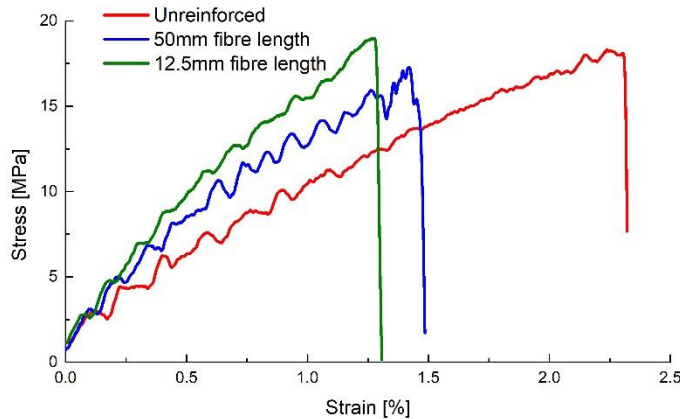


Figure 4.3 Influence of fibreglass reinforcements on the dynamic tensile behaviour of a PUR foam

As the main application of polyurethane foams as structural components is related to their energy absorption capabilities, dynamic tests were also performed. Though predominantly subjected to compression, structural parts that integrate PUR materials can also be subjected to bending, thus both dynamic tensile and compressive tests were performed. The same trends were observed: the increase in fibre weight content and in the density of the PUR foam determined an increase in stiffness and plateau stress, while the optimal fibre length was around 25mm, the 50mm fibres determining lower properties (Figure 4.3).

The modelling of polyurethane foams was performed using the Deshpande-Fleck plasticity model, which assumes an elliptic yield surface in the meridian plane (hydrostatic pressure – equivalent von Mises stress plane) [37], Figure 4.4.

$$\sqrt{(\sigma_{Mises})^2 + \alpha^2 [(\sigma_{Hid}^c)' - \sigma_{Hid}^c]^2} - B = 0 \quad (4.1)$$

where

$$\alpha = \frac{3k}{(3k_t + k)(3 - k)} \quad (4.2)$$

$$k = \frac{\sigma_c}{|\sigma_{Hid}^c|} \quad (4.3)$$

$$k_t = \frac{\sigma_{Hid}^t}{|\sigma_{Hid}^c|} \quad (4.4)$$

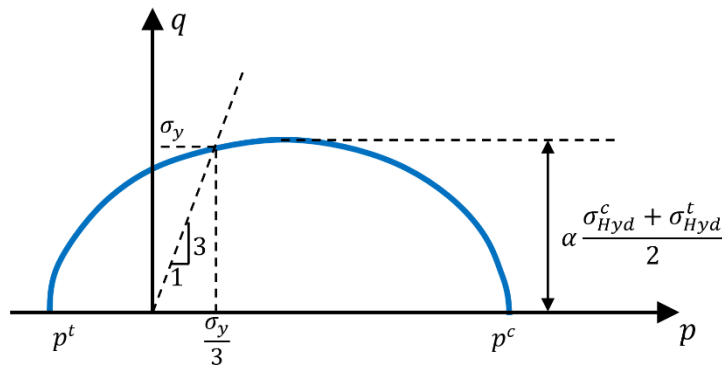


Figure 4.4 Yield surface of a PUR foam in the meridian plane [35]

The flow potential of the Deshpande-Fleck model is defined as

$$\Phi = \frac{\sigma_c(\varepsilon^{pl}) \left[\sigma_c(\varepsilon^{pl}) \left(\frac{1}{\alpha^2} + \frac{1}{9} \right) + \frac{\sigma_{Hid}^t}{3} \right]}{\sigma_{Hid}^t + \frac{\sigma_c(\varepsilon^{pl})}{3}} \quad (4.5)$$

The D-F material model was calibrated using the experimental data and numerical analyses were performed for both static and dynamic loading, yielding accurate results (Figure 4.5).

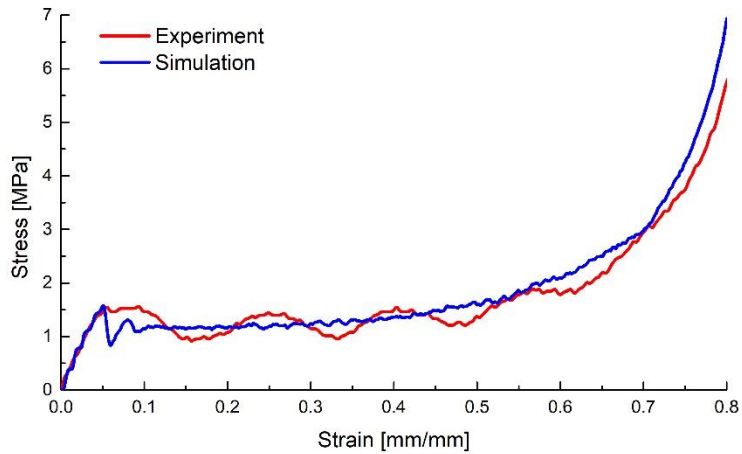


Figure 4.5 Experimental and numerical results for the dynamic compressive stress-strain variation for an unreinforced PUR foam [38]

For additional investigations into the dynamic properties of PUR foams, impulse excitation and DMA tests were performed. The impulse excitation tests measure the resonance frequency of the materials through the excitation generated by an impulse strike [39], Figure 4.6.

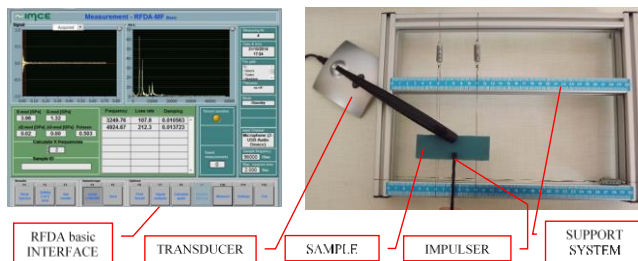


Figure 4.6 Determination of dynamic properties of PUR foams using impulse excitation technique [39]

Dynamical mechanical analyses were performed using a temperature and frequency sweep. Using the experimental data and applying Boltzmann's superposition principle, the time-temperature superposition was generated, obtaining a variation of the dynamic properties with frequency from very low values (10^{-18}Hz) up to very high values (10^{12}Hz), Figure 4.7 [39].

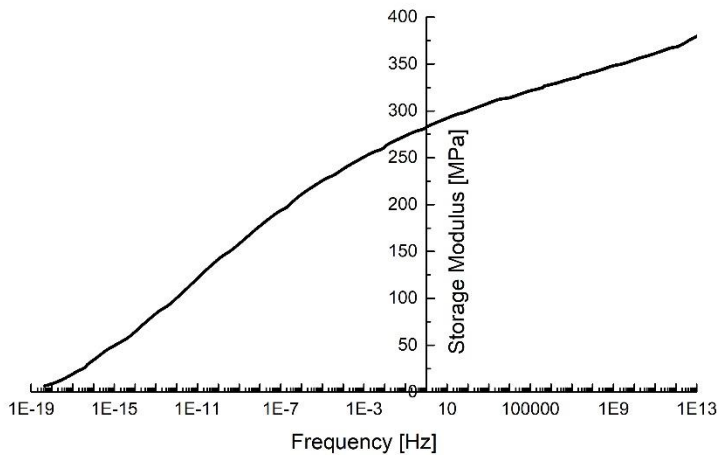


Figure 4.7 Time-temperature superposition resulting in the variation of the storage modulus with frequency for a PUR foam [39]

Studies regarding the influence of the morphology and microstructure of polymeric foams on their mechanical properties

In order to gather more information regarding the mechanical behaviour of cellular structures, studies were performed in order to link the microstructures to the mechanical properties of the materials.

A first step in this direction was the development of microstructures with cell parameters similar to those measured from SEM images (Figure 4.8). The gather data was used in determining various types of 2D (circles, squares, hexagons etc. [40]) and 3D structures (hollow spheres, Kelvin tessellations [32]).

The variation of the relative density of the structures with structural parameters were investigated, in order to determine the respective values for various densities (Figure 4.10).

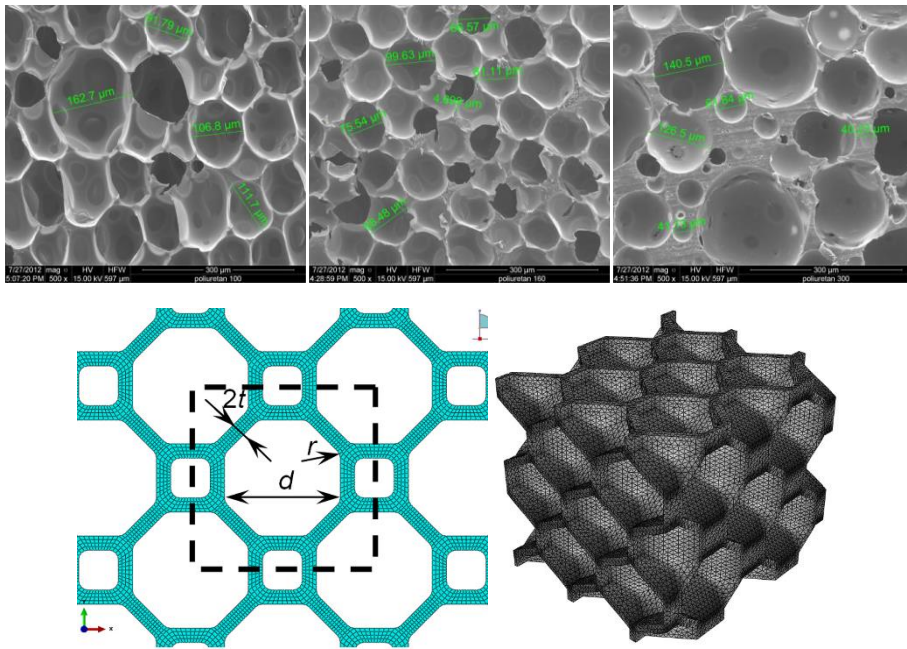


Figure 4.8 Cell diameter measurements from SEM images for three PUR densities and geometric models [39, 40, 32]

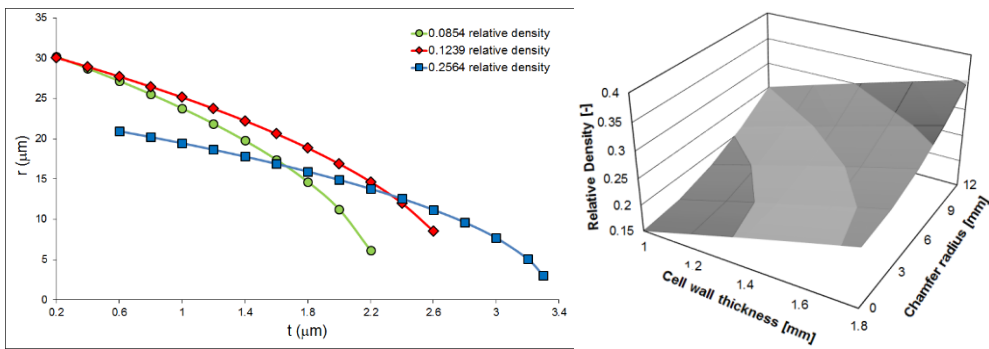


Figure 4.9 Variation the structural parameters for various densities for 2D and 3D geometires [40, 32]

The resulting structures were subjected to numerical analyses in order to determine whether the chosen parameters determine accurate results when compared to the experimental values (Figure 4.10).

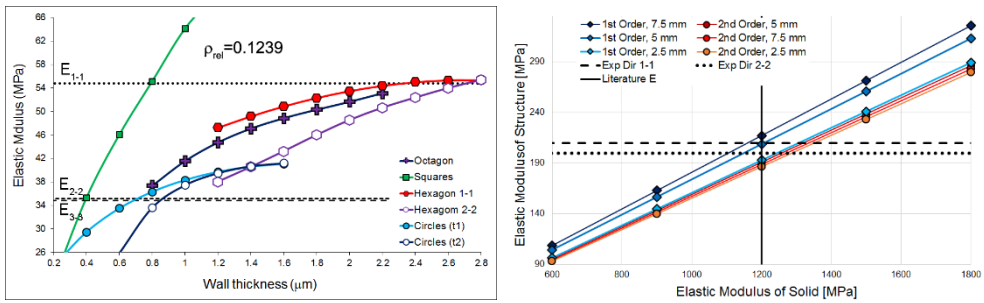


Figure 4.10 Variation of Young’s modulus with structural parameters for a micromechanical PUR foam model [40, 32]

For the fibre reinforced PUR foams, SEM images and CT scans helped determine the correlation between the microstructure and the mechanical properties (Figure 4.11). The fibre orientation and microstructural defects caused by the inclusions helped explain the scatter in results and helped identify some manufacturing parameters that caused these phenomena [36].



Figure 4.11 SEM image of the fracture area and CT scan showcasing the glass fibre distribution [36]

Fracture and damage of polymeric foams

An important topic of the researched conducted by Prof. Marşavina dealt with the determination of the fracture properties of PUR foams for various modes and the evaluation of several fracture mechanics criteria (averaged strain energy density, theory of critical distances) for the gathered data [41, 42].

The author’s contribution in this research was the development of numerical analyses that replicate the tests conditions of the experimental procedures and the post-processing of the results.

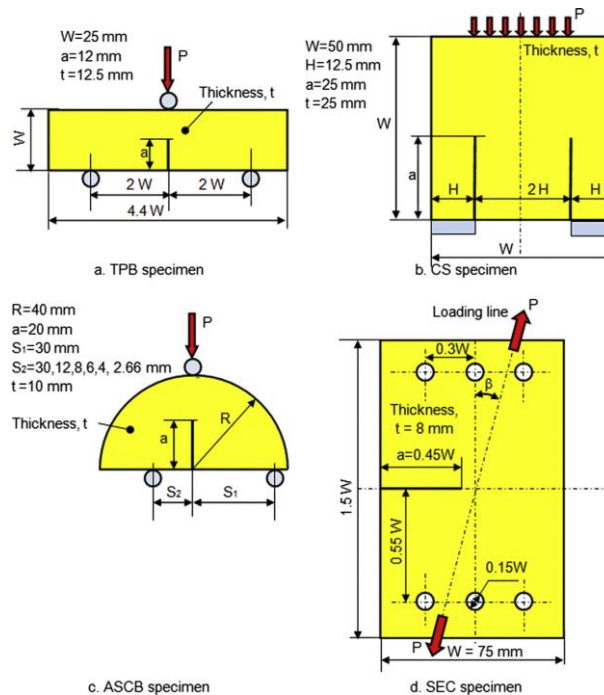


Figure 4.12 A sample of fracture mechanics tests specimens [41]

Another topic related to the fracture mechanics of PUR foams was the evaluation of the properties on microstructural models. For this purpose, the micromechanical models developed earlier were subjected to finite element analysis with the introduction of artificial cracks (Figure 4.13). The stress states in the cell walls were evaluated and with the results, the stress intensity factor was evaluated and compared to the experimental values [43].

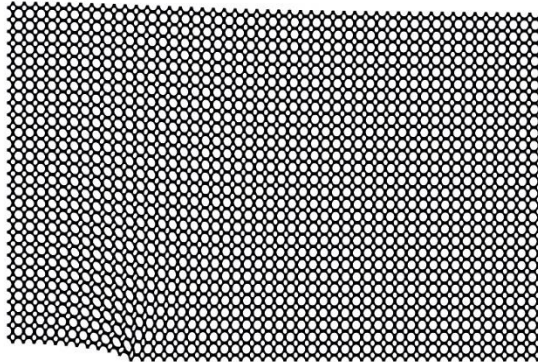


Figure 4.13 Crack simulation using micromechanical model [43]

The failure of PUR foams was also investigated considering macroscopic phenomena, namely, the influence of the triaxial state of stress on the critical plastic strain [35]. The theoretical background regarding this approach was presented extensively in the previous chapter. For PUR foams, cylindrical specimens with various fillet radii were obtained through turning, using profiled knives (Figure 4.14).



Figure 4.14 PUR specimens used in the triaxial state of stress-critical plastic strain study

Finite element analyses were performed on specimens with identical geometries with the imposed displacement identical to the recorded fail travel. From the results, the variation of the plastic strain, stress triaxiality and the Lode angle parameter with the specimen diameter was obtained, resulting in the variations presented in Figure 4.15.

The obtained damage models were evaluated on tests performed on sandwich structures with aluminium faces and PUR cores [44], yielding accurate results both in

terms of the force-deflection curves and regarding the fracture mode of the composite beams [35].

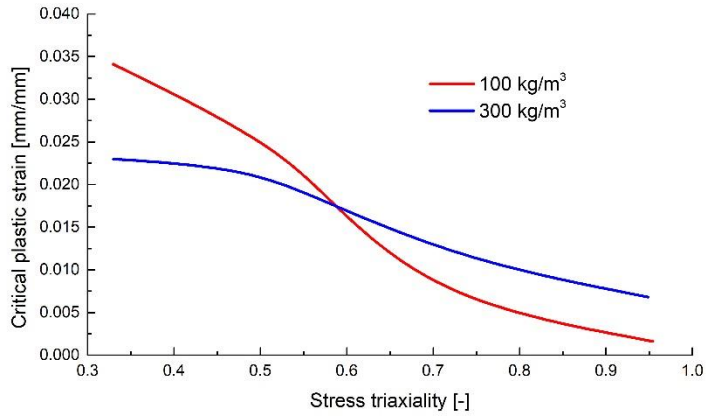


Figure 4.15 Variation of the critical plastic strain with the stress triaxiality for PUR foams of two densities

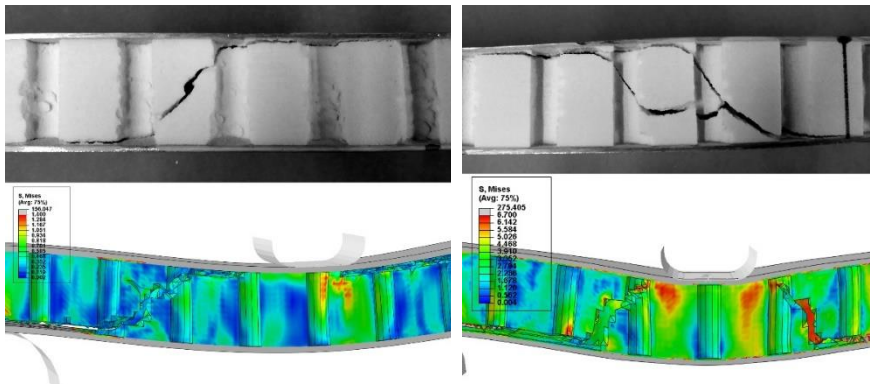
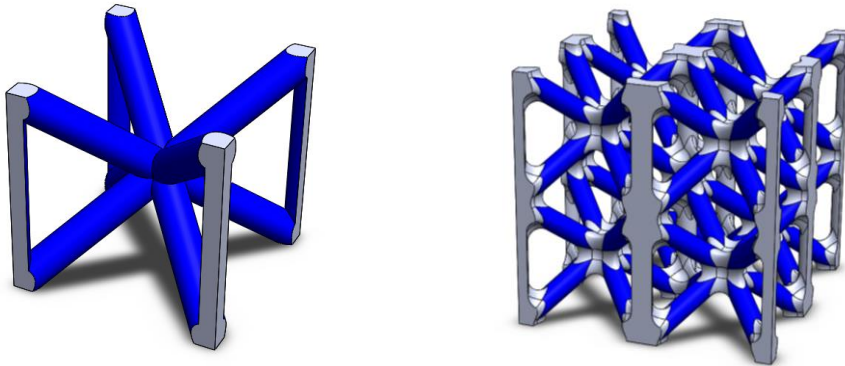


Figure 4.16 Simulation results for the validation of the failure model [35]

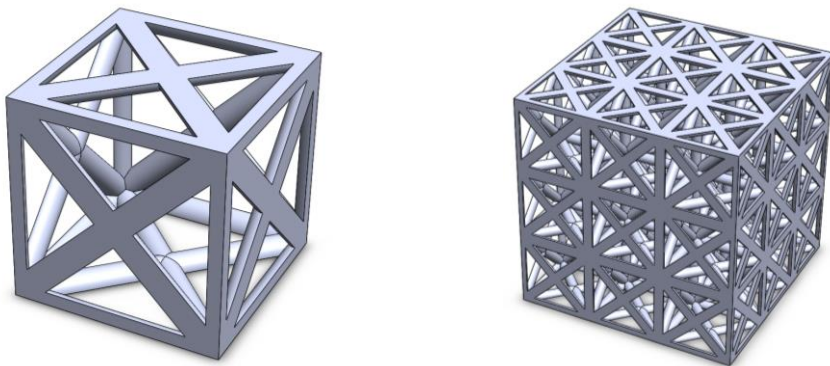
4.5.2. Research into metamaterial structures

The micromechanical modelling of PUR foams opened up new research directions for the Author, in the field of metamaterial structures that can be manufactured through rapid prototyping. Through the research Grant awarded to the Author regarding this topic, an in-depth analysis was performed concerning the various types of structures that can be prototyped.

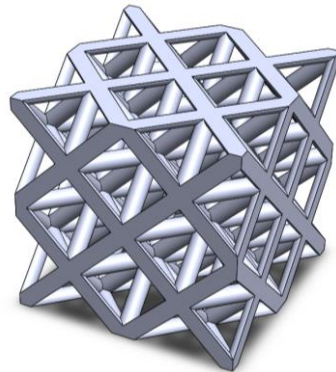
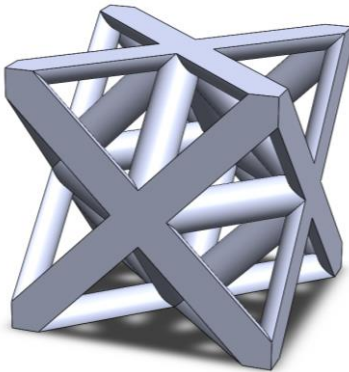
The investigated structures consisted of tessellations of various cell types and associated lattices. The most commonly used type of cell has a cubic geometry (prismatic variants can be designed for anisotropy), as the tessellation is easily performed through mirroring operations (Figure 4.17). The cubic structures described in literature are based on crystalline structures: the positions of the atoms represent connection nodes between the structure trusses.



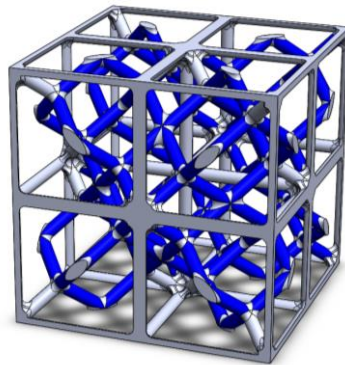
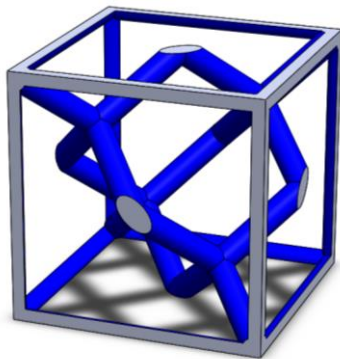
Body-centered cubic structure



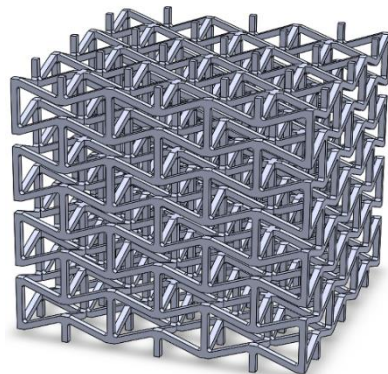
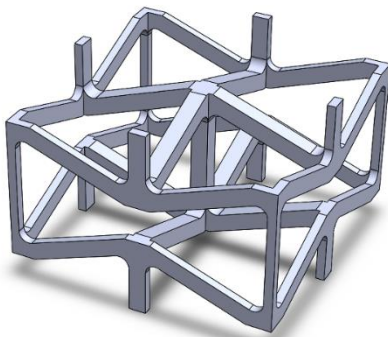
Face-centered cubic structure



Octet truss structure



Diamond structure



Auxetic structure

Figure 4.17 Cubic structures

Several parametric cubic structures were investigated: body-centred, face-centred, octet-truss and diamond. In addition, a particular type of structure was also investigated, consisting of re-entrant elements that determine a negative Poisson ratio (auxetic).

Another type of structure that possesses a peculiar cell shape is the Kagome. This type of structure was influenced by Japanese basket weaves and is presented in Figure 4.18.

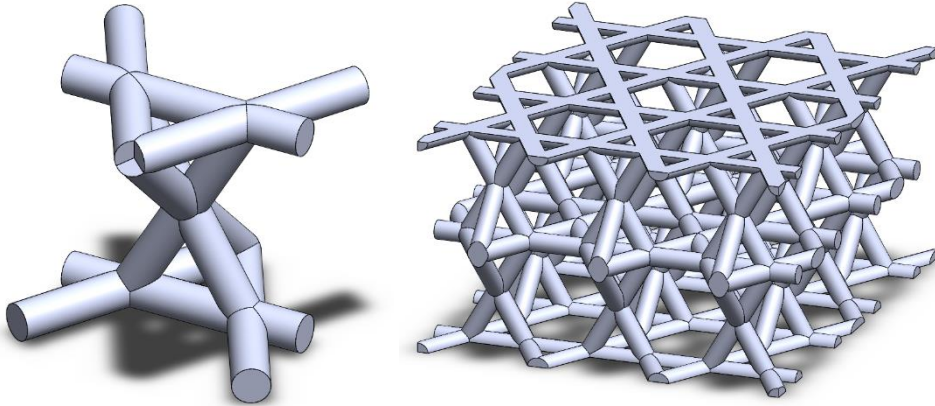
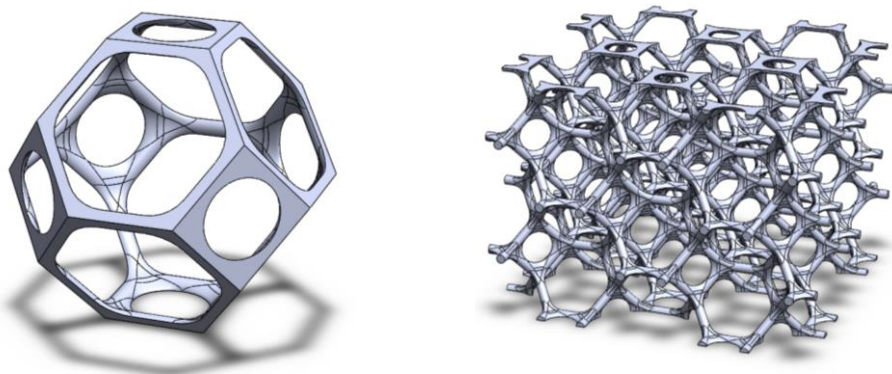
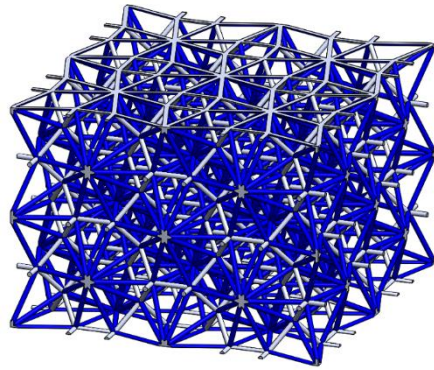
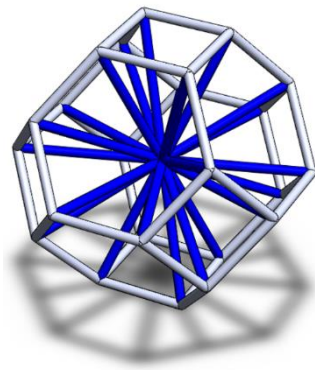


Figure 4.18 Kagome structure

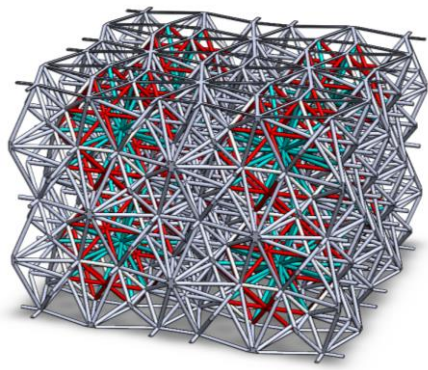
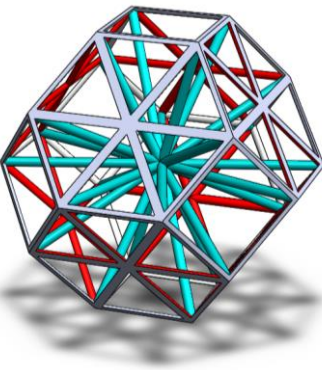
The third type of cell that was studied was the regular dodecahedron (truncated pyramid) also known as the Kelvin cell (Figure 4.19). This structure is known to be one of the most efficient natural occurring geometry, having one of the lowest surface to volume ratios [32].



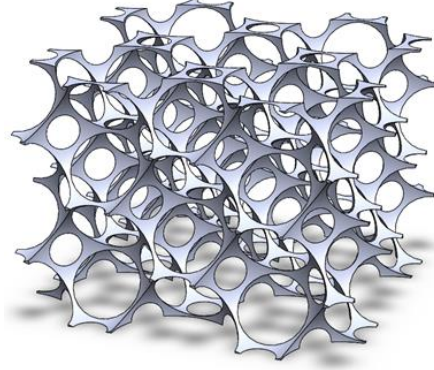
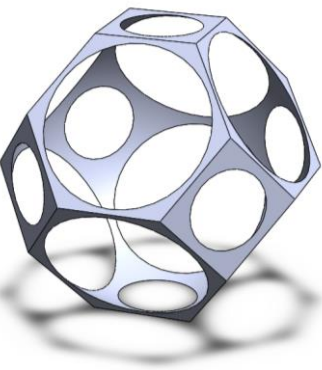
Basic Kelvin structure



Central reinforced Kelvin structure



Central and face reinforced Kelvin structure



Spherical Kelvin structure

Figure 4.19 Kelvin structures

Several variations of the Kelvin structure were investigated, having various reinforcements in order to reduce the value of Maxwell's stability parameter and to transform it into a stretch-dominated structure.

All the structures presented above were modelled using parametric geometries, namely the fillet radius and the strut thickness to length ratio. Thus, the relative density of the structures varied through the modification of the structural parameters (Figure 4.20).

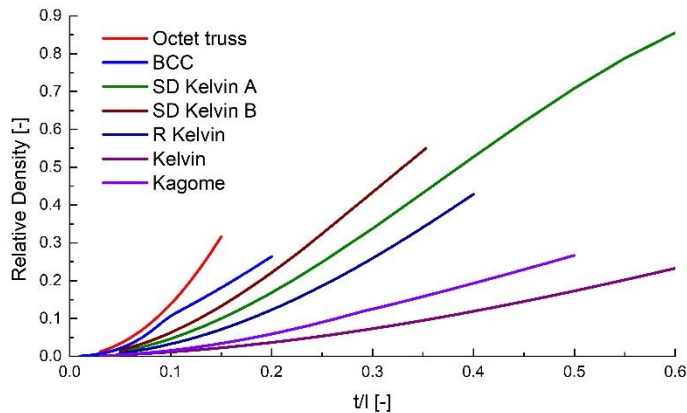


Figure 4.20 Relative density variation with the t/l ratio

Polynomial equations were fitted to the curves presented in Figure 4.20 and structures were generated with set relative densities for comparison purposes. The structures were subjected to finite element analyses using the material model for the rapid prototyped ABS presented in the previous chapter.

Stress-strain curves were obtained for each structure at the set relative densities and from them, the relative density and relative strength. The comparison of the results is presented in Figure 4.21.

It was observed that the stiffness of the structures falls in between the values characteristic of bending and stretch dominated structures, while the strength is closer to the bending dominated behaviour.

It was observed that the strength of the structure is proportional with the t/l ratio of the structure at a given density while the stiffness is also influenced by Maxwell's stability criterion.

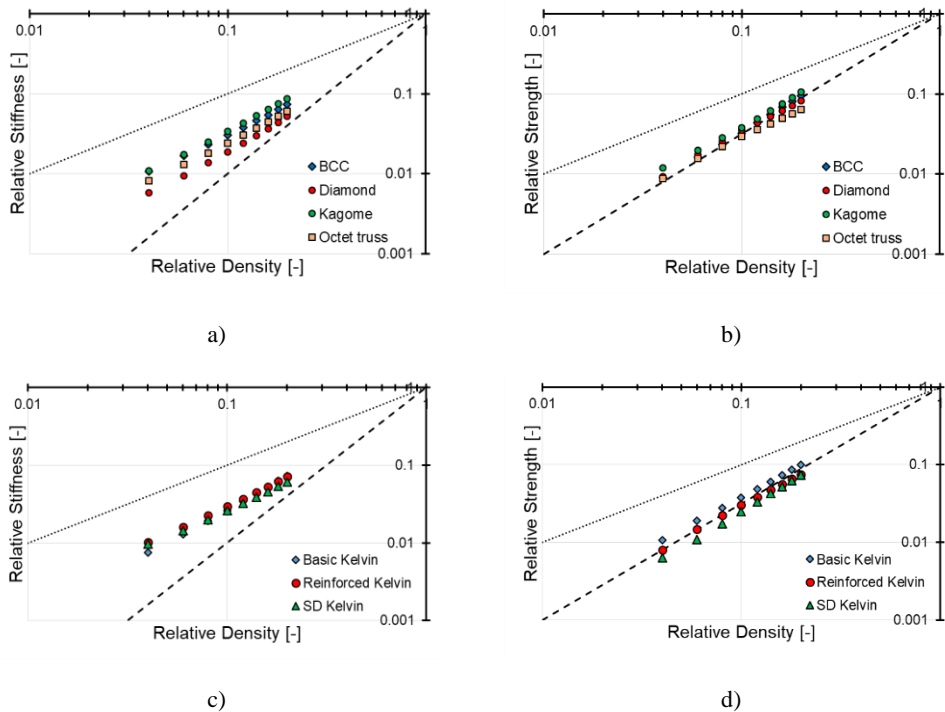


Figure 4.21 Relative stiffness and strength variation with the relative density for the investigated structures

4.5.3. Research into geopolimer composites

The Horizon 2020 EraNet LAC ELAC2015/T02-0721 research Grant dealt with the development and testing of geopolimer composites manufactured from waste materials, as a part of urban mining and waste management. Several compositions were considered, based on the waste materials resulting from industrial activities specific for each region.

The composites investigated by the Romanian partner were based on fly ash resulted from the burning of coal in thermal power plants and wood chips resulted from timber processing.

The composite materials were developed in Babeş-Bolyai University of Cluj Napoca and tested at Politehnica University Timișoara. A cross-section of a geopolimer composite sample is presented in Figure 4.22 showing the distribution of the wood fibres and the defects that occurred during curing [45].

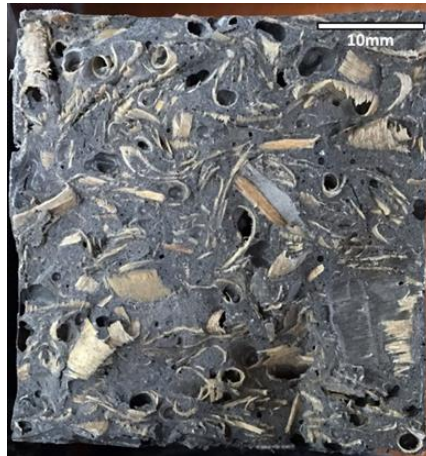


Figure 4.22 Geopolymer – wood fibre composite cross section

This study investigated the influence of the wood fibre content on the mechanical properties in compression and three-point bending.

Compression tests were performed on cubic samples at a strain rate of 1mm/min. Unreinforced samples showed a brittle behaviour, while the increase in wood fibre content determine lower stiffness and strength, but higher failure strain (Figure 4.23 and Figure 4.24).

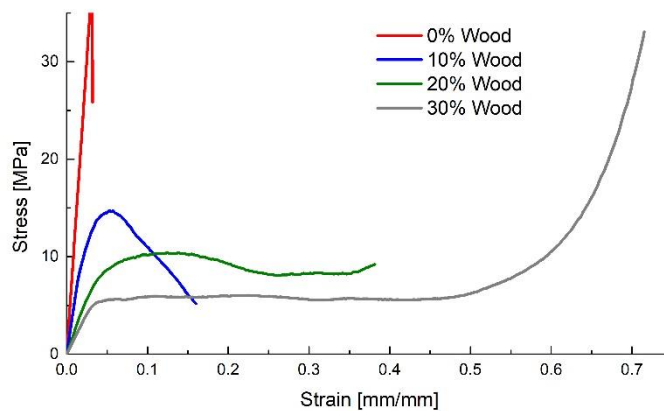


Figure 4.23 Stress-strain response in compression of the composites with various wood fibre content

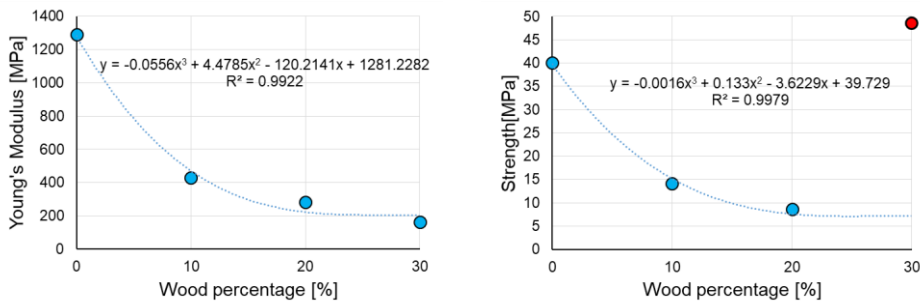


Figure 4.24 Variation of Young's modulus and compressive strength with wood fibre content

Three-point bending tests were performed on prismatic samples at a strain rate of 1mm/min and, similar to the compression tests, the unreinforced samples showed a brittle behaviour and the increase in wood fibre content determine lower stiffness and higher failure strain (Figure 4.25 and Figure 4.26).

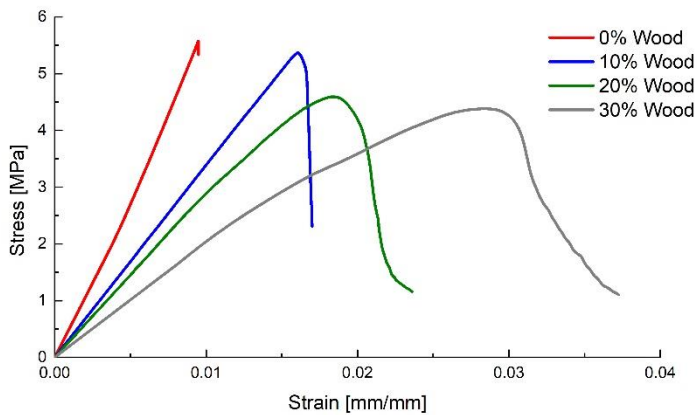


Figure 4.25 Stress-strain response in bending of the composites with various wood fibre content

The next step in this study consisted of the development of numerical models that can accurately replicate the tensile and compressive behaviour of the wood chip reinforced geopolymers.

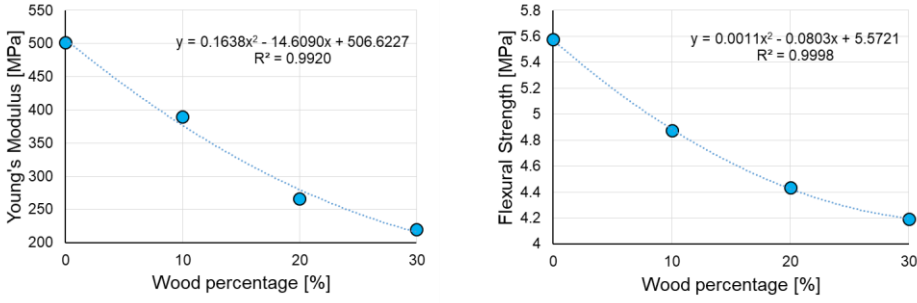


Figure 4.26 Variation of Young's modulus and flexural strength with wood fibre content

The chosen constitutive model was the *Concrete damage plasticity* formulation, which assumes a Drucker-Prager yield function, which, in the meridian plane is expressed as

$$q = p \cdot \tan \beta + c \quad (4.6)$$

where q is the equivalent stress, p is the hydrostatic pressure, β is the friction angle defined as:

$$\beta = \arctan(-3B\sqrt{3}) \quad (4.7)$$

and c is the cohesion, expressed as

$$c = \left(1 - \frac{1}{3} \tan \beta\right) \sigma_y^c = \left(1 + \frac{1}{3} \tan \beta\right) \sigma_y^t \quad (4.8)$$

The modified Drucker-Prager formulation assumes a hyperbolic curve in the $p - q$ plane (Figure 4.27) and is defined as

$$\sqrt{l_0^2 + q^2} = p \cdot \tan \beta + c \quad (4.9)$$

where

$$l_0 = c - p_t \cdot \tan \beta \quad (4.10)$$

p_t being the yield stress in hydrostatic tension.

The hardening law is expressed as the yield stress as a function of plastic strain and the flow potential can be incompressible or dilatant.

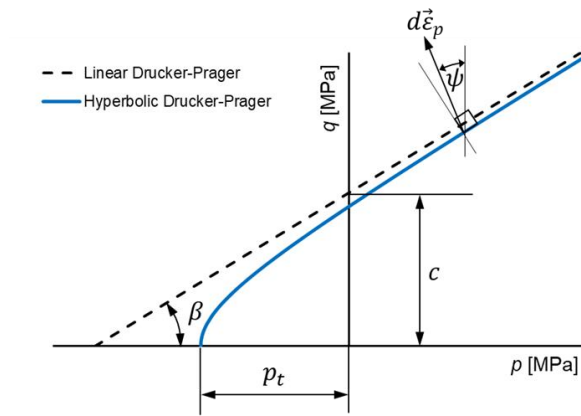


Figure 4.27 Linear and hyperbolic Drucker-Prager models

The damage model implies a damage variable δ that progressively reduces the initial stiffness of the elastic response of the material, the effective stress being defined as

$$\bar{\sigma} = (1 - \delta)E_0(\bar{\epsilon}^{tot} - \bar{\epsilon}^{pl}) \quad (4.11)$$

where the plastic strain is a function of the inelastic strain

$$\bar{\epsilon}^{pl} = \bar{\epsilon}^{in} - \frac{\delta}{1 - \delta} \frac{\bar{\sigma}}{E_0} \quad (4.12)$$

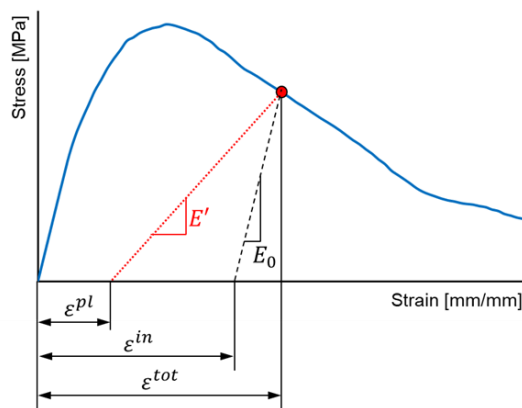


Figure 4.28 Concrete damage plasticity model

If cyclic tests are not available, the damage parameter can be estimated with the relation

$$\delta(\bar{e}^{in}) = \begin{cases} 0, & \bar{e}^{in} \leq \bar{e}^{in}|_{\bar{s}_{max}} \\ 1 - \frac{\bar{s}(\bar{e}^{in})}{\bar{s}_{max}}, & \bar{e}^{in} > \bar{e}^{in}|_{\bar{s}_{max}} \end{cases} \quad (4.13)$$

where \bar{s} is the effective true stress and \bar{s}_{max} is the strength of the material.

This model was calibrated using the experimental data for both compressive and tensile damage (from three-point bending tests) and simulations were performed replicating the physical tests.

Compression tests show the damage initiates at the edges of the specimens and it propagates at an angle of 45 degrees (Figure 4.29). The results show an excellent correlation with the experimental data (Figure 4.30).

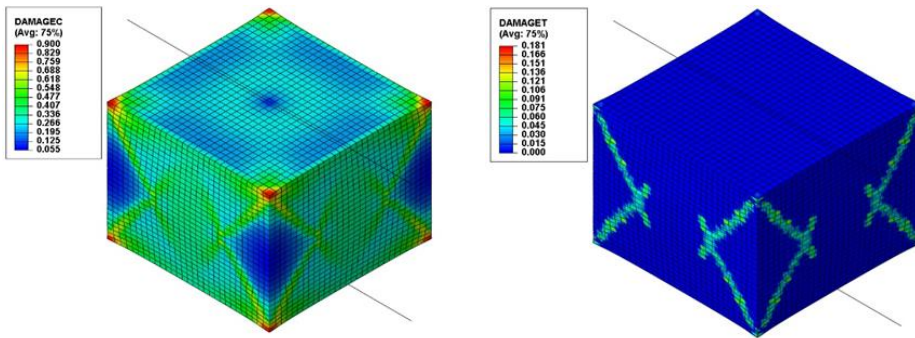


Figure 4.29 Compressive and tensile damage variation for compression simulations

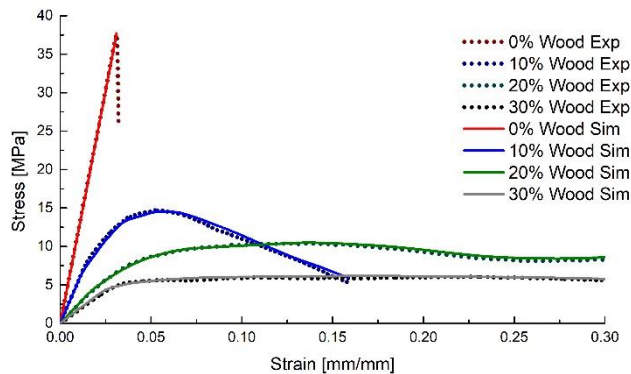


Figure 4.30 Experimental and numerical results for compression tests

The three-point bending simulations show that the specimen fails due to the tensile damage that occurs in the mid region (Figure 4.31). Similar to the compressive simulations, the flexural analyses determine accurate results, thus validating the model (Figure 4.32).

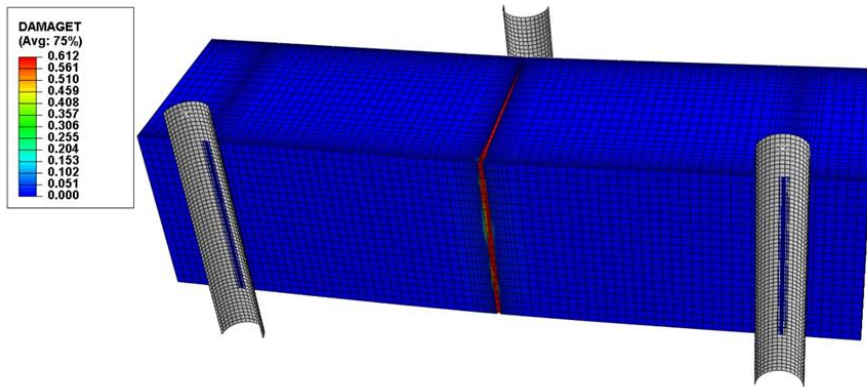


Figure 4.31 Tensile damage variation for the flexural simulations

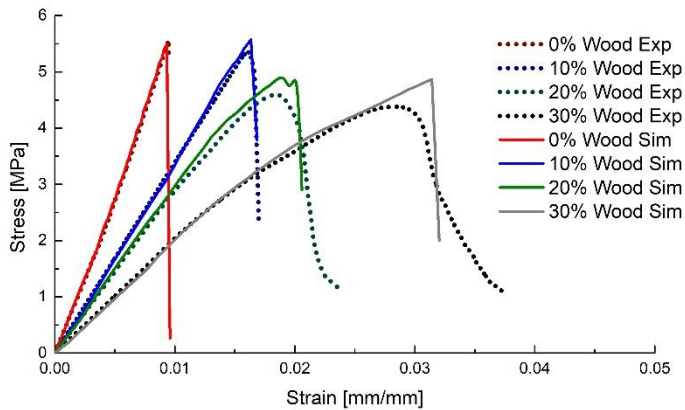


Figure 4.32 Experimental and numerical results for flexural tests

5. Scientific and academic development plan

This chapter will highlight the research fields that the author is considering to pursue for the future development of his scientific career.

5.1. Viscosity, plasticity, fatigue and failure of polymers

The research into the testing and numerical modelling of the mechanical behaviour of polymers will progress through the expansion of the range of investigated materials. An in-depth look into the viscosity (time- and temperature-dependency), plasticity (yield surfaces, flow potentials), fatigue (notch influence on fatigue life) and failure will be considered.

5.1.1. Mechanical testing

As with the rapid prototyped ABS compound, investigations will be carried out on other compounds with regards to the yield and damage loci. These investigation will require the manufacturing of specimens with specific geometries, and injection moulds will be required. Some examples of such specimens are presented in Figure 5.1 (uniaxial tensile, bi-axial, plane strain and shear).

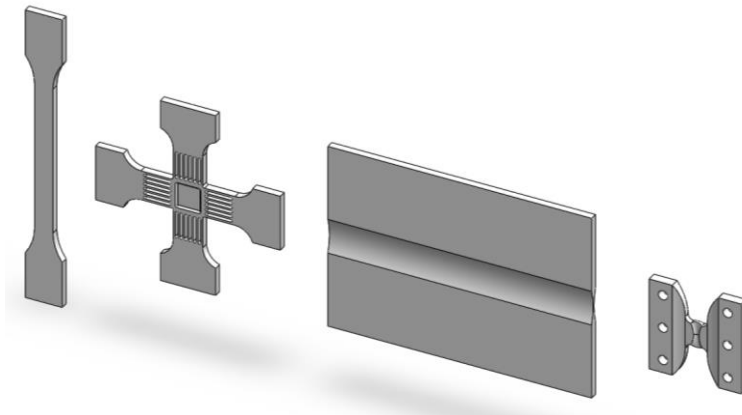


Figure 5.1 Examples of specimen geometries required for plasticity studies

If the adequate experimental facilities are available, the aforementioned specimens will also be subjected to fatigue tests, as literature studies determined limited data for these types of loadings.

5.1.2. Numerical models

One of the main objectives of the author with respect to the study of polymers is the development of yield criteria capable of accurately modelling the plasticity of polymers. The exhaustive planned experimental procedures will provide sufficient data regarding yielding and failure for various stress states so that existing models can be calibrated and new models can be developed.

Another important aspect regarding numerical modelling is the implementation of the developed plasticity and failure models in finite element analysis software using user subroutines. This aspect will allow the analysis of complex structures and thus it constitutes an essential step in validating the models.

5.2. Metamaterial structures

The research into metamaterial structures that the candidate has performed is in its incipient state. There are numerous ways in which the knowledge regarding this field can be extended, from different manufacturing approaches to optimized design and the possibility of designing metamaterial based composite structures.

5.2.1. Manufacturing

One of the objectives regarding this topic is the consideration of other manufacturing technologies (selective laser sintering/melting, stereolithography) and other base materials (metals and ceramics). In addition, conventional manufacturing methods (casting, machining) could be included in hybrid manufacturing procedures.

5.2.2. Structure design and optimization

The research into determining the optimal configuration of metamaterial structures will include investigations regarding the opportunity of reducing stress concentration and improving the rigidity and strength through the addition of various types of reinforcements. Additional structures will also be developed and investigated considering the previous results.

5.2.3. Composite metamaterial structures

The properties of the developed metamaterial structures will be augmented through their inclusion in composite structures. Some options can include the filling of cells with materials with good impact absorption capabilities (polyurethane rigid and/or flexible foams) or the inclusion of higher stiffness materials such as fibre reinforced resins in sandwich structures.

5.3. Woven fibre reinforced polymers

The study of the mechanical properties of woven fibre reinforced composites will represent a new research direction for the author. The study regarding this topic will include both mechanical testing as well as numerical modelling.

5.3.1. Mechanical testing

A particularity of woven composites is their peculiar type of anisotropy. Not only that the strength and stiffness decrease with the angle of rotation from the principal direction of the weave, but the behaviour changes drastically, from linear elastic with brittle failure to elastic-plastic with relatively high failure strains (Figure 2.1).

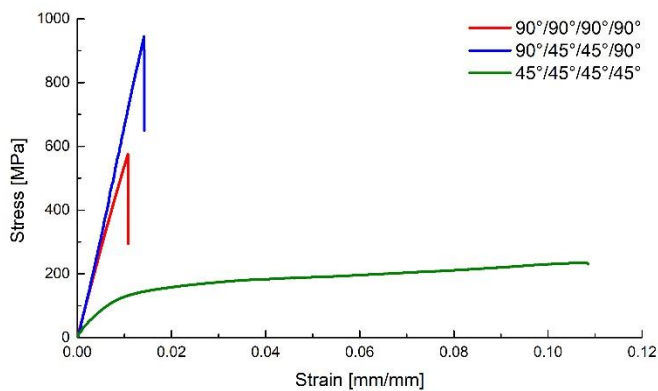


Figure 5.2 Tensile stress-strain behaviour of plane weave carbon fibre reinforced epoxy

90°

5.3.2. Multi-scale modelling

Considering the data provided by the manufacturer and preliminary tests, multi-scale modelling approaches will be considered in simulating the behaviour of these materials. Starting from the fibre count/density and dimensions, the properties of the yarn will be evaluated. Microscopic observations will aid in developing the weave pattern, which will be applied to periodic geometries (Figure 5.3).

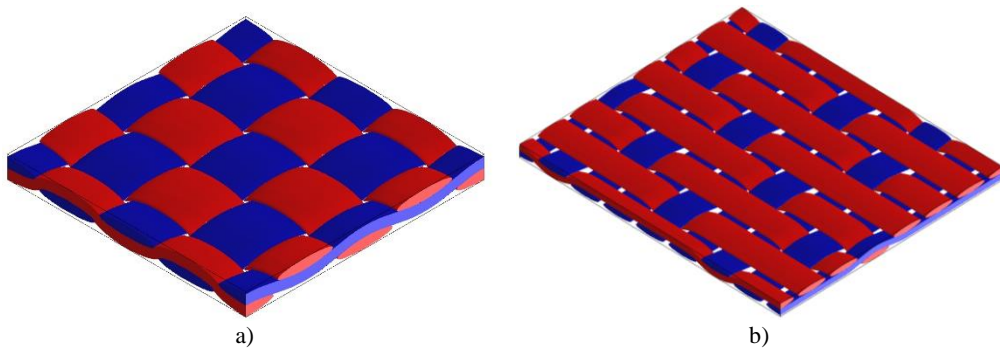


Figure 5.3 Plain (a) and Satin 5N (b) weave patterns

Numerical analyses will be performed with the properties of the yarn and of the matrix in order to determine the orthotropic properties of the structures (Figure 5.4).

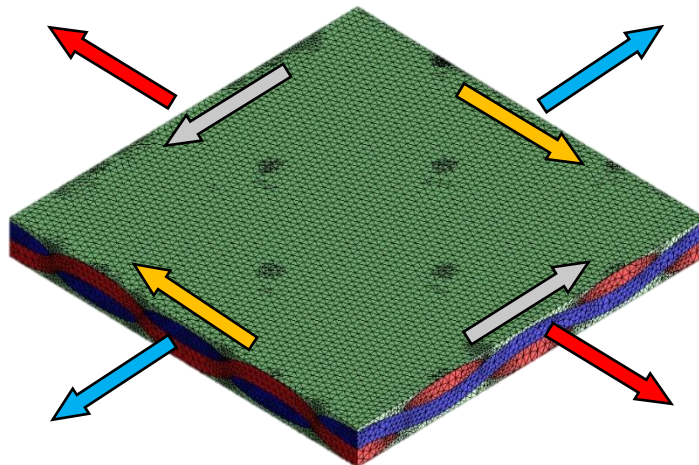


Figure 5.4 Tensile stress-strain behaviour of plane weave carbon fibre reinforced epoxy

The final step in the multi-scale modelling approach is to develop constitutive models that can accurately predict the stiffness, strength and failure of these materials. Some novel approaches will be considered, such as defining the mechanical properties with respect to a polar/cylindrical coordinate system, as the orientation angle of the weave determines significantly different responses.

5.4. Academic development plan

The doctorate themes of the future PhD students that the candidate will coordinate will be in line with the main research directions presented in this chapter. The candidate intends to start working with his future PhD students during their Master studies, so they can get familiar with the research topics before enrolling.

The candidate has showcased his abilities in leading research teams through the successful implementation of three research Grants as Project Manager, leading research teams composed of Professors, senior researchers, postdocs and engineers, as presented in Chapter 4.3.

The majority of the experimental investigations were performed in two laboratories of the Politehnica University Timișoara: The Ștefan Nădășan Laboratory (<http://erris.gov.ro/St-Nadasan-Research-Laborato>) and The Medical Engineering Research Center (<http://erris.gov.ro/Medical-Engineering-Research>). Through his ability of attracting financing, the candidate has acquired and updated a number of experimental facilities that helped him during his research. Examples include:

- Environmental chamber for testing materials at different temperatures (ranging from -100 °C to 350 °C) for the biaxial Instron 8874 testing machine;
- digital inverted optical microscope Insize ISM-M1000, with magnifying powers up to 1000 ×;
- Testing devices for various loading types such as a flexural fatigue, multiaxial loadings (Arcan device), tensile tests for ribbons etc.
- Various load cells and accelerometers that can be mounted on existing testing machines (adequate load ranges for different types of materials/specimens);
- Acquisition of a high performance computer and the optimisation of other machines for finite element analyses.

If the infrastructure available in the aforementioned laboratories is not adequate for some types of experimental procedures, the candidate has access to the facilities of other institutions.

Given his long term collaboration with Institut für Leichtbau und Kunststofftechnik, Technische Universität Dresden (as seen in Section 4.4), the candidate can arrange research stages for future PhD students that can be financially advantageous (the experimental procedures performed at ILK were free of charge and in some instances, the host institution also provided a stipend for the duration of the stage).

Other research institutes and universities that could provide assistance in experimental investigations as well as know-how and resources for various numerical analyses include Loughborough University, UK, Technische Universität München, Germany or Lublin University of Technology, Poland.

Considering the future research directions of the candidate and available collaborations, a potential PhD student can opt for co-tutoring with Professors from the aforementioned Universities (if the parties agree on various terms and the framework is available):

- Prof. Niels Modler or Prof. Maik Gude of Technische Universität Dresden, for research in the field of composite materials, polymers and/or metamaterial structures;
- Prof. Vadim Silberschmidt of Loughborough University, for research into the mechanical behaviour of polymers and biomaterials;
- Prof. Ewald Werner of Technische Universität München, for research in the field of plasticity and/or metamaterial structures;
- Prof. Tomasz Sadowski of Lublin University of Technology, for research in the field of composite materials.

Apart from the financial support offered by Politehnica University Timișoara and the potential support of the co-tutoring institutions, the candidate will include PhD student roles in his future projects. As of the writing of this thesis, the candidate has submitted a project proposal for the UEFISCDI PN-III-P4-ID-PCE-2020-2 competition that includes vacant positions for PhD students as well as Master students (that can continue their work through doctorate studies after their dissertation defense).

6. Bibliography

- [1] J. Mark, *Physical Properties of Polymers Handbook*, Springer, 2007.
- [2] D. Şerban, G. Weber, L. Marşavina, V. Silberschmidt and W. Hufenbach, “Tensile properties of semi-crystalline thermoplastic polymers: Effects of temperature and strain rates,” *Polymer Testing*, no. 32, p. 413–425, 2013.
- [3] D. Şerban, “Viscoplastic Behaviour of Polyamides,” in *Viscoelastic and Viscoplastic Materials*, InTech, 2016.
- [4] G. Strobl, *The Physics of Polymers*, Springer, 2007.
- [5] D. Şerban, H. Hanson, L. Marşavina and V. Silberschmidt, “Viscoelastic properties of semi-crystalline thermoplastic polymers: dynamic analysis and creep,” *Solid State Phenomena*, vol. 188, no. Advanced Materials and Structures IV, pp. 211-218, 2011.
- [6] D. Şerban, L. Marşavina and V. Silberschmidt, “Behaviour of semi-crystalline thermoplastic polymers: Experimental studies and simulations,” *Computational Material Science*, vol. 52, p. 139–146, 2012.
- [7] D. Şerban, *Experimental Investigations and Numerical Simulations of the Mechanical Behaviour of Polyamides - PhD Thesis*, Timișoara: Polytechnic University of Timișoara Press, 2012.
- [8] D. Şerban, L. Marşavina, L. Culea and V. Silberschmidt, “Experimental determination of Mullins effect in semi-crystalline thermoplastic polymers,” *Acta Technica Napocensis*, 2010.
- [9] D. Şerban, L. Marşavina and N. Modler, “Low-cycle fatigue behaviour of polyamides,” *Fatigue and Fracture of Engineering Materials and Structures*, vol. 38, p. 1383–1394, 2015.
- [10] H. Brinson and L. Brinson, *Polymer Engineering Science and Viscoelasticity: An Introduction*, Springer Science, 2008.
- [11] D. Şerban, *Introducere în mecanica solidului deformabil*, Timișoara: Editura Politehnica, 2019.

- [12] P. Hajikarimi, S. Mohammadi and S. Aflaki, "Two dimensional creep analysis of a linear cracked viscoelastic medium using," in *European Congress on Computational Methods in Applied Sciences and Engineering*, Vienna, Austria, 2012.
- [13] D. Şerban, L. Marşavina and V. Silberschmidt, "Response of semi-crystalline thermoplastic polymers to dynamic loading: A finite element study," *Computational Material Science*, vol. 64, p. 116–121, 2012.
- [14] F. J. Zerilli and R. W. Armstrong, "Dislocation-mechanics-based constitutive relations for material dynamics calculations," *Journal of Applied Physics*, vol. 61, no. 5, pp. 1816-1825, 1987.
- [15] G. Johnson and W. Cook, "A constitutive model and data for metals subjected to large strains, high strain rates and high temperatures," in *Proceedings of the Seventh International Symposium on Ballistics*, Hague, The Netherlands, 1983.
- [16] P. Kelly, *An introduction to Solid Mechanics*, Auckland, New Zealand: University of Auckland.
- [17] R. Seltzer, A. P. Cisilino, P. Frontini and Y.-W. Mai, "Determination of the DruckerPrager parameters of polymers exhibiting pressure-sensitive plastic behaviour by depth-sensing indentation," *International Journal of Mechanical Sciences*, vol. 53, no. 6, pp. 471-478, 2011.
- [18] D. Drucker and W. Prager, "Soil Mechanics and Plastic Analysis or Limit Design," *Journal of applied Mathematics*, vol. 10, no. 2, pp. 157-165, 1952.
- [19] D. Şerban, T. Voiconi, L. Marşavina and V. Silberschmidt, "Flexural properties of polyamides: influence of strain rate, friction and moulding-induced anisotropy," in *Key Engineering Materials: Proceedings of the 14th Symposium on Experimental Stress Analysis and Materials Testing*, Timişoara, Romania, 2014.
- [20] R. Hill, "A Theory of the Yielding and Plastic Flow of Anisotropic Metals," *Proceedings of the Royal Society of London, Series A*, no. 193, p. 281–297, 1948.
- [21] W. Hosford, "A Generalized Isotropic Yield Criterion," *Journal of Applied Mechanics*, vol. 39, no. 2, pp. 607-609, 1972.
- [22] K. Runesson, *Constitutive Modelling of Engineering Materials*, Goteborg: Chalmers University of Technology, Goteborg, 2005.

- [23] J. Burša and J. P., “Systemic approach to modelling of constitutive behaviour of various types of matter,” Institute of Solid Mechanics, Mechatronics and Biomechanics, Brno University of Technology, Brno, Czech Republic.
- [24] J. Kang, A. Becker and W. Sun, “Determination of elastic and viscoplastic material properties obtained from indentation tests using a combined finite element analysis and optimization approach,” *Journal of Materials: Design and Applications*, vol. 229, no. 3, pp. 175-188, 2015.
- [25] Y. Bao, Prediction of Ductile Crack Formation in Uncracked Bodies. Ph.D Thesis, Cambridge, Massachusetts: Massachusetts Institute of Technology, 2003.
- [26] Y. Bai, Effect of Loading History on Necking and Fracture, PhD Thesis, Cambridge, Massachusetts: Massachusetts Institute of Technology, 2008.
- [27] Y. Bai and T. Wierzbicki, “A new model of metal plasticity and fracture with pressure and Lode dependence,” *International Journal of Plasticity*, vol. 24, p. 1071–1096, 2008.
- [28] P. Bridgman, Studies in large plastic flow and fracture—with special emphasis on the effects of hydrostatic pressure, New York: McGraw-Hill, 1952.
- [29] Abaqus, “User's Manual,” vol. Analysis, 2017.
- [30] H. Hooputra, H. Gese, H. Dell and H. Werner, “A comprehensive failure model for crashworthiness simulation of aluminium extrusions,” *International Journal of Crashworthiness*, vol. 9, no. 5, pp. 449-464, 2004.
- [31] M. Murugesan and D. Jung, “Johnson Cook Material and Failure Model Parameters Estimation of AISI-1045 Medium Carbon Steel for Metal Forming Applications,” *Materials*, vol. 12, p. 609, 2019.
- [32] D. Şerban, E. Linul, S. Sărăndan and M. L., “Development of parametric Kelvin structures with closed cells,” *Solid State Phenomena*, vol. 254, pp. 49-54, 2016.
- [33] ISO 527, Plastics – Determination of Tensile Properties, 1996.
- [34] E. Linul, D. Şerban, T. Voiconi, L. Marşavina and T. Sadowski, “Energy-absorption and efficiency diagrams of rigid PUR foams,” *Key Engineering Materials*, vol. 601, no. Proceedings of the 14th Symposium on Experimental Stress Analysis and Material Testing, pp. 246-249, 2014.

- [35] D. Şerban, R. Negru, H. Filipescu and L. Marşavina, “Investigations on the influence of the triaxial state of stress on the failure of polyurethane rigid foams,” *Accepted for publication in Continuum Mechanics and Thermodynamics, SI: Computational Mechanics of Materials*, 2020.
- [36] D. Şerban, O. Weissenborn, S. Geller, L. Marşavina and M. Gude, “Evaluation of the mechanical and morphological properties of long fibre reinforced polyurethane rigid foams,” *Polymer Testing*, vol. 49, p. 121–127, 2016.
- [37] V. Deshpande and N. Fleck, “Multi-axial Yield Behaviour of Polymer Foams,” *Acta Materialia*, no. 49, p. 1859–1866, 2001.
- [38] E. Linul, D. Şerban, L. Marşavina and T. Sadowski, “Assessment of collapse diagrams of rigid polyurethane foams under dynamic loading conditions,” *Archives of Civil and Mechanical Engineering*, vol. 17, p. 457 – 466, 2017.
- [39] D. Şerban, T. Voiconi, E. Linul, L. Marşavina and N. Modler, “Viscoelastic Properties of PUR Foams: Impact excitation and dynamic mechanical analysis,” *Materiale Plastice*, vol. 52, p. 537–541, 2015.
- [40] D. Şerban, E. Linul, T. Voiconi, L. Marsavina and N. Modler, “Numerical evaluation of two-dimensional micromechanical structures of anisotropic cellular materials: case study for polyurethane rigid foams,” *Iranian Polymer Journal*, vol. 24, pp. 515-529, 2015.
- [41] L. Marşavina, F. Berto, R. Negru, D. Şerban and E. Linul, “An engineering approach to predict mixed mode fracture of PUR foams based on ASED and micromechanical modelling,” *Theoretical and Applied Fracture Mechanics*, vol. 91, pp. 148-154, 2017.
- [42] R. Negru, D. Şerban, C. Pop and L. Marşavina, “Notch effect assessment in a PUR material using a ring shaped specimen,” *Theoretical and Applied Fracture Mechanics*, vol. 97, pp. 500-506, 2018.
- [43] E. Linul, D. Şerban and L. Marşavina, “Influence of Cell Topology on Mode I Fracture Toughness of Cellular Structures,” *Physical Mesomechanics*, vol. 21, pp. 178-186, 2018.
- [44] L. Marşavina, D. Şerban, C. Pop and R. Negru, “Experimental investigation of failure modes for sandwich beams,” *Key Engineering Materials*, vol. 754, no. 16th International Conference on Fracture and Damage Mechanics, pp. 115-118, 2017.

- [45] D. Șerban, G. Furtos, L. Marșavina, C. Șoșdean and R. Negru, “Numerical modelling of the mechanical behaviour of wood fibre-reinforced geopolymers,” *Continuum Mechanics and Thermodynamics*, 2020.
- [46] D. Șerban, L. Marșavina and N. Modler, “Finite element modelling of the progressive damage and failure of thermoplastic polymers in puncture impact,” *Procedia Engineering*, vol. 109, no. Proceedings of the XXIII Italian Group of Fracture Meeting, p. 97–104, 2015.
- [47] D. Șerban, L. Marșavina, L. Rusu and R. Negru, “Numerical study of the behavior of magnesium alloy AM50 in tensile and torsional loadings,” *Archive of Applied Mechanics*, vol. 89, no. 5, pp. 911-917, 2019.